Structure-performance relationships for supported cobalt Fischer-Tropsch catalysts

Relatie tussen Synthese en Prestatie van Gedragen Kobalt-Fischer-Tropsch-Katalysatoren

(met een samenvatting in het Nederlands)

PROEFSCHRIFT

ter verkrijging van de graad van doctor aan de Universiteit Utrecht op gezag van de rector magnificus, prof. dr. G. J. van der Zwaan, ingevolge het besluit van het college voor promoties in het openbaar te verdedigen op
woensdag 21 oktober 2015 des middags te 2.30 uur

door

Thomas Oliver Eschemann

geboren op 5 oktober 1984 te Leverkusen, Duitsland

Promotor: Prof. dr. ir. K. P. de Jong

The work described in this thesis was financially supported by Shell Global Solutions.

to my family

meiner Familie

ISBN 978-90-393-6417-8

Contents

Chapter 1

Introduction

History and drivers of the Fischer-Tropsch synthesis

In the beginning of the 20th century the first successful experiments on the heterogeneously catalyzed hydrogenation of CO and CO_2 were carried out by *Sabatier* and *Senderens*, who discovered that methane could be formed in presence of nickel catalysts at 523 K.[1] BASF researchers *Mittasch* and *Schneider* patented processes for the heterogeneously catalyzed formation of a variety of liquid hydrocarbons and water from synthesis gas, a mixture of carbon monoxide and hydrocarbons that can be generated from coal, natural gas or biomass.[2–4]

$$n\,CO + (2n+1)\,H_2 \rightarrow C_nH_{2n+2} + n\,H_2O \quad (1)$$

$$n\,CO + 2n\,H_2 \rightarrow C_nH_{2n} + n\,H_2O \quad (2)$$

The potential of the hydrogenation of carbon monoxide for the generation of liquid fuels and chemicals was realized by *Franz Fischer* and *Hans Tropsch* at the Kaiser-Wilhelm Institute for Coal Research in Mülheim/Ruhr, Germany. Their studies led to the development of base-promoted supported cobalt catalysts for the conversion of coal-derived synthesis gas and the low-temperature Fischer-Tropsch process (473 K – 503 K).[4–8] Commercialization was carried out in the 1930s by Ruhrchemie in Oberhausen, Germany, and striving for independence from oil imports, production capacities in Germany were rapidly expanded up to more than 120.000 bpd in the beginning of 1944.[9] With the end of World War II, these plants were either destroyed or dismantled, but interest in the Fischer-Tropsch process continued overseas, since crude oil reserves were estimated to be very limited. The discovery of oil fields in the Middle East and advances in drilling technology led to the closure of the Fischer-Tropsch plant in Brownsville, TX, after short operation time. Based on large coal reserves, Sasol implemented coal-based Fischer-Tropsch plants in South Africa which eventually helped the Apartheid regime to reduce oil dependencies during the embargos in the late 1980s. [10,11]

The economic competitiveness of Fischer-Tropsch plants depends on the oil price, the choice of feedstock for synthesis gas generation, the investment and operating costs of the plant, and the process technology and catalyst performance.[10,12,13] Due to relatively low and stable oil prices, the worldwide interest in Fischer-Tropsch remained

relatively low from the 1950s until the 1970s, when the oil price increased drastically as a consequence of the Yom Kippur war and the Iranian revolution. Considering the estimated break-even prices of GTL (gas to liquids), CTL (coal to liquids) and BTL (biomass to liquids) processes[14] and the oil price development in the recent 60 years, it can be noted that the break-even price of GTL was exceeded by the oil price for the first time in the 1970s and has been continuously surpassed by the oil price since the 2000s, making it an increasingly interesting process for commercial implementation. (Figure 1)

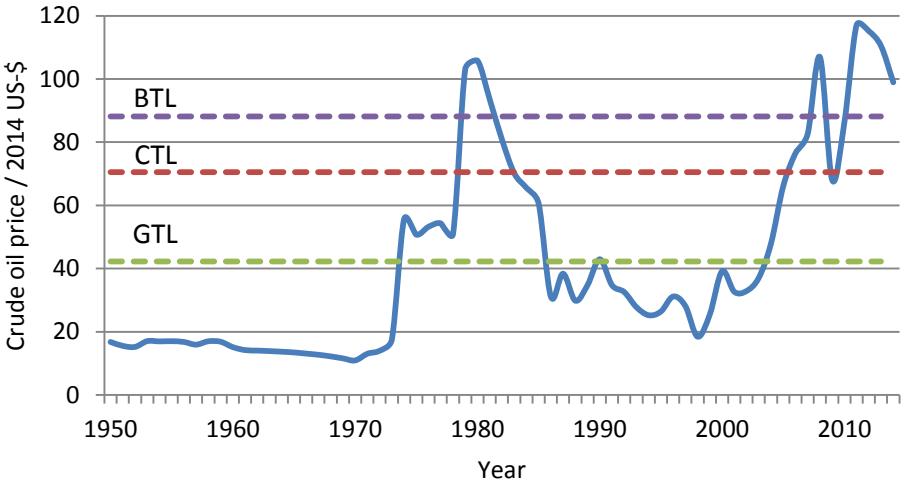

Figure 1: Inflation-corrected annual average crude oil price development from 1950 until 2013.[15] The dotted lines mark the inflation-corrected break-even prices for BTL, CTL and GTL.[14]

Another driver of the GTL process is the fact that stranded natural gas reserves can be converted to liquid and solid products, which can be transported to the relevant markets more easily. Nevertheless, alternative technologies as pipelines, CNG (compressed natural gas), LNG (liquefied natural gas) and GTW (gas to wire) need to be considered, but these tend to be economically less favorable for long distances to the markets and high gas field capacities.[12] The use of natural gas or coal as a feedstock for synthesis gas production may also provide a useful alternative to crude oil, which is estimated to reach its peak production earlier than the other primary energy sources.[16] On the other hand, these feedstocks are still of fossil nature, net-generating carbon dioxide emissions in their combustion. Theoretically carbon-neutral fuels can only be achieved via BTL processes,

but these see relatively few applications due to their high break-even prices and the technical challenges associated with the use of biomass for synthesis gas generation, gas cleanup and subsequent conversion.[17–20]

Road traffic with internal combustion engines has been one of the major sources for the emission of unconverted hydrocarbons, carbon monoxide, nitric and sulphuric oxides and soot. While combustion fuels derived from crude oil typically comprise contaminations of sulphur- and nitrogen containing compounds, metal salts and polyaromatic hydrocarbons, these compounds are virtually absent for Fischer-Tropsch derived fuels.[21] Therefore, the use of ultraclean Fischer-Tropsch fuels or blends thereof may, along with suitable catalytic converters, reduce the emissions of the pollutants stated above in order to meet environmental legislation, which has continuously become more stringent since the 1960s, both in respect to fuel quality and automotive emissions.[21–24]

Probably all of the driving factors described have led to growing interest in the Fischer-Tropsch synthesis both in industry and academia, indicated by increasing numbers of patents and publications, respectively.[4] This regained interest has resulted in the construction of several large-scale Fischer-Tropsch plants such as Secunda by Sasol, a 160,000 bpd CTL plant (now also supplemented with natural gas) built in South Africa in the 1980s based on Sasol's long term experience in the CTL process from smaller plants. In 2005 Sasol has started to carry out further GTL activities in their Oryx plant in Qatar at a capacity of 34,000 bpd. After demonstrating the feasibility of their Shell Middle Distillate Synthesis (SMDS) GTL process in Bintulu, Malaysia, in 2011 Shell has launched Pearl GTL in Las Raffan, Qatar, with a capacity of over 140,000 bpd. In 2014, Chevron has launched its Escravos GTL plant in Nigeria, based on Sasol technology and with a capacity of 34,000 bpd.[10,25] Up to date, the largest operational BTL plant has been built in Freiberg, Germany, with a capacity of only 300 bpd.[18]

In 2013, the total production capacity for Fischer-Tropsch synthesis capacity was estimated to exceed 400,000 bpd, which is still a low share compared to the oil production of currently about 90 mio bpd. Despite the high necessary investment costs, further Fischer-Tropsch projects are continuously evaluated in respect to their technical and economic feasibility. Areas of interest for future investment include, but are not limited to, Australia, Bolivia, China, Iran, Russia, United States, and Uzbekistan.[13,18,25]

The GTL process

After desulphurization, the synthesis gas necessary for Fischer-Tropsch synthesis can be generated from natural gas by steam reforming, partial oxidation or autothermal reforming. Although the latter two options require the construction of large air separation units, it appears to be the economically most favorable route for large Fischer-Tropsch plants.[26]

In the subsequent step, the generated synthesis gas is catalytically converted into water and a mixture of hydrocarbons. The performance of this step has been identified to be of great importance for the overall economic performance of GTL plants.[13] Fischer-Tropsch synthesis can be carried out in the presence of iron catalysts at high temperatures of 573 K – 623 K (HTFT) to yield mainly short-chain products. Operation in the presence of iron or cobalt catalysts at lower temperatures of 473 K – 553 K (LTFT) is the base for all plants recently commissioned in Qatar and Nigeria[25] and leads to the production of long chain hydrocarbon products, which are most interesting for diesel production.[10,27] Different reactor systems have been studied for the implementation of LTFT, of which slurry bubble column and multitubular fixed bed reactors are the most relevant ones. Slurry bubble columns are mainly operated by Sasol (and Exxon at pilot scale) and have the advantage of good heat transfer, an important point in the case of the highly exothermic Fischer-Tropsch reaction. Moreover, mass transfer limitations are likely to be absent during operation and loading and unloading of the catalyst can easily be performed during operation. On the other hand, these type of reactors require separation of the solid catalyst from the reaction products, attrition of the catalyst may occur and upscaling may be difficult.[10,28–30] Multitubular fixed bed reactors are the design of choice for the Shell GTL plants in Bintulu and Las Raffan. They allow relatively easy upscaling, but are prone to heat and mass transfer limitations. Also, the fact that the reactors need to be shut down for the catalyst to be exchanged makes catalyst stability a particularly important point in catalyst development.[10,28,31]

The Fischer-Tropsch reaction is a catalyzed chain growth reaction, in which alkyl chains are formed on the surface of the catalyst particles. The probability for these chains to grow by a single methylene unit is defined as α, the probability of desorption to yield the olefin or paraffin is then $1-\alpha$. The parameter α is a function of the process temperature and

pressure, the synthesis gas composition, and the catalyst used. The expected weight fraction W_n of products containing n carbon atoms is given by:[25,32,33]

$$W_n/n = (1-\alpha)^2 \alpha^{n-1} \quad (3)$$

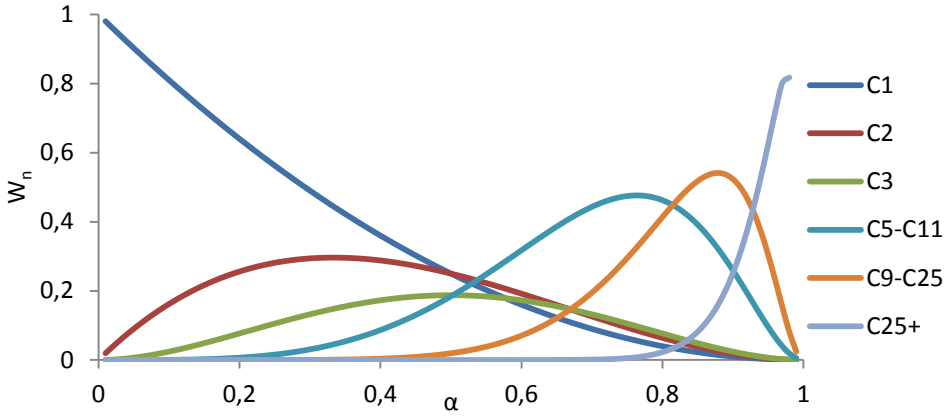

Figure 2: Anderson-Schulz-Flory distribution for Fischer-Tropsch synthesis products.

The expected production distribution for Fischer-Tropsch synthesis can be described by the Anderson-Schulz-Flory distribution (Figure 2). As the figure illustrates, the reaction always yields a wide variety of hydrocarbon species, which need to be separated and/or upgraded. These steps can typically be carried out with conventional refinery technologies as distillation and catalytic cracking. The final products may include ultraclean diesel and naphtha fractions as well as higher molecular lubricants and food grade waxes.[31,34,35] Further product workup also includes separation and purification of water, the stoichiometric main product of the Fischer-Tropsch synthesis. If the plant is located in an arid environment such as Pearl GTL, the generated water can be used not only for steam generation and cooling, but also for plant watering.[36]

Fischer-Tropsch catalysts

It has been demonstrated before that all group 8-10 metals are active in the hydrogenation of carbon monoxide, with ruthenium, nickel, iron, and cobalt being the most relevant.[37] Although being the most active metal in the Fischer-Tropsch reaction, the scarcity and the high price exclude the ruthenium for the use in large scale commercial applications. Relatively high activities are also found for nickel catalysts, but these catalysts show a high selectivity towards methane, which is obviously not wanted in the GTL process. These factors leave iron and cobalt to be considered for commercial Fischer-Tropsch applications, as both elements combine reasonable activities and high selectivities towards heavier hydrocarbons. Cobalt catalysts ($ 30/kg for 99.8% Co[38]) are significantly more expensive than iron catalysts ($ 0.4/kg for scrap iron[38]), but they feature higher stabilities and higher productivities at high conversions due to a less significant effect of water on their activity. Compared to their iron counterparts, cobalt catalysts also show a lower activity in the undesired water-gas shift reaction,

$$CO + H_2O \rightarrow CO_2 + H_2 \quad (4)$$

leading to less formation of carbon dioxide and making them the preferred catalysts for LTFT GTL processes.[39–41]

While the first work of *Fischer* and *Tropsch* was based on using alkalized iron chips as catalysts,[5–7] they later developed co-precipitated Co/ThO_2/kieselguhr catalysts, which also became the first commercial catalyst to be used in the Ruhrchemie plants.[4,42] The naturally-occuring and porous kieselguhr as support material facilitated heat and mass transfer and stabilized the dispersed cobalt nanoparticles against growth. In later Fischer-Tropsch catalyst development, the support material was in most cases replaced by well-defined and readily available synthetic oxides like SiO_2, Al_2O_3 or TiO_2.[39–41] Furthermore, other oxides as ZrO_2,[43–51] CeO_2[52–55] or Nb_2O_5[56–64] have been proposed as support materials for cobalt Fischer-Tropsch catalysts. Highly acidic zeolite support materials have the advantage of catalyzing cracking reactions and thus directly yield gasoline products with less need for further upgrading, making them interesting for small scale Fischer-Tropsch plants.[65–79] Non-oxidic materials studied include different carbon support materials[80–90] and SiC.[91–101]

In general, the support material should combine high porosity and high chemical and mechanical stability under hydrothermal conditions during Fischer-Tropsch synthesis. At a moderate price and good availability, it should allow the preparation of highly dispersed supported catalysts and the reduction of the supported metal oxide nanoparticles to their metallic form. The support materials can be categorized by their extent of interaction with the supported particles. Strongly-interacting supports materials like Al_2O_3 or TiO_2 allow the preparation of highly dispersed supported nanoparticles, but may inhibit their reduction to the catalytically active metal form or show a tendency to form mixed metal-support compounds, which are catalytically not active.[33,39–41] Also, in the presence of supported metal nanoparticles, transition metal oxides as TiO_2 or Nb_2O_5 may be partly reduced to form mobile suboxide species, which may then migrate over the active metal surface to reduce its capability to chemisorb the reactant molecules. This phenomenon called strong metal support interaction (SMSI) has first been studied for Pt/TiO_2 catalysts,[102,103] but needs to be considered for Fischer-Tropsch catalysts supported on reducible transition metals, too.[61,104] Weakly interacting support materials as carbon, SiC or SiO_2, on the other hand, typically allow a facile reduction of cobalt oxide to the metallic form, but may not provide sufficient anchoring sites for the preparation of highly dispersed supported metal catalysts.[39–41]

Industrial catalysts do not only contain a support material and the active metal species, but also one or more promoters. These promoters are not catalytically active themselves, but improve the activity, selectivity and stability of the catalysts. Many names are found for the different kind of promoters in literature, so an attempt has been made to categorize them into structural and electronic promoters. Structural promoters influence the formation and stability of the active phase, e.g. by suppressing the formation of metal-support compounds, increasing the dispersion of the active phase or increasing its stability against particle growth. Electronic promoters directly affect the reactivity of the active metal by decorating its surface or forming an alloy. Promoters featuring both structural and electronic aspects, so-called synergistic promoters, can also be present. While transition metal oxides are often used in order to increase the selectivity to heavier hydrocarbons, noble metals are added in order to facilitate the reduction to the active phase or to increase the dispersion of the active metal.[25,105,106]

Titania-supported Fischer-Tropsch catalysts

While Sasol and Syntroleum seem to have focused exclusively on alumina-supported catalysts, both Exxon and Shell have also focused on other supports like titania.[25,40,107] For industrial use, titania is often not applied in its pure form, but stabilized with other oxides such as Al_2O_3 or SiO_2 in order to preserve its porosity and crystallographic properties under the hydrothermal conditions applied during Fischer-Tropsch synthesis.[40,108–112] The attrition resistance of Co/TiO_2 catalysts has been reported to be lower than for Co/SiO_2 or Co/Al_2O_3 catalysts, although this is a minor problem when operating a fixed-bed process.[113] For research in academia, pyrogenic Evonik Degussa P25 has been established as a standard titania support material, featuring relatively high porosities (BET surface area 50 m^2/g, pore volume 0.3 mL/g) at high purities and a phase composition of 70 % anatase and 30 % rutile. Since the two crystalline structures may have a different impact on the catalytic properties,[114] the ratio of rutile to anatase in this material can be increased by calcination prior to deposition of cobalt.[40,115,116] Well-defined mesoporous and one-dimensional titania support materials have also been developed for academic studies,[117–126] some of which have also been suggested as support materials for Fischer-Tropsch catalysts.

Various studies have been carried out in order to study the differences between titania-supported cobalt Fischer-Tropsch catalysts and systems based on different support materials. *Bartholomew et al.* found increasing turnover frequencies in the order Co/MgO < Co/C < Co/Al_2O_3 < Co/SiO_2 < Co/TiO_2 and selectivities Co/SiO_2 ~ Co/Al_2O_3 < Co/TiO_2 for catalytic testing under atmospheric pressure,[127] *Iglesia et al.* found the impact of the support material on turnover frequencies to be negligible for catalysts with moderate dispersions(< 0.12) at 20 bar and CO conversions above 40 %.[128,129] Both *Iglesia et al.*[128] and *Holmen et al.*[116,130] rationalize the high C_{5+} selectivities of titania-supported catalysts with their porosity and resulting diffusion effects rather than the interaction of the support material with the active metal species, while *Kuipers et al.*[131] discuss effects of the heat of physisorption of olefins on the catalyst surface and their heat of dissolution in and their diffusivity through the wax layer. Both *Shimura et al.*[132]. and *Jongsomijt et al*.[114] found that the increased rutile to anatase ratio could facilitate the reduction to cobalt leading to increased activities at atmospheric pressure. The use of mixed oxides as support materials has also been a topic studied extensively in academia.

Jongsomijt et al.[133] and *Venezia et al.*[134] found that increasing titania contents increased the activity and C_{5+} selectivtity in Co/SiO_2-TiO_2 catalysts.

One of the most important properties of the support material is its interaction with the metal species and the consequences on the dispersions and degree of reductions that can be achieved. The degree of metal-support interaction and the tendency to form irreducible ternary oxides for the most relevant support materials is described to decrease in the order Co/Al_2O_3 > Co/TiO_2 > Co/SiO_2,[25,32] therefore the use of titania offers a compromise between high dispersions and cobalt reducibility. The most remarkable feature about titania as a support material is its own partial reducibility, an aspect that was first studied for Pt/TiO_2 catalysts by *Tauster et al.* in the 1970s.[102,103] This effect known as strong metal support interaction (SMSI) occurs during reduction at elevated temperatures, allowing titania to be partially reduced to TiO_{2-x}, forming mobile species that can cover the surface of the metal nanoparticles and inhibit H_2 chemisorption and thus catalytic activity. The SMSI effect has recently been visualized for Co/TiO_2 catalysts by high resolution electron microscopy[104] and is also possible for other reducible oxide support materials such as Nb_2O_5[56,58,59,61,62,135] and CeO_2.[52] Since this partial reduction of the reducible support material can be reverted when the atmospheric conditions change, it is particularly important to consider the effect of conversion during Fischer-Tropsch synthesis, or resulting water partial pressures,[86,136–143] and the presence of noble metal promoters for this kind of support materials.[57,60,61,128,129,144–146]

The effect of different methods and cobalt precursors in the preparation of Co/TiO_2 catalysts has been studied extensively by *Baerns et al*. They found that the use of cobalt acetate, oxalate or acetyl acetonate precursors led to increased activities but reduced C_{5+} selectivities, while impregnations with Co-EDTA led to slightly increased C_{5+} selectivity. The precipitation of cobalt from high pH did not lead to active catalysts, presumably because cobalt oxide could not be reduced to the active metallic form.[53] Homogeneous deposition precipitation from low pH using urea was shown to yield highly disperse Co/TiO_2 catalysts, which were more active during Fischer-Tropsch synthesis at atmospheric pressure, but showed lower C_{5+} selectivities.[105] Cobalt cations typically present in impregnation solutions show electrostatic interaction with the support surface if the pH of the impregnation solution is above the point of zero charge(PZC, 6.5 for

TiO_2[147]).[39,148,149] This has been modeled in numerous studies[150–154] and shown experimentally for impregnations of TiO_2 in which impregnations with higher pH yielded higher cobalt dispersions.[155] This is also the base for new preparation protocols involving the use of deposition precipitation from high pH.[156–158]

Manganese promoted Co/TiO_2 catalysts have been in the focus of both academia and industry because of their increased C_{5+} selectivities.[25,39] Simultaneous homogeneous deposition precipitation of cobalt and manganese has led to a more intimate contact of the active metal and the promoter as compared to co-impregnated catalysts.[159] The co-precipitated catalysts were reported to show higher activities and C_{5+} selectivities, presumably due to the formation of $Mn_{1-x}Co_xO$ species identified by *in-situ* EXAFS.[160] Using DRIFTS it could be shown that the presence of manganese led to a relative increase in linearly bonded CO, resulting in lower hydrogenation rates during Fischer-Tropsch synthesis.[161] Using selective electrostatic adsorption, manganese promoted Co/TiO_2 catalysts with close contact of active metal and could also be prepared by subsequent impregnation steps.[162,163] The addition of zinc to Co/TiO_2 catalysts has been shown to increase the activity during Fischer-Tropsch synthesis, but comes with the penalty of lower selectivities to heavy hydrocarbons for increasing amounts of zinc.[164–167] The addition of small amounts of boron has been reported to increase dispersion and to increase activity and selectivity to higher hydrocarbons, higher amounts of boron resulted in lower selectivities to heavy hydrocarbons.[168,169] The use of increasing amounts of lanthanum has also been demonstrated to lead to higher activities, but also to lower C_{5+} selectivities.[170]

The characterization of titania-supported cobalt catalysts is a non-straightforward issue, due to the low contrast between the support and the active metal in conventional electron microscopy and the possible occurrence of SMSI effects hampering the determination of dispersion by hydrogen chemisorption or the degree of reduction by temperature-programmed reduction.[116,171] Therefore, both *ex-situ* and *in-situ* techniques have been developed and applied to better understand the properties of the supported catalysts. Synchrotron-based spectroscopy techniques XANES and EXAFS have been applied and combined with traditional characterization methods to gain insight into the degree of reduction of the active metal and the chemical state of promoters.[172] These techniques are particularly useful for monitoring dynamic processes as the

activation[173] or deactivation[174,175] of the catalysts during more or less realistic conditions.[176] It has also been demonstrated that the chemical state of promoters can be well studied using synchrotron based x-ray spectroscopy, providing a useful addition to modern electron microscopy techniques.[159,160,177–180]

Noble metal promoters are used for commercial catalysts, mainly in order to improve the cobalt dispersion and the reduction properties.[181] *Iglesia et al*.[129,144,145] found that bimetallic particles present in Ru-promoted Co/TiO_2 catalysts calcined at high temperatures showed a higher intrinsic activity and higher C_{5+} selectivity than their unpromoted counterparts at 20 bar. This so-called bimetallic synergy was not observed for Ru-promoted Co/SiO_2 catalysts, but has also been found for noble metal promoted Co/Nb_2O_5, a different reducible oxide support material.[56] As reported by *Storsæter et al.*, the use of rhenium as a promoter for Co/TiO_2 catalysts has led to a slight increase in the degree of cobalt reduction without affecting the metal dispersion. During Fischer-Tropsch synthesis at 20 bar these catalysts were found to have distinctly higher activities and increased C_{5+} selectivities.[116] According to *Bertole et al.*, the intrinsic activity of cobalt is not changed in the presence of rhenium.[182] Distinctly cheaper nickel has been discussed to be used as a substitute for rhenium as a reduction activity promoters by *Rytter et al.* and *Jothimurugesan et al.*, although the catalysts prepared by co-impregnation showed low initial activities.[183,184] The addition of small amounts of gold led to an increased cobalt dispersion and activity, but also to increasing selectivities to lighter hydrocarbon products.[185]

The interesting properties of TiO_2 as a support material have generated interest in also studying its properties as a promoter in Fischer-Tropsch synthesis. This has first been attempted in a study on titania promoted Ru/SiO_2 catalysts, in which both higher activities and higher selectivities to heavy hydrocarbons were found for increasing amounts of titania.[186] More recent studies include the addition of titania to Co/SiO_2[187,188] and Co/SiC[189–191] catalysts, in both cases leading to increased activities and selectivities to heavy hydrocarbons. Based on XPS and CO-DRIFTS studies, this effect is rationalized by cobalt being more electron rich, resulting in lower relative H_2 coverages of the metal particles.[187]

Scope of this thesis

It is the goal of this work to contribute to the understanding how the catalyst preparation methods influence the structure and the performance of supported cobalt Fischer-Tropsch catalysts.

In **chapter 2** conventional incipient wetness impregnation (IWI) with subsequent static drying is compared with two deposition precipitation protocols, starting from low (DPU) and from high (DPA) pH, for the preparation of Co/TiO_2 catalysts over a broad Co loading range (4-24 wt.-%). The impact on the the dispersion and distribution of the supported cobalt species is studied using TEM, XRD and DRIFTS. The catalysts are tested under industrially relevant conditions, showing that the superior cobalt distribution for catalysts prepared by deposition precipitation from high pH features higher activities that can be explained with higher hydrogen uptake determined by chemisorption. Moreover, distinctly higher C_{5+} selectivities are measured for catalysts prepared using the DPA technique at similar CO conversion levels.

Chapter 3 deals with the problem of commercial Fischer-Tropsch catalysts undergoing deactivation under realistic conditions. Beside the catalysts prepared by conventional IWI and DPA, incipient wetness impregnation with subsequent fluidized bed drying is applied in order to prepare a system with cobalt distributions more uniform than in the statically dried impregnated catalysts but less uniform than in the DPA catalysts. The catalysts are tested under industrially relevant conditions, showing superior activities for catalysts dried in a fluidized bed compared to their statically dried counterparts. Again, the highest activities and selectivities are found for the DPA catalysts. After one week of Fischer-Tropsch synthesis, all catalyst have lost about 20 % of their initial activity, regardless the preparation procedure and cobalt distribution or the metal loading. The deactivation roughly follows a second order deactivation curve as discussed previously. TEM histogram analysis of the fresh and spent catalysts after 200 h allows to draw conclusions on the deactivation mechanism, the loss in activity is found to correlate well with the loss in cobalt surface area, making average cobalt particle growth the most likely deactivation mechanism.

In **chapter 4** noble metal promoted Co/TiO_2 catalysts are studied in order to obtain further insight on if and how the turnover frequency increases in the presence of these promoters

on reducible oxide support materials. Therefore, the reduction properties and the cobalt particle sizes are studied using TPR and TEM in order to calculate turnover frequencies, both based on the initial cobalt particle sizes and on the particle sizes of the spent catalysts. The results for catalytic testing under industrially relevant conditions indicate that increased activities can be achieved using all promoters in this study, platinum, silver, rhenium and ruthenium. Based on TEM histogram analysis of the spent catalysts, the turnover frequency of the promoted samples has also distinctly increased.

While commercially available titania was kept as a constant in the first chapters of this thesis, **chapter 5** focuses on carbon nanotubes (CNT) supported cobalt catalysts. For this part, the support material is functionalized using both liquid and gas phase oxidation protocols, leading to different degrees of surface functionalized and structural distortion. Impregnations with organic solvents and careful drying protocols are developed in order to yield catalysts with homogeneously distributed and highly-disperse supported cobalt nanoparticles. During Fischer-Tropsch synthesis under industrial conditions, the catalysts supported on unfunctionalized CNT show distinctly higher activities and C_{5+} selectivities, while the catalysts on functionalized CNT are more stable against particle growth when being exposed to Fischer-Tropsch synthesis at elevated temperatures.

Finally, **chapter 6** provides a summary and concluding remarks on the work presented in this thesis. Suggestions are made for future studies in order to provide further insight in the synthesis-structure-performance relationships of cobalt catalysts for Fischer-Tropsch synthesis.

References

[1] P. Sabatier, J.B. Senderens, Comptes Rendus l'Academie Des Sci. Paris. 134 (1902) 689.

[2] A. Mittasch, C. Schneider, DRP 293,787, 1913.

[3] A. Mittasch, C. Schneider, DRP 295,202, 1914.

[4] J.L. Casci, C.M. Lok, M.D. Shannon, Catal. Today. 145 (2009) 38–44.

[5] H. Fischer, F. Tropsch, Brennstoff-Chemie. 4 (1923) 276.

[6] H. Fischer, F. Tropsch, Brennstoff-Chemie. 5 (1924) 201.

[7] H. Fischer, F. Tropsch, Brennstoff-Chemie. 7 (1926) 97.

[8] H. Fischer, F. Tropsch, Berichte Der Dtsch. Chem. Gesellschaft. 59 (1926) 830.

[9] U.S.D. of Energy, (n.d.). http://energy.gov/fe/early-days-coal-research.

[10] M.E. Dry, Catal. Today. 71 (2002) 227–241.

[11] Y. Li, A. de Klerk, Industrial Case Studies, in: P.M. Maitlis, A. de Klerk (Eds.), Greener Fischer-Tropsch Process. Fuels Feestocks, Wiley-VCH, 2013: pp. 107–129.

[12] R. Khalilpour, I.A. Karimi, Energy. 40 (2012) 317–328.

[13] R. Zennaro, Fischer – Tropsch Process Economics, in: P.M. Maitlis, A. de Klerk (Eds.), Greener Fischer-Tropsch Process., Wiley-VCH, 2013: pp. 149–169.

[14] O.P.R. van Vliet, A.P.C. Faaij, W.C. Turkenburg, Energy Convers. Manag. 50 (2009) 855–876.

[15] BP Statistical Review of World Energy June 2014, 2014.

[16] G. Maggio, G. Cacciola, Fuel. 98 (2012) 111–123.

[17] E. Rytter, E. Ochoa-Fernández, A. Fahmi, Biomass-to-Liquids by the Fischer – Tropsch Process, in: P. Imhof, J.C. van der Waal (Eds.), Catal. Process Dev. Renew. Mater., Wiley-VCH, 2013: pp. 265–308.

[18] R. Luque, A.R. de la Osa, J.M. Campelo, A.A. Romero, J.L. Valverde, P. Sanchez, Energy Environ. Sci. 5 (2012) 5186–5202.

[19] P.K. Swain, L.M. Das, S.N. Naik, Renew. Sustain. Energy Rev. 15 (2011) 4917–4933.

[20] L. Petrus, M.A. Noordermeer, Green Chem. 8 (2006) 861–867.

[21] M.E. Dry, J. Chem. Technol. Biotechnol. 77 (2002) 43–50.

[22] E.B. Fox, Z.-T.Z.-W. Liu, Z.-T.Z.-W. Liu, Energy & Fuels. 27 (2013) 6335–6338.

[23] E.S.J. Lox, Automotive Exhaust Treatment, in: G. Ertl, H. Knozinger, F. Schuth, J. Weitkamp (Eds.), Handb. Heterog. Catal., Wiley-VCH, 2008: pp. 2366–2438.

[24] H. Wang, H. Hao, X. Li, K. Zhang, M. Ouyang, Appl. Energy. 86 (2009) 2257–2261.

[25] J. ven de Loosdrecht, F.G. Botes, I.M. Ciobica, A. Ferreira, P. Gibson, D.J. Moodley, A.M. Saib, J.L. Visagie, C.J. Westrate, J.W. Niemantsverdriet, Fischer-Tropsch Synthesis: Catalysts and Chemistry, in: J. Reedijk, K. Poeppelmeier (Eds.), Compr. Inorg. Chem. II, Vol. 7, 2013: pp. 525–554.

[26] J.R. Rostrup-Nielsen, Catal. Today. 71 (2002) 243–247.

[27] A. de Klerk, Y.-W. Li, R. Zennaro, Fischer – Tropsch Technology, in: P.M. Maitlis, A. de Klerk (Eds.), Greener Fischer-Tropsch Process. Fuels Feestocks, Wiley-VCH, 2013: pp. 53–79.

[28] S.T. Sie, R. Krishna, Appl. Catal. A Gen. 186 (1999) 55–70.

[29] T. Wang, J. Wang, Y. Jin, Ind. Eng. Chem. Res. 46 (2007) 5824–5847.

[30] B.H. Davis, Catal. Today. 71 (2002) 249–300.

[31] A. de Klerk, Energy Environ. Sci. 4 (2011) 1177–1205.

[32] Q. Zhang, J. Kang, Y. Wang, ChemCatChem. 2 (2010) 1030–1058.

[33] Q. Zhang, W. Deng, Y. Wang, J. Energy Chem. 22 (2013) 27–38.

[34] D. Kubi, C. Radek, Ind. Eng. Chem. Res. 51 (2012) 8849–8857.

[35] E.F. Sousa-Aguiar, F.B. Noronha, A. Faro, Jr., Catal. Sci. Technol. 1 (2011) 698–713.

[36] Shell Glob. Solut. (2015). http://www.shell.com/global/aboutshell/major-projects-2/pearl/water-treatment.html (accessed January 25, 2015).

[37] M.A. Vannice, J. Catal. 37 (1975) 449–461.

[38] Metalprices.com. (2015). www.metalprices.com (accessed January 25, 2015).

[39] A.Y. Khodakov, W. Chu, P. Fongarland, Chem. Rev. 107 (2007) 1692–1744.

[40] B.H. Davis, Cobalt FT Catalysts, in: P.M. Maitlis, A. de Klerk (Eds.), Greener Fischer-Tropsch Process. Fuels Feestocks, First edit, 2013: pp. 193–207.

[41] M.E. Dry, Stud. Surf. Sci. Catal. 152 (2004) 533–600.

[42] H. Fischer, F. Tropsch, Brennstoff-Chemie. 13 (1932) 61.

[43] H.X. Zhao, H.L. Lü, Adv. Mater. Res. 850-851 (2013) 120–123.

[44] X. Zhang, H. Su, X. Yang, J. Mol. Catal. A Chem. 360 (2012) 16–25.

[45] O.L. Eliseev, M. V. Tsapkina, O.S. Dement'eva, P.E. Davydov, A. V. Kazakov, A.L. Lapidus, Kinet. Catal. 54 (2013) 207–212.

[46] A.L. Lapidus, D.A. Grigorev, M.N. Mikhailov, A.N. Loginova, Russ. Chem. Bull. Int. Ed. 59 (2010) 1675–1679.

[47] H. Zhao, H. Lu, React. Kinet. Catal. Lett. 97 (2009) 289–293.

[48] Y.C. Liu, H.T. Wu, L.T. Jia, Z.H. Fu, J.G. Chen, D.B. Li, D.L. Yin, Y.H. Sun, Adv. Mater. Res. 347-353 (2011) 3788–3793.

[49] J. Panpranot, N. Taochaiyaphum, P. Praserthdam, React. Kinet. Catal. Lett. 87 (2006) 185–190.

[50] D. Enache, Appl. Catal. A Gen. 268 (2004) 51–60.

[51] L.A. Bruce, G.J. Hope, J.F. Mathewsly, Appl. Catal. 8 (1983) 349–358.

[52] M.K. Gnanamani, M.C. Ribeiro, W. Ma, W.D. Shafer, G. Jacobs, U.M. Graham, B.H. Davis, Appl. Catal. A Gen. 393 (2011) 17–23.

[53] M. Kraum, M. Baerns, Appl. Catal. A Gen. 186 (1999) 189–200.

[54] L.A. Bruce, M. Hoang, A.E. Hughes, T.W. Turney, Appl. Catal. A Gen. 100 (1993) 51–67.

[55] M. Hoang, A.E. Hughes, T.W. Turney, 72 (1993) 55–65.

[56] J.H. den Otter, K.P. de Jong, Top. Catal. 57 (2013) 445–450.

[57] F.M.T. Mendes, F.B. Noronha, C.D.D. Souza, M.A.P. da Silva, A.B. Gaspar, M. Schmal, Stud. Surf. Sci. Catal. 147 (2004) 361–366.

[58] R.R.C.M. Silva, M. Schmal, R. Frety, J.A. Dalmon, J. Chem. Soc. Faraday Trans. 89 (1993) 3975–3980.

[59] R.R. Soares, A. Frydman, M. Schmal, Catal. Today. 16 (1993) 361–370.

[60] F.B. Noronha, A. Frydman, D.A.G. Aranda, C. Perez, R.R. Soares, B. Morawek, D. Castner, C.T. Campbell, R. Frety, M. Schmal, Catal. Today. 28 (1996) 147–157.

[61] F.M.T. Mendes, A. Uhl, D.E. Starr, S. Guimond, M. Schmal, H. Kuhlenbeck, S.K. Shaikhutdinov, H.-J. Freund, Catal. Letters. 111 (2006) 35–41.

[62] F.B. Noronha, C. a. Perez, M. Schmal, R. Fre´ty, Phys. Chem. Chem. Phys. 1 (1999) 2861–2867.

[63] M. Schmal, D.A.. Aranda, R.. Soares, F.B. Noronha, A. Frydman, Catal. Today. 57 (2000) 169–176.

[64] A. Frydman, D.G. Castner, C.T. Campbell, M. Schmal, 13 (1999) 1–13.

[65] S. Sartipi, J.E. van Dijk, J. Gascon, F. Kapteijn, Appl. Catal. A Gen. 456 (2013) 11–22.

[66] S. Sartipi, M. Alberts, M.J. Meijerink, T.C. Keller, J. Pérez-Ramírez, J. Gascon, F. Kapteijn, ChemSusChem. 6 (2013) 1646–50.

[67] S. Sartipi, K. Parashar, M. Makkee, J. Gascon, F. Kapteijn, Catal. Sci. Technol. 3 (2013) 572.

[68] S. Sartipi, M. Alberts, V.P. Santos, M. Nasalevich, J. Gascon, F. Kapteijn, ChemCatChem. 6 (2014) 142–151.

[69] S. Sartipi, K. Parashar, M.J. Valero-Romero, V.P. Santos, B. van der Linden, M. Makkee, F. Kapteijn, J. Gascon, J. Catal. 305 (2013) 179–190.

[70] C. Xing, W. Shen, G. Yang, R. Yang, P. Lu, J. Sun, Y. Yoneyama, N. Tsubaki, Catal. Commun. 55 (2014) 53–56.

[71] S. Wang, Q. Yin, J. Guo, B. Ru, L. Zhu, Fuel. 108 (2013) 597–603.

[72] M. Dalil, M. Sohrabi, S.J. Royaee, J. Ind. Eng. Chem. 18 (2012) 690–696.

[73] S.-H. Kang, J.-H. Ryu, J.-H. Kim, P.S. Sai Prasad, J.W. Bae, J.-Y. Cheon, K.-W. Jun, Catal. Letters. 141 (2011) 1464–1471.

[74] A.S. Zola, A.M.F. Bidart, A. d C. Fraga, C.E. Hori, E.F. Sousa-Aguiar, P.A. Arroyo, Stud. Surf. Sci. Catal. 167 (2007) 129–134.

[75] S. Bessel, Appl. Catal. A Gen. 126 (1995) 235–244.

[76] G. Calleja, A. de Lucas, R. van Grieken, Fuel. 74 (1995) 445–451.

[77] S. Bessel, Stud. Surf. Sci. Catal. 81 (1994) 461–466.

[78] G. Calleja, A. De Lucas, R. Van Grieken, Appl. Catal. 68 (1991) 11–29.

[79] V. Udaya, S. Rao, R.J. Gormley, Catal. Today. 6 (1990) 207–234.

[80] G.L. Bezemer, Cobalt supported on carbon nanofibers as catalysts for the Fischer-Tropsch synthesis, Utrecht University, 2006.

[81] G.L. Bezemer, U. Falke, A.J. van Dillen, K.P. de Jong, Chem. Commun. (2005) 731–733.

[82] G.L. Bezemer, P.B. Radstake, V. Koot, A.J. van Dillen, J.W. Geus, K.P. de Jong, J. Catal. 237 (2006) 291–302.

[83] J.P. den Breejen, P.B. Radstake, G.L. Bezemer, J.H. Bitter, V. Frøseth, A. Holmen, K.P. de Jong, J. Am. Chem. Soc. 131 (2009) 7197–7203.

[84] T.O. Eschemann, W.S. Lamme, R.R. Manchester, T.E. Parmentier, A. Cognigni, M. Ronning, J Catal. 328 (2015) 130–138.

[85] H. Xiong, M. a. M. Motchelaho, M. Moyo, L.L. Jewell, N.J. Coville, Catal. Today. 214 (2013) 50–60.

[86] Ø. Borg, Z. Yu, D. Chen, E.A. Blekkan, E. Rytter, A. Holmen, Top. Catal. 57 (2013) 491–499.

[87] J.A. Díaz, M. Martínez-Fernández, A. Romero, J.L. Valverde, Fuel. 111 (2013) 422–429.

[88] M. Moyo, M.A.M. Motchelaho, H. Xiong, L.L. Jewell, N.J. Coville, Appl. Catal. A Gen. 413-414 (2012) 223–229.

[89] T. Fu, C. Huang, J. Lv, Z. Li, Fuel. 121 (2014) 225–231.

[90] K.P. de Jong, J.W. Geus, Catal. Rev. 42 (2000) 481–510.

[91] B. Lee, H.M. Koo, M.-J. Park, B. Lim, D.J. Moon, K.J. Yoon, J.W. Bae, Catal. Letters. 143 (2012) 18–22.

[92] J.S. Lee, J.S. Jung, D.J. Moon, J. Nanosci. Nanotechnol. 15 (2015) 396–399.

[93] X. Zhu, X. Lu, X. Liu, D. Hildebrandt, D. Glasser, Chem. Eng. J. 247 (2014) 75–84.

[94] J.A. Díaz, M. Calvo-Serrano, A.R. de la Osa, A.M. García-Minguillán, A. Romero, A. Giroir-Fendler, J.L. Valverde, Appl. Catal. A Gen. 475 (2014) 82–89.

[95] Y. Liu, O. Ersen, C. Meny, F. Luck, C. Pham-Huu, ChemSusChem. 7 (2014) 1218–39.

[96] A. Lillebø, S. Håvik, E.A. Blekkan, A. Holmen, Top. Catal. 56 (2013) 730–736.

[97] Y. Liu, D. Edouard, L.D. Nguyen, D. Begin, P. Nguyen, C. Pham, C. Pham-Huu, Chem. Eng. J. 222 (2013) 265–273.

[98] A.R. de la Osa, A. De Lucas, J. Díaz-Maroto, A. Romero, J.L. Valverde, P. Sánchez, Catal. Today. 187 (2012) 173–182.

[99] A.R. de la Osa, A. de Lucas, L. Sánchez-Silva, J. Díaz-Maroto, J.L. Valverde, P. Sánchez, Fuel. 95 (2012) 587–598.

[100] B. de Tymowski, Y. Liu, C. Meny, C. Lefèvre, D. Begin, P. Nguyen, C. Pham, D. Edouard, F. Luck, C. Pham-Huu, Appl. Catal. A Gen. 419-420 (2012) 31–40.

[101] M. Lacroix, L. Dreibine, B. de Tymowski, F. Vigneron, D. Edouard, D. Bégin, P. Nguyen, C. Pham, S. Savin-Poncet, F. Luck, M.-J. Ledoux, C. Pham-Huu, Appl. Catal. A Gen. 397 (2011) 62–72.

[102] S.J. Tauster, S.C. Fung, R.L. Garten, J. Am. Chem. Soc. 100 (1978) 170–175.

[103] S.J. Tauster, Acc. Chem. Res. 20 (1987) 389–394.

[104] V.A. de la Peña O'Shea, M.C.Á. Galván, A.E. Prats Platero, J.M. Campos-Martin, J.L.G. Fierro, Chem. Commun. 47 (2011) 7131–7133.

[105] F. Morales Cano, Manganese Promotion in Titania-Supported Cobalt Fischer-Tropsch Catalysis, 2006.

[106] F. Morales, B.M. Weckhuysen, Promotion Effects in Co-based Fischer – Tropsch Catalysis, in: J.J. Spivey, K.M. Dooley (Eds.), Catal. Vol. 19, The Royal Society of Chemistry, Cambridge, 2006: pp. 1–20.

[107] R. Oukaci, A.H. Singleton, J.G. Goodwin, Appl. Catal. A Gen. 186 (1999) 129–144.

[108] W.C. Behrmann, S.M. Davis, C.H. Mauldin, US 5,258,411, 1992.

[109] S.L. Soled, E. Iglesia, R.A. Fiato, G.B. Ansell, 1995.

[110] A.H. Singleton, R. Oukaci, US 6,537,945, 2003.

[111] S. Plecha, C.H. Mauldin, L.E. Pedrick, US 6,124,367, 2000.

[112] S.L. Soled, E. Iglesia, R.A. Fiato, G.B. Ansell, 1991.

[113] D. Wei, J.G. Goodwin, R. Oukaci, A.H. Singleton, Appl. Catal. A Gen. 210 (2001) 137–150.

[114] B. Jongsomjit, C. Sakdamnuson, P. Praserthdam, Mater. Chem. Phys. 89 (2005) 395–401.

[115] S. Rane, Ø. Borg, J. Yang, E. Rytter, A. Holmen, Appl. Catal. A Gen. 388 (2010) 160–167.

[116] S. Storsæter, B. Tøtdal, J.C. Walmsley, B.S. Tanem, A. Holmen, J. Catal. 236 (2005) 139–152.

[117] Y. Wu, J. Yu, H.-M. Liu, B.-Q. Xu, J. Nanosci. Nanotechnol. 10 (2010) 6707–6719.

[118] K. Das, S.K. Panda, S. Chaudhuri, J. Cryst. Growth. 310 (2008) 3792–3799.

[119] Y. Zhang, Mater. Lett. 54 (2002) 375–381.

[120] R. Zhang, B. Tu, D. Zhao, Chem. - A Eur. J. 16 (2010) 9977–9981.

[121] J.G. Dos Santos, T. Ogasawara, R. a. Corrêa, Brazilian J. Chem. Eng. 26 (2009) 555 – 561.

[122] K. Zimny, J. Ghanbaja, C. Carteret, M.-J. Stébé, J.-L. Blin, New J. Chem. 34 (2010) 2113–2117.

[123] K. Zimny, T. Roques-Carmes, C. Carteret, M.J. Stebe, J.L. Blin, J. Phys. Chem. C. (2012).

[124] K. Assaker, C. Carteret, P. Durand, L. Aranda, M.J. Stebe, J.L. Blin, J. Phys. Chem. C. (2013).

[125] S. Yu, Y. Ma, Y. Zhi, H. Jing, H.-Q. Su, Integr. Ferroelectr. 147 (2013) 59–66.

[126] W. Kongsuebchart, A. Methachittipan, T. Kongviwatanakul, P. Praserthdam, O. Mekasuwandumrong, J. Panpranot, Adv. Mater. Res. 634-638 (2013) 595–598.

[127] C.H. Bartholomew, R.C. Reuel, Ind. Eng. Chem. Prod. Res. Dev. 24 (1985) 56–61.

[128] E. Iglesia, S.L. Soled, R.A. Fiato, J. Catal. 137 (1992) 212–224.

[129] E. Iglesia, Appl. Catal. A Gen. 161 (1997) 59–78.

[130] M. Lualdi, S. Lögdberg, G. Carlo, S. Järås, M. Boutonnet, A.M. Venezia, E.A. Blekkan, A. Holmen, Top. Catal. 54 (2011) 1175–1184.

[131] E.W. Kuipers, I.H. Vinkenburg, H. Oosterbeek, J. Catal. 152 (1995) 137–146.

[132] K. Shimura, T. Miyazawa, T. Hanaoka, S. Hirata, Appl. Catal. A Gen. 460-461 (2013) 8–14.

[133] B. Jongsomjit, T. Wongsalee, P. Praserthdam, Mater. Chem. Phys. 97 (2006) 343–350.

[134] A.M. Venezia, V. La Parola, L.F. Liotta, G. Pantaleo, M. Lualdi, M. Boutonnet, S. Järås, Catal. Today. 197 (2012) 18–23.
[135] F.M.T. Mendes, C.A.C. Perez, F.B. Noronha, M. Schmal, Catal. Today. 101 (2005) 45–50.
[136] S. Lögdberg, M. Boutonnet, J.C. Walmsley, S. Järås, A. Holmen, E.A. Blekkan, Appl. Catal. A Gen. 393 (2011) 109–121.
[137] S. Storsæter, Ø. Borg, E.A. Blekkan, A. Holmen, J. Catal. 231 (2005) 405–419.
[138] C. Bertole, C.A. Mims, G. Kiss, J. Catal. 210 (2002) 84–96.
[139] S. Storsæter, Ø. Borg, E.A. Blekkan, B. Tøtdal, A. Holmen, Catal. Today. 100 (2005) 343–347.
[140] M. Lualdi, S. Lögdberg, M. Boutonnet, S. Järås, Catal. Today. 214 (2013) 25–29.
[141] J. Li, G. Jacobs, T. Das, B.H. Davis, Appl. Catal. A Gen. 233 (2002) 255–262.
[142] A.K. Dalai, B.H. Davis, Appl. Catal. A Gen. 348 (2008) 1–15.
[143] R.O. James, T.W. Healy, J. Colloid Interface Sci. 40 (1972) 42–52.
[144] E. Iglesia, S.L. Soled, R.A. Fiato, H. V Grayson, J. Catal. 143 (1993) 345–368.
[145] E. Iglesia, S.L. Soled, R.A. Fiato, G.H. Via, Dispersion, support, and bimetallic effects in Fischer-Tropsch synthesis on cobalt catalysts, in: H.E. Curry-Hide, R.F. Howe (Eds.), Nat. Gas Convers. II, Elsevier, 1994: pp. 433–442.
[146] F. Mendes, F.B. Noronha, R.R. Soares, C.A.C. Perez, G. Marcheti, M. Schmal, Stud. Surf. Sci. Catal. (2001) 177.
[147] G.A. Parks, Chem. Rev. 65 (1965) 177–198.
[148] J.A. Schwarz, Catal. Today. 15 (1992) 395–405.
[149] J.R. Regalbuto, Electrostatic Adsorption, in: K.P. de Jong (Ed.), Synth. Solid Catal., Wiley-VCH, Weinheim, 2009: pp. 33–58.
[150] K. Bourikas, C. Kordulis, J. Vakros, A. Lycourghiotis, Adv. Colloid Interface Sci. 110 (2004) 97–120.
[151] A. Lycourghiotis, Interfacial Chemistry, in: K.P. de Jong (Ed.), Synth. Solid Catal., Wiley-VCH, Weinheim, 2009: pp. 13–30.
[152] G.D. Panagiotou, T. Petsi, K. Bourikas, C.S. Garoufalis, A. Tsevis, N. Spanos, C. Kordulis, A. Lycourghiotis, Adv. Colloid Interface Sci. 142 (2008) 20–42.
[153] K. Bourikas, C. Kordulis, A. Lycourghiotis, Catal. Rev. 48 (2006) 363–444.
[154] T. Petsi, G.D. Panagiotou, C.S. Garoufalis, C. Kordulis, P. Stathi, Y. Deligiannakis, A. Lycourghiotis, K. Bourikas, Chemistry. 15 (2009) 13090–104.
[155] Z.-Q. Zhu, K.-G. Fang, J.-G. Chen, Y.-H.J. Sun, J. Fuel Chem. Technol. 33 (2005) 506.

[156] J.J.C. Geerlings, H.M. Huisman, C.M.A.M. Mesters, US 6,130,184, 2000.
[157] C.M. Lok, US 7,851,404, 2010.
[158] C.M. Lok, EP 1 542 794, 2010.
[159] F. Morales, D. Grandjean, F.M.F. de Groot, O. Stephan, B.M. Weckhuysen, Phys. Chem. Chem. Phys. 7 (2005) 568–572.
[160] F. Morales, D. Grandjean, A. Mens, F.M.F. de Groot, B.M. Weckhuysen, J. Phys. Chem. B. 110 (2006) 8626–8639.
[161] F. Morales, E. de Smit, F.M.F. de Groot, T. Visser, B.M. Weckhuysen, J. Catal. 246 (2007) 91–99.
[162] T.E. Feltes, Y. Zhao, R.F. Klie, R.J. Meyer, J.R. Regalbuto, ChemCatChem. 2 (2010) 1065–1068.
[163] T.E. Feltes, L. Espinosa-Alonso, E. de Smit, L. D'Souza, R.J. Meyer, B.M. Weckhuysen, J.R. Regalbuto, J. Catal. 270 (2010) 95–102.
[164] N.N. Madikizela-Mnqanqeni, N.J. Coville, J. Mol. Catal. A Chem. 225 (2005) 137–142.
[165] N.N. Madikizela-Mnqanqeni, N.J. Coville, Appl. Catal. A Gen. 272 (2004) 339–346.
[166] N.N. Madikizela-Mnqanqeni, N.J. Coville, Appl. Catal. A Gen. 317 (2007) 195–203.
[167] N.N. Madikizela, N.J. Coville, J. Mol. Catal. A Chem. 181 (2002) 129–136.
[168] J. Li, G. Jacobs, Y. Zhang, T.K. Das, B.H. Davis, G. Racoillet, Appl. Catal. A Gen. 223 (2002) 195–203.
[169] J. Li, N.J. Coville, Appl. Catal. A Gen. 181 (1999) 201–208.
[170] Y. Zhang, K. Liew, J. Li, X. Zhan, Catal. Letters. 139 (2010) 1–6.
[171] M. Voß, D. Borgmann, G. Wedler, J. Catal. 212 (2002) 10–21.
[172] G. Jacobs, W. Ma, P. Gao, B. Todic, T. Bhatelia, D.B. Bukur, B.H. Davis, Catal. Today. 214 (2013) 100–139.
[173] G. Jacobs, W. Ma, B.H. Davis, D.C. Cronauer, J.A.. Kropf, C.L. Marshall, Catal. Letters. 140 (2010) 106–115.
[174] K.H. Cats, I.D. Gonzalez-Jimenez, Y. Liu, J. Nelson, D. van Campen, F. Meirer, A.M.J. van der Eerden, F.M.F. de Groot, J.C. Andrews, B.M. Weckhuysen, Chem. Commun. (Camb). 49 (2013) 4622–4.
[175] N.E. Tsakoumis, M. Rønning, Ø. Borg, E. Rytter, A. Holmen, Catal. Today. 154 (2010) 162–182.
[176] H. Oosterbeek, Phys. Chem. Chem. Phys. 9 (2007) 3570–3576.

[177] F. Morales, F. de Groot, O. Gijzeman, A. Mens, O. Stephan, B.M. Weckhuysen, J. Catal. 230 (2005) 301–308.

[178] G. Jacobs, W. Ma, P. Gao, B. Todic, T. Bhatelia, D.B. Bukur, S. Khalid, B.H. Davis, Top. Catal. 55 (2012) 811–817.

[179] T. Jermwongratanachai, G. Jacobs, W. Ma, W.D. Shafer, M.K. Gnanamani, P. Gao, B. Kitiyanan, B.H. Davis, J.L.S. Klettlinger, C.H. Yen, D.C. Cronauer, J.A. Kropf, C.L. Marshall, Appl. Catal. A Gen. 464-465 (2013) 165–180.

[180] G. Jacobs, M.C. Ribeiro, W. Ma, Y. Ji, S. Khalid, P.T.A. Sumodjo, B.H. Davis, Appl. Catal. A Gen. 361 (2009) 137–151.

[181] F. Diehl, A.Y. Khodakov, Oil&Gas Sci. Technol. 64 (2009) 11–24.

[182] C.J. Bertole, C.A. Mims, G. Kiss, J. Catal. 221 (2004) 191–203.

[183] E. Rytter, T.H. Skagseth, S. Eri, A.O. Sjåstad, Ind. Eng. Chem. Res. 49 (2010) 4140–4148.

[184] K. Jothimurugesan, S.K. Gangwal, Ind. Eng. Chem. Res. 37 (1998) 1181–1188.

[185] K. Jalama, N.J. Coville, D. Hildebrandt, D. Glasser, L.L. Jewell, J.A. Anderson, S. Taylor, D. Enache, G.J. Hutchings, Top. Catal. 44 (2007) 129–136.

[186] T. Komaya, A.T. Bell, Z. Weng-Sieh, R. Gronsky, F. Engelke, T.S. King, M. Pruski, J. Catal. 150 (1994) 400–406.

[187] H. Wu, Y. Yang, H. Suo, M. Qing, L. Yan, B. Wu, J. Xu, H. Xiang, Y. Li, J. Mol. Catal. A Chem. 390 (2014) 52–62.

[188] S. Hinchiranan, Y. Zhang, S. Nagamori, T. Vitidsant, N. Tsubaki, Fuel Process. Technol. 89 (2008) 455–459.

[189] Y. Liu, I. Florea, O. Ersen, C. Pham-huu, C. Meny, Chem. Commun. 51 (2014) 145–148.

[190] Y. Liu, B. de Tymowski, F. Vigneron, I. Florea, O. Ersen, C. Meny, P. Nguyen, C. Pham, F. Luck, C. Pham-Huu, ACS Catal. 3 (2013) 393–404.

[191] Y. Liu, C. Pham-Huu, P. Nguyen, C. Pham, WO 2014/001697 A1, 2014.

Chapter 2

Effects of loading and synthesis method of Co/TiO_2 Fischer-Tropsch catalysts

Abstract: Because of their high activity and selectivity to C_{5+} hydrocarbons in the Fischer-Tropsch process, titania-supported cobalt catalysts have received great interest from industrial and academic institutions. Here, we report on three catalyst preparation procedures, incipient wetness impregnation (IWI), deposition precipiration using urea hydrolysis (DPU) or ammonia evaporation (DPA) to prepare Co/TiO_2 catalysts with 4-24 wt.-% Co. The results reveal a strong impact of the catalyst preparation procedure on dispersion and distribution of cobalt over the titania surface. IWI led to clustered cobalt oxide particles of ~10 nm, while for the DPA catalysts similarly sized nanoparticles were found to be well-distributed over the support surface. Co/TiO_2 catalysts prepared by DPU showed the presence of ~2 nm supported cobalt oxide particles beside large unsupported particles. Catalytic tests under industrially relevant conditions show that the DPA catalysts displayed a superior activity and C_{5+} selectivity for the entire cobalt loading range studied.

Introduction

Ever since its invention in the 1920s the Fischer-Tropsch (FT) reaction, the catalytic conversion of synthesis gas into hydrocarbons, has been a topic of great interest for both academic and industrial research. Depleting reserves and increasing prices of crude oil have been a driving force for a growing number of large scale FT applications, as synthesis gas can be generated from alternative feedstock such as coal, biomass or natural gas. In the low temperature FT process, synthesis gas is converted to a mixture of linear high molecular mass hydrocarbons, which is further converted to fuels, lubricants and chemicals.[1–3] For the economic viability of FT plants a good catalyst performance in terms of high activity, selectivity and stability at affordable costs is essential, which makes supported cobalt catalysts the material of choice for modern plants.[4–7] Titania-supported cobalt catalysts have the benefit of particularly high selectivities to heavy (C_{5+}) hydrocarbons,[8,9] although it should be noted that the support is a reducible oxide and, therefore, catalysts are potentially prone to strong metal support interactions (SMSI).[10]

Previous research has shown that particle sizes of supported cobalt nanoparticles have a strong impact on the activities and selectivities in the FT reaction. Turnover frequencies (TOF) and selectivities to higher hydrocarbons are reported to be constant for larger cobalt particles. However, both the TOF and the selectivity to C_{5+} products decrease below a critical particle size.[11–14] Aside the well-studied metal dispersion effects on activity and selectivity in case of cobalt FT catalysts, it has very recently been shown for methanol synthesis catalysts, that the distribution of the active metal species over the support material strongly affects catalysts stability.[15] Furthermore, the chemical nature of the compounds used in the catalyst synthesis can have a strong influence on reducibility and catalytic properties.[16]

Catalyst synthesis methods that have been applied for supported cobalt catalysts for the FT reaction include impregnations with different precursors, co-precipitation, deposition precipitation, sol-gel methods, chemical vapor deposition and colloidal methods. The theoretical background and the obtained results for various combinations of support materials and synthesis methods have been reviewed extensively before.[6] SiO_2 and γ-Al_2O_3 are by far the most widely used support materials for the preparation of cobalt-based FT catalysts. These supports feature large specific surface areas and appreciable

pore volumes and are suitable for incipient wetness impregnations (IWI), in which the metal precursor is deposited within the pores upon drying.[17] Modifications in both drying[18] and the subsequent decomposition of the metal precursor[19] have led to highly active and selective catalysts. For commercially available TiO_2 support materials, however, the maximum applicable metal loadings by IWI are limited by relatively low pore volumes.

A potential solution to this problem is using deposition precipitation (DP), in which the support material is suspended in excess solution of the metal precursor, which can be precipitated on the solid-liquid interface, e.g. upon change of pH of the suspension.[20] The method allows the preparation of highly loaded catalysts with highly dispersed supported nanoparticles. For the deposition of small nanoparticles with narrow size distributions nucleation at the support must outweigh that in solution. This can either proceed via epitaxial growth of support oxide compounds, as has been well studied for the formation of cobalt phyllosilicates.[21] Alternatively, in the case of nickel deposition on oxidized carbon nanofibers, [22] ion-adsorption can precede the nucleation of a hydroxide. In case that an attractive electrostatic interaction between the metal precursor and the support surface prevails, concentration and charge of the metal precursor need to be considered as well as the net surface charge of the oxidic support material.[23,24] In case of pH values above the point of zero charge (PZC, 6.5 for TiO_2), the surface of the oxide is deprotonated and negatively charged, thus adsorption of cations is favored. For pH values below the PZC the surface is positively charge and anions will adsorb. For titania-supported cobalt catalysts, two different DP methods have been put forward in the literature. The first method uses cobalt nitrate as metal precursors and hydrolysis of urea to increase pH such that deposition of cobalt hydroxy species occurs.[25] The second method[26,27] involves a cobalt ammine complex in alkaline solution as metal precursor, which is decomposed by evaporation of ammonia to bring about precipitation.

In this study, we have investigated three catalyst preparation methods, being incipient wetness impregnation (IWI) and the two DP methods described above. We have prepared titania-supported cobalt catalysts in the range of 4-24 wt.-% metal loading and show that the preparation method has a strong impact on both the physicochemical properties and the activities and selectivities during FT synthesis under industrially relevant conditions.

Materials and methods

Catalyst synthesis

For incipient wetness impregnation (IWI), TiO_2 (Aeroxide P25, Evonik Degussa) was pre-sieved to 75-150 µm and dried under vacuum. The support material was impregnated with an aqueous solution of $Co(NO_3)_2 \cdot 6H_2O$ (Acros, p.a.). Subsequently, the material was dried in an oven under static air at 333 K overnight. After that, the catalyst was heat-treated at 623 K(2 h, 2 K/min) in a fluidized bed under a flow of N_2. Note that for higher loadings up to three subsequent impregnations and heat-treatments were required. The catalysts are labeled IWI-XX, XX being the weight percentage of Co, assuming Co to be in the form of Co_3O_4.

In order to prepare Co/TiO_2 catalysts by urea hydrolysis DP (DPU) [25,27] with loadings of 4-24 wt.-% Co, 2 g of TiO_2 powder were suspended in 150 mL of an aqueous solution of an appropriate amount of $Co(NO_3)_2 \cdot 6H_2O$ (0.5-4.0 g) in a double-walled thermostated vessel, which allows pressure release along the axis of the overhead stirrer. The pH was adjusted to 3 using HNO_3 and the suspension was heated to 90°C under vigorous stirring, then 10 mL of an aqueous solution of urea (Acros, p.a., threefold molar amount of Co^{2+}) were added. The suspension was stirred for further 20 h, before it was left to cool to ambient temperature. The solid was filtered off, washed thoroughly with water and dried at 333 K overnight. The obtained filter cake was crushed and sieved to 75-150 µm and then heat-treated in a flow of N_2 at 673 K (4 h, 5 K/min). The catalysts are labeled DPU-XX.

For the preparation of Co/TiO_2 catalysts by ammonia evaporation DP (DPA) [26,27] with loadings of 4-24 wt.% Co, 24.75 g of $CoCO_3$ (Acros, p.a.) were dissolved in 255.6 g of 25 wt.-% ammonia solution (Merck, p.a.). 24.75 g of $(NH_4)_2CO_3$ (Acros, p.a.) were added and the mixture was diluted to give a total of 500 mL. 8 mL of this stock solution were mixed with 70 mL of 9 wt.-% ammonia solution and used to suspend an appropriate amount of TiO_2 powder (0.5-4.0 g) in a PTFE round-bottom flask. The flask was equipped with a reflux cooler and the suspension was stirred and heated to 373 K for 3 h while air was not excluded. After cooling to ambient temperature, the material was filtered off, washed thoroughly with water and dried at 333 K overnight. The obtained filter cake was crushed

and sieved to 75-150 µm and then heat-treated in a flow of N_2 at 673 K (4 h, 5 K/min). The catalysts are labeled DPA-XX.

For selected catalysts prepared by the DPA or DPU method, the vessel was equipped with a pH electrode to record the pH as a function of time during the first hours of precipitation. For comparison, pH curves were also recorded for analogous experiments in absence of the support material.

Elemental analysis using AAS was performed on selected catalysts. The results show that the experimentally determined cobalt loadings are in good accordance with the nominated metal loadings. For the experimental procedure and results the reader is referred to the supporting information.

Catalyst characterization

X-ray powder diffraction (XRD) was performed on a Bruker D2 Phaser with a Cu K_α (λ = 1.789 Å) source. Co_3O_4 crystallite size estimation was performed using the Co_3O_4 peak at 37° 2Θ with an automatic calculation routine in DiffracEvaluation V2.0 software by Bruker, which is based on the Debye-Scherrer-equation.

For Transmission Electron Microscopy (TEM), the heat-treated catalysts were ground with a mortar, suspended in ethanol using an ultrasonic bath and dropped onto a copper grid with holey carbon film. Alternatively, the catalyst particles were embedded in a two component resin (Epofix, EMS) and cured at 333 K overnight. The embedded samples were cut into slices of 50 nm using a Diatome Ultra 35° diamond knife mounted on a Reichert-Jung Ultracut E microtome and then transferred to a copper TEM grid. The samples were analyzed using a Tecnai T10/Tecnai T12 microscope, with electron beam voltage of 100 kV, 120 kV, respectively.

Temperature-programmed reduction (TPR) was carried out using a Micromeritics Autochem II ASAP 2920. Typically, 50 mg of the sample were dried in a flow of Ar at 393 K for 1 h and then reduced in a flow of H_2/Ar (1:19 v/v) at a temperature ramp of 5 K/min.

Hydrogen chemisorption was carried out on a Micromeritics Autochem ASAP 2020. Typically 100 mg of catalyst were dried in a flow of He at 393 K for 2 h and then reduced in

a flow of H_2 at 623 K for 2 h. After evacuation hydrogen chemisorption was measured at 413 K.

Fischer-Tropsch synthesis

Fischer-Tropsch synthesis was carried out in a 16 reactor catalytic testing setup (Flowrence, Avantium). The catalysts were diluted with SiC (200 µm) to arrive at the same amount of Co in every reactor, giving a catalyst bed volume of 200 µL. The catalysts were dried in a flow of He for 2 h and then reduced in-situ in a flow of H_2/He (1:3 v/v) at 623 K (8 h, ramp 1 K/min). Subsequently, the reactors were cooled to 353 K and pressurized to 20 bar under a flow of H_2. After switching to H_2/CO (2:1 v/v) the temperature was increased to 493 K (1 K/min), the products were analyzed using online gas chromatography (Agilent 7890A). The permanent gases were separated on a Shincarbon column and quantified against He as an internal standard using a TCD detector. CO conversions were calculated as

$$X_{CO} = (mol_{CO\ in}\text{-}mol_{CO\ out})/mol_{CO\ in} \quad (1)$$

Hydrocarbons (C1-C9) were separated on a PPQ column, detected using an FID detector and quantified against the TCD signal of the internal standard He. Selectivities to the lower hydrocarbon fractions S_{CX} were calculated from converted CO and the corresponding yields as

$$S_{CX} = Y_{CX}/(mol_{CO\ in}\text{-}mol_{CO\ out}) \quad (2)$$

The selectivities to products with 5 and more carbon atoms are calculated from the yields to lower hydrocarbons as

$$S_{C5+} = 1 - S_{C1\text{-}C4} \quad (3)$$

Stable CO conversions and hydrocarbon selectivities were reached after about 50 h on stream and were between 25 and 35 %. Activities are reported as weight time yields (WTY, $mol_{CO}/(g_{Cat}\cdot s)$).

Results and discussion

Co_3O_4 crystallite sizes for the heat-treated catalysts prepared as calculated from XRD line broadening are given in table 1. The results show that for all applied methods crystallite sizes increase with metal loadings.

Table 1: Co_3O_4 crystallite sizes (nm) obtained from XRD line broadening.

Method/wt.-% Co	4	8	12	16	24
IWI	8.0	8.9	15	15	15
DPA	9.0	8.9	9.4	12	14
DPU	19	25	23	39	51

While the values for the catalysts prepared by IWI and DPA were similar for all studied loadings, distinctly larger values for the crystallites were found for the systems prepared by DPU. For the IWI and DPA catalysts, the XRD line broadening crystallite sizes are in good accordance with the particle sizes obtained from TEM studies. Both IWI and DPA catalyst showed relatively narrow particle size distributions, although few isolated unsupported Co_3O_4 particles of up to ~50 nm were found for the DPA catalysts. In case of the DPU catalysts, TEM studies showed a bimodal particle size distribution of very small (~2-3 nm) supported Co_3O_4 particles besides very large (50-300 nm) unsupported Co_3O_4 particles (Figure 1) for all metal loadings studied. When comparing the similarly sized titania-supported Co_3O_4 particles for the IWI and DPA method, TEM revealed distinct differences in the distribution of the metal oxide nanoparticles over the support surface. While for IWI catalysts, the Co_3O_4 particles were mostly found clustered and wide areas of the support material are empty, the Co_3O_4 nanoparticles appear to be more homogeneously distributed over the support surface in case of the DPA catalysts (Figure 2). The different distributions of the nanoparticles are also observed on the µm length scale when studying TEM micrographs (supplementary data) of ultramicrotomed sections.

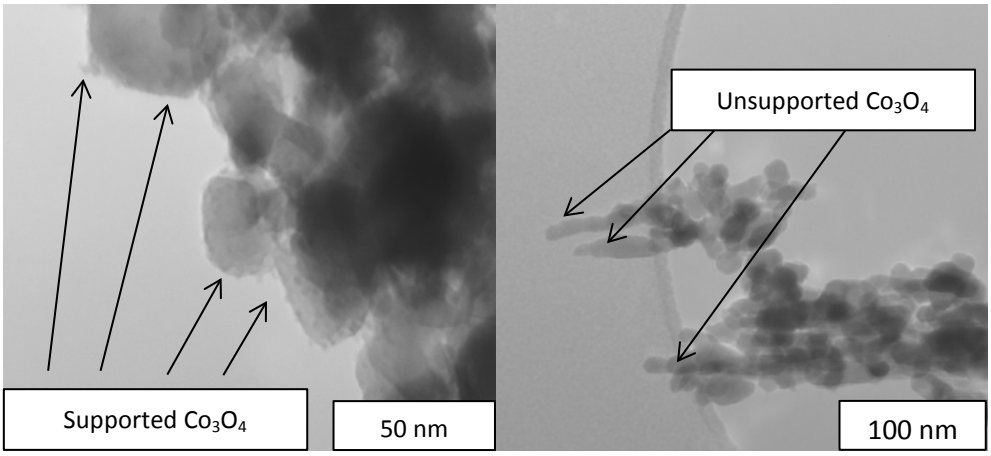

Figure 1: TEM micrographs of DPU-08 showing very small supported (left) and very large unsupported (right) Co_3O_4 particles.

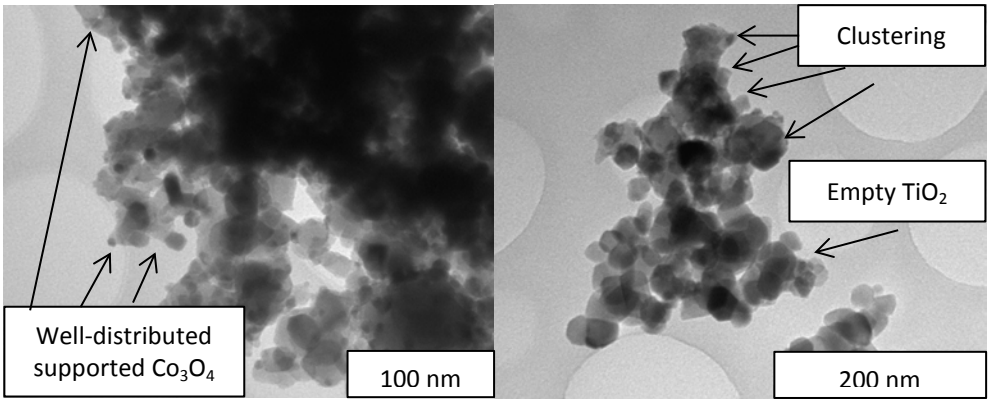

Figure 2: TEM micrographs showing homogeneous distribution of Co_3O_4 nanoparticles in case of DPA-08 (left) and clustering in case of IWI-08 (right).

The observation of clustered supported cobalt oxide particles in case of the IWI catalysts can be explained as a consequence of the deposition of the cobalt precursor during static drying within the pores of the impregnated material as has been published for Ni[28–31] and Co[18,31–33] nitrates. For the DPA catalysts, the well-dispersed and well-distributed supported cobalt oxide nanoparticles can be understood as a consequence of nucleation induced by electrostatic adsorption of the positively charged cobalt precursor on the support surface, being negatively charged above the PZC of TiO_2. The bulk precipitation of cobalt species in the case of the DPU catalysts can be explained by insufficient interaction of the surface and the cobalt precursor. These results are in line with the observations made from the pH curves recorded during the preparation of selected precipitated catalysts. For cobalt deposition by urea hydrolysis, the curve recorded in absence of titania shows a maximum at pH~6.2 (Figure 3), which can be attributed to supersaturation and the nucleation of a solid phase, in this case presumably bulk $Co(OH)_2$ in the liquid.[22] In the presence of titania the rise in pH was much slower for the first 100 min which shows enhanced hydrolysis of $Co(H_2O)_6^{2+}$ ions that coincide with Co-ion adsorption on the support. For longer precipitation times (>100 min) in DPU, however, pH curves with and without support coincide and in both cases precipitation in the bulk liquid prevails, apparently. These observations can be linked to the bimodal particle size distribution described above. The small supported Co particles are linked to ion adsorption whereas the large unsupported particles are linked to bulk precipitation. For cobalt deposition by ammonia evaporation, the interpretation of the recorded pH curves (Figure 4) is less straightforward, as both the curve for DP in absence and in presence do not show a significant minimum, which could be attributed to the formation of a new solid phase. However, the small but apparently significant difference in pH beyond 50 minutes is sufficient with DPA to assure selective deposition of Co species on the titania support.

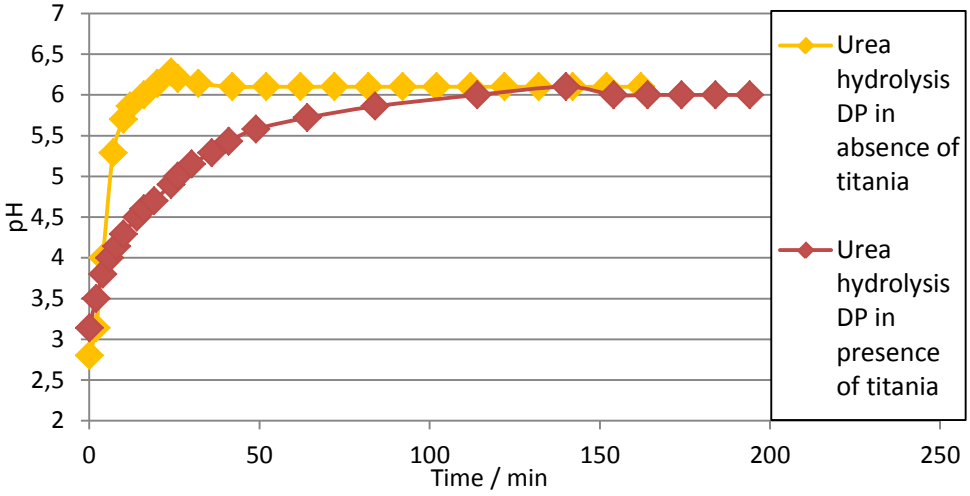

Figure 3: Recorded pH curves for urea hydrolysis DP in presence (DPU-08) and absence of titania.

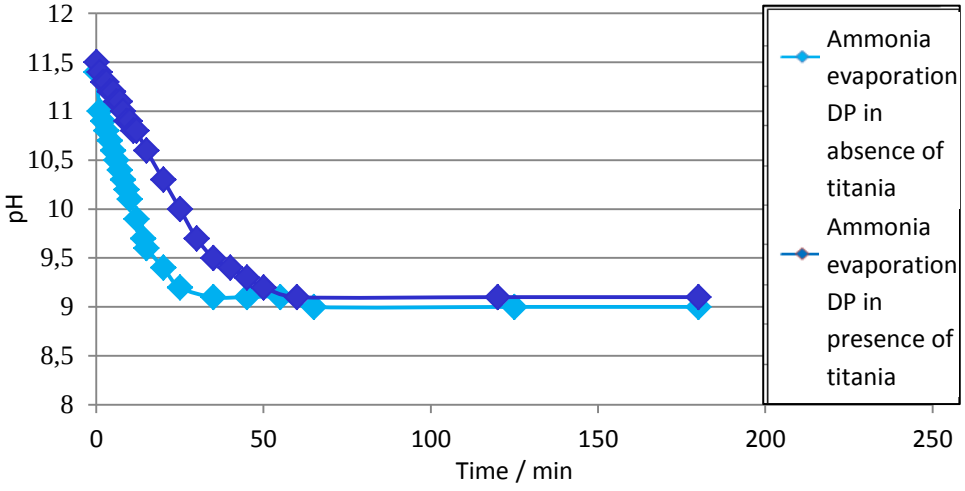

Figure 4: Recorded pH curves for ammonia evaporation DP in presence (DPA-08) and absence of titania.

In order to learn more about the chemical nature of the precipitated species, the heat-treatment procedure of the dried catalysts was mimicked and followed by *in-situ*-DRIFTS. The results (appendix) reveal that for the IWI catalysts, cobalt nitrate hexahydrate was the deposited cobalt precursor that it was dehydrated at 373 K and decomposed into Co_3O_4 at 523 K. In case of the DPU catalysts, the precipitated species was identified as cobalt hydroxynitrate, which was decomposed into cobalt oxide at 493 K. For the DPA catalysts, cobalt hydroxycarbonates were found, which were decomposed upon heating to 523 K.

Results obtained from TPR (Figure 5) support the observations made in the TEM studies. For the IWI catalysts, two peaks were found in a characteristic two-step reduction pattern, with the first one at 590 K indicating the reduction of Co_3O_4 to CoO and the second one at 720 K for the reduction of CoO to metallic cobalt. In the TPR pattern of the DPU sample, the high temperature peak at 720 K was found to be comparable with the IWI catalyst, however, the peak at 590 K featured a distinct shoulder at lower temperatures and a further peak was observed at 440 K. For the DPA sample, the peak at 720 K was observed to be less intense, the peak at 600 K showed a distinct shoulder and an additional peak was observed at 543 K. The presence of a shoulder in the low temperature peaks as seen in the DP samples has previously been interpreted as a result of the better reducibility of bigger supported Co_3O_4 particles or the presence of a promoting species.[34–36] The additional peak below 450 K for the DPU catalyst indicated the presence of organic residues from urea decomposition.

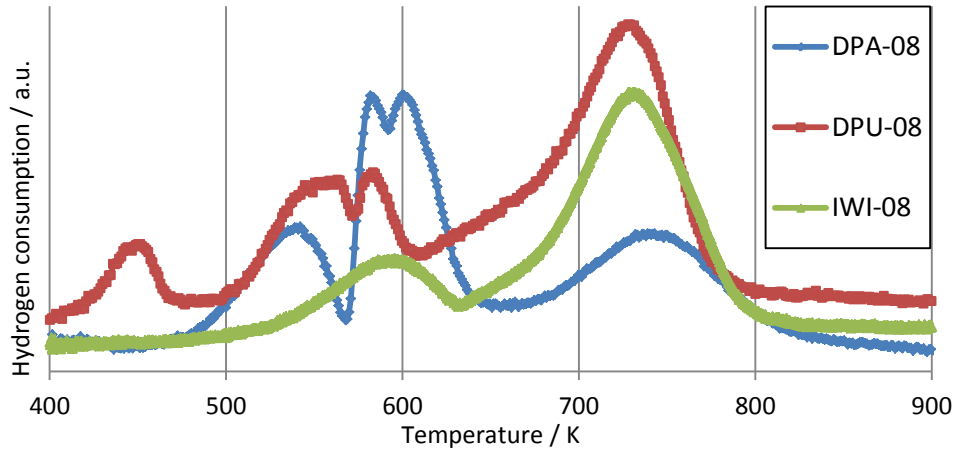

Figure 5: TPR profiles for Co/TiO_2 catalysts DPU-08, DPA-08 and IWI-08.

Results from catalytic testing at industrially relevant conditions are shown in figure 6. For all preparation methods the WTY was found to increase with Co loading with a steep increase for low loadings and a modest increase for higher loadings. The results showed the lowest activities for the catalysts prepared by the DPU method, which can be explained as a result of vast amounts of cobalt being precipitated as unsupported species. Higher activities were obtained for catalysts prepared by IWI and the highest activities were found for catalysts prepared by the DPA method. To explain the different activities of IWI and DPA catalysts, the hydrogen chemisorption uptake after reduction of selected catalysts (Table 2) was compared. The results indicate that the clustered IWI catalysts are more prone to particle growth during reduction than their well-distributed DPA counterparts. The apparent turnover frequencies were found to be similar and the difference in activity can be explained by different accessible metal surface area.

Table 2: H_2 chemisorption uptake, apparent Co particle sizes and TOF for selected catalysts.

Catalyst	H_2 uptake / µmol/g	Apparent d_{Co} / nm	Apparent TOF / s^{-1}
IWI-08	23	32	0.11
DPA-08	43	17	0.12

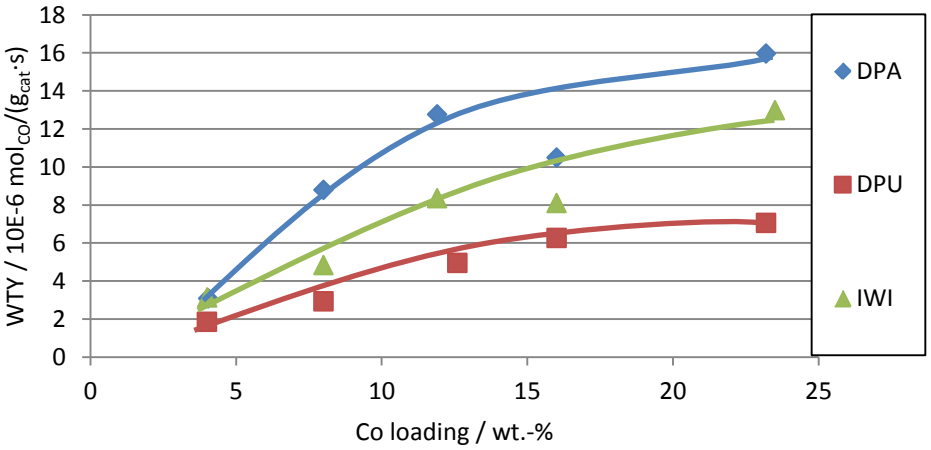

Figure 6: Catalyst weight-based FT activities (WTY) at 20 bar, 493 K, H_2/CO 2.0 for Co/TiO_2 catalysts prepared by different methods.

When comparing the selectivites to C_{5+} hydrocarbons, the lowest selectivities were found for the catalysts prepared by IWI. (Figure 7) The values observed are in good accordance with the literature.[37] Slightly higher selectivites were obtained for catalysts prepared by DPU and by far the highest C_{5+} selectivities for catalysts prepared by the DPA method. This observation is in line with the lowest methane selectivities observed for the DPA catalysts as compared to the other systems. (Figure 8) Both from own results and from the literature[38], it can be excluded that these significant differences in selectivities are a consequence of different CO conversion levels. No impact on selectivities of the metal loading was apparent. It is possible that the higher selectivities observed for the DP catalysts are a consequence of nitrogen being incorporated during catalyst preparation and having a promoting effect under the catalytic testing conditions. Dissolution of the support material during DP and subsequent decoration of the cobalt oxide particles could provide an alternative explanation, especially for the highly selective DPA catalysts. For titania-promoted Ru/SiO_2 catalysts, it was found before that moderate decoration of the active metal particles with reducible oxides can lead to increased activities and selectivities.[39–41] On the other hand, excessive surface coverage of the active metal particles can reverse both these trends. Strong metal support interactions (SMSI), the reduction of the support material to mobile TiO_x species during high temperature reduction, have been studied thoroughly before and mainly found to lead to site blockage and reduced hydrogen chemisorption uptake, showing that the degree of surface coverage can be a key factor in varying the catalytic properties of Co FT catalysts.

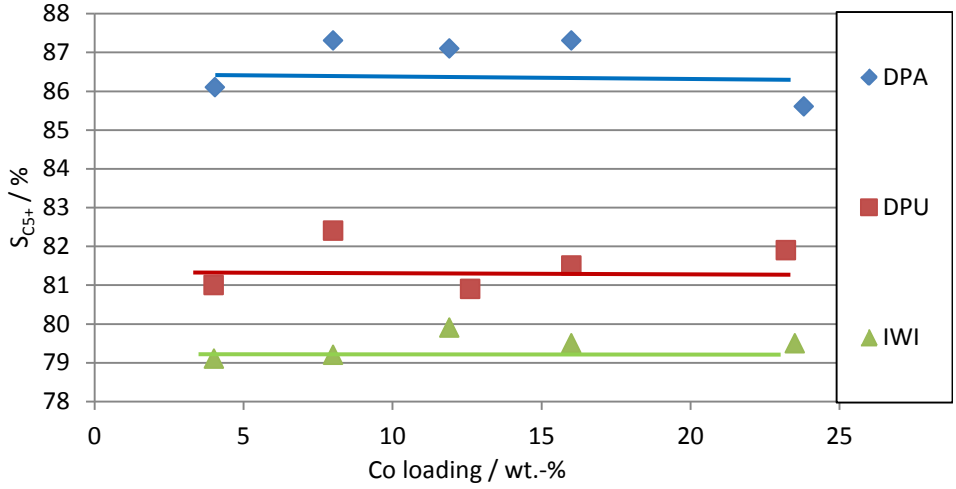

Figure 7: C_{5+} selectivities at 20 bar, 493 K, H_2/CO 2.0 for Co/TiO_2 catalysts prepared by different methods.

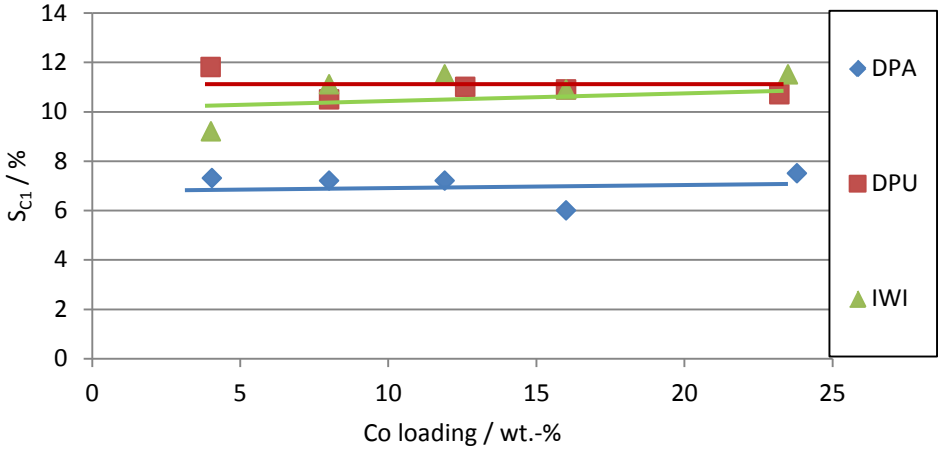

Figure 8: Methane selectivities at 20 bar, 493 K, H_2/CO 2.0 for catalysts prepared by different methods.

Conclusions and outlook

Using incipient wetness impregnation (IWI) and two different deposition precipitation (DP) methods, we have prepared Co/TiO_2 catalysts with fundamentally different physicochemical and catalytic properties. Incipient Wetness Impregnation led to the formation of small, but clustered supported Co_3O_4 particles. Similarly-sized, but more uniformly distributed supported particles were found for catalysts prepared by the ammonia evaporation method. For the catalysts prepared by the urea hydrolysis method, very small particles were found beside very large unsupported particles. The observations in respect to the catalyst structure are in reasonable accordance with pH curves recorded.

Having tested the catalysts in FT synthesis under industrially relevant conditions, we have shown that the activity of the tested systems follows the order DPA > IWI > DPU over a broad range of cobalt loading (4-24 wt.-% Co). Catalyst weight based activities increased with Co loading for all systems studied. Different activities could mainly be attributed to different accessible Co surface areas. The C_{5+} selectivity trend DPA>>DPU>IWI was significant and did not depend on the metal loading in the studied range. Clearly, the distinctly higher activities and selectivities in case of the DPA catalysts require further studies. We tentatively ascribe the high C_{5+} selectivities to an uncontrolled promotion occurring during DP catalyst preparation procedures, either by incorporation of nitrogen in the catalyst or by dissolution of titania and subsequent decoration of the cobalt metal nanoparticles. These decoration effects can be compared with surface coverage of Co with TiO_x species occurring during high temperature reduction, also known as strong metal support interactions (SMSI). Future research will address these issues, e.g. using infrared spectroscopy of adsorbed CO[42] and advanced TEM studies.[43,44]

Acknowledgements

We gratefully acknowledge Shell Global Solutions for financial support. We also thank Johan den Breejen and Sander van Bavel for fruitful discussions, Peter Munnik for carrying out *in-situ*-DRIFTS studies, Arjan den Otter and Tomas van Haasterecht for hydrogen chemisorption measurements and Rien van Zwienen for technical assistance on high pressure catalytic testing.

References

[1] M.E. Dry, Catal. Today. 71 (2002) 227–241.

[2] J.L. Casci, C.M. Lok, M.D. Shannon, Catal. Today. 145 (2009) 38–44.

[3] M.E. Dry, J. Chem. Technol. Biotechnol. 77 (2002) 43–50.

[4] M.E. Dry, Stud. Surf. Sci. Catal. 152 (2004) 533–600.

[5] E. Iglesia, Appl. Catal. A Gen. 161 (1997) 59–78.

[6] A.Y. Khodakov, W. Chu, P. Fongarland, Chem. Rev. 107 (2007) 1692–1744.

[7] Q. Zhang, J. Kang, Y. Wang, ChemCatChem. 2 (2010) 1030–1058.

[8] C.H. Bartholomew, R.C. Reuel, J. Catal. 85 (1984) 78–88.

[9] A.R. de la Osa, A. De Lucas, A. Romero, J.L. Valverde, P. Sánchez, Catal. Today. 176 (2011) 298–302.

[10] V.A. de la Peña O'Shea, M.C.Á. Galván, A.E. Prats Platero, J.M. Campos-Martin, J.L.G. Fierro, Chem. Commun. 47 (2011) 7131–7133.

[11] E. Iglesia, S.L. Soled, R.A. Fiato, J. Catal. 224 (1992) 212–224.

[12] J.P. den Breejen, P.B. Radstake, G.L. Bezemer, J.H. Bitter, V. Frøseth, J. Am. Chem. Soc. 131 (2009) 7197–7203.

[13] G.L. Bezemer, J.H. Bitter, H.P.C.E. Kuipers, H. Oosterbeek, J.E. Holewijn, X. Xu, F. Kapteijn, A.J. van Dillen, K.P. de Jong, J. Am. Chem. Soc. 128 (2006) 3956–64.

[14] G. Prieto, A. Martínez, P. Concepción, R. Moreno-Tost, J. Catal. 266 (2009) 129–144.

[15] G. Prieto, J. Zečević, H. Friedrich, K.P. de Jong, P.E. de Jongh, Nat. Mater. 12 (2013) 34–9.

[16] J.W. Bae, S.-M. Kim, S.-H. Kang, K.V.R. Chary, Y.-J. Lee, H.-J. Kim, K.-W. Jun, J. Mol. Catal. A Chem. 311 (2009) 7–16.

[17] E. Marceau, X. Carrier, M. Che, Impregnation and Drying, in: K.P. de Jong (Ed.), Synthesis of Solid Catalysts, Wiley-VCH, Weinheim, 2009: pp. 59–78.

[18] T.M. Eggenhuisen, P. Munnik, H. Talsma, P.E. de Jongh, K.P. de Jong, J. Catal. 297 (2013) 306–313.

[19] J.P. den Breejen, J.R.A. Sietsma, H. Friedrich, J.H. Bitter, K.P. de Jong, J. Catal. 270 (2010) 146–152.

[20] K.P. de Jong, Deposition Precipitation, in: K.P. de Jong (Ed.), Synthesis of Solid Catalysts, Wiley-VCH, Weinheim, 2009: pp. 111–132.

[21] R. Trujillano, J.-F. Lambert, C. Louis, J. Phys. Chem. C. (2008) 18551–18558.

[22] M.K. van der Lee, A.J. van Dillen, J.H. Bitter, K.P. de Jong, J. Am. Chem. Soc. 127 (2005) 13573–13582.

[23] A. Lycourghiotis, Interfacial Chemistry, in: K.P. de Jong (Ed.), Synthesis of Solid Catalysts, Wiley-VCH, Weinheim, 2009: pp. 13–30.

[24] J.R. Regalbuto, Electrostatic Adsorption, in: K.P. de Jong (Ed.), Synthesis of Solid Catalysts, Wiley-VCH, Weinheim, 2009: pp. 33–58.

[25] F. Morales, D. Grandjean, A. Mens, F.M.F. de Groot, B.M. Weckhuysen, J. Phys. Chem. B. 110 (2006) 8626–8639.

[26] C.M. Lok, EP 1 542 794 A1, 2010.

[27] G.L. Bezemer, P.B. Radstake, V. Koot, A.J. van Dillen, J.W. Geus, K.P. de Jong, J. Catal. 237 (2006) 291–302.

[28] X. Liu, J.G. Khinast, B.J. Glasser, Chem. Eng. Sci. 79 (2012) 187–199.

[29] X. Liu, J.G. Khinast, B.J. Glasser, Chem. Eng. Sci. 63 (2008) 4517–4530.

[30] A. Lekhal, B.J. Glasser, J.G. Khinast, Chem. Eng. Sci. 56 (2001) 4473–4487.

[31] M. Wolters, P. Munnik, J.H. Bitter, P.E. de Jongh, K.P. de Jong, J. Phys. Chem. C. 115 (2011) 3332–3339.

[32] T.M. Eggenhuisen, H. Friedrich, F. Nudelman, J. Zečevic, N.A.J.M. Sommerdijk, P.E. de Jongh, K.P. de Jong, Chem. Mater. 25 (2013) 890–896.

[33] M. Wolters, L.J.W. van Grotel, T.M. Eggenhuisen, J.R.A. Sietsma, K.P. de Jong, P.E. de Jongh, Catal. Today. 163 (2011) 27–32.

[34] A.M. Saib, A. Borgna, J. van de Loosdrecht, P.J. van Berge, J.W. Geus, J.W. Niemantsverdriet, J. Catal. 239 (2006) 326–339.

[35] G. Jacobs, T.K. Das, Y. Zhang, J. Li, G. Racoillet, B.H. Davis, Appl. Catal. A Gen. 233 (2002) 263–281.

[36] A.Y. Khodakov, J. Lynch, D. Bazin, B. Rebours, N. Zanier, B. Moisson, P. Chaumette, J. Catal. 25 (1997) 16–25.

[37] S. Storsæter, B. Tøtdal, J.C. Walmsley, B.S. Tanem, A. Holmen, J. Catal. 236 (2005) 139–152.

[38] D.B. Bukur, Z. Pan, W. Ma, G. Jacobs, B.H. Davis, Catal. Letters. 142 (2012) 1382–1387.

[39] T. Komaya, A.T. Bell, Z. Weng-Sieh, R. Gronsky, F. Engelke, T.S. King, M. Pruski, J. Catal. 150 (1994) 400–406.

[40] A. Dinse, M. Aigner, M. Ulbrich, G.R. Johnson, A.T. Bell, J. Catal. 288 (2012) 104–114.

[41] F. Morales, B.M. Weckhuysen, Promotion Effects in Co-based Fischer – Tropsch Catalysis, in: J.J. Spivey, K.M. Dooley (Eds.), Catalysis Vol. 19, The Royal Society of Chemistry, Cambridge, 2006: pp. 1–20.

[42] V.P. Santos, B. Van Der Linden, A. Chojecki, G. Budroni, S. Corthals, H. Shibata, G.R. Meima, F. Kapteijn, M. Makkee, J. Gascon, ACS Catal. 3 (2013) 1634–1637.

[43] F. Morales, F. de Groot, O. Gijzeman, A. Mens, O. Stephan, B.M. Weckhuysen, J. Catal. 230 (2005) 301–308.

[44] G.L. Bezemer, U. Falke, A.J. van Dillen, K.P. de Jong, Chem. Commun. (Camb). (2005) 731–733.

Appendix

Atomic Absorption Spectroscopy

Elemental analysis was performed on an AnalytikJena ContrAA 700 Flame Atomic Absorption Spectrometer. Therefore, typically 50-100 mg of catalyst was heated to reflux in 2 mL of nitric acid for 1 h to dissolve supported cobalt. After cooling to ambient, the solid was filtered off, washed with water and the sample was diluted to the linear working range of 0-10 mg_{Co}/L. The absorption was measured at the primary line (λ = 240.73 nm), an acetylene-air mixture (1:1 v/v, 50 L/h) was used as fuel for the flame.

The results from experimental analysis using AAS are shown in table S1. The results show that the experimentally determined cobalt loadings are in good accordance with the nominal values for low, medium and high metal loadings. The small deviations can be explained with inaccuracies during weighing the starting materials or with low amounts of cobalt remaining in solution in case of the catalysts prepared by deposition precipitation.

Table S1: Experimentally determined cobalt loadings using AAS for selected catalysts.

Method/nominal wt-% Co	4	12	24
IWI	4.01	11.9	23.5
DPA	4.04	11.9	23.8
DPU	4.00	12.6	23.2

In-situ DRIFTS

In-situ DRIFTS experiments were performed using a Bruker Tensor 27 and a HVC-DRP-3 diffuse reflectance reaction chamber with CaF_2 windows and a mercury-cadmium-telluride (MCT) detector. The bottom of the sample cup was filled with silicon carbide and covered by a grid to minimize temperature gradients, creating a cup of about 1-2 mm deep for the pre-dried sample (±15 mg). N_2 was flowed through the sample from top to bottom at a flow rate of 10 mL/min. 50 scans were recorded from 4000 to 1000 cm^{-1} at a resolution of 4cm^{-1}. Spectra were taken at 2 min intervals. In a typical experiment the cell was first flushed with N_2 at ambient temperature, then the temperature was increased to 350°C with a ramp of 2°C/min.

The results of the in-situ DRIFTS studies for the catalyst prepared by IWI (Figure S1) show that cobalt nitrate was first dehydrated, before it decomposed under formation of cobalt oxide from 150°C onwards. In case of the DPU catalysts, the spectra (Figure S2) showed sharp hydroxide (3500 cm^{-1}) and nitrate (1500 cm^{-1}) bands, indicating that the cobalt species were precipitated as a hydroxynitrate. This is supported by the disappearance of both bands at ~ 225 °C. In case of the DPA catalysts, the hydroxide band was not less distinct than in case of the DPU catalysts.(Figure S3) Carbonate bands (1400 and 1600 cm^{-1}) were found between 150 and 250 °C, indicating that mainly cobalt carbonate was deposited on the titania support. The decomposition of this species occurred at ~ 250°C.

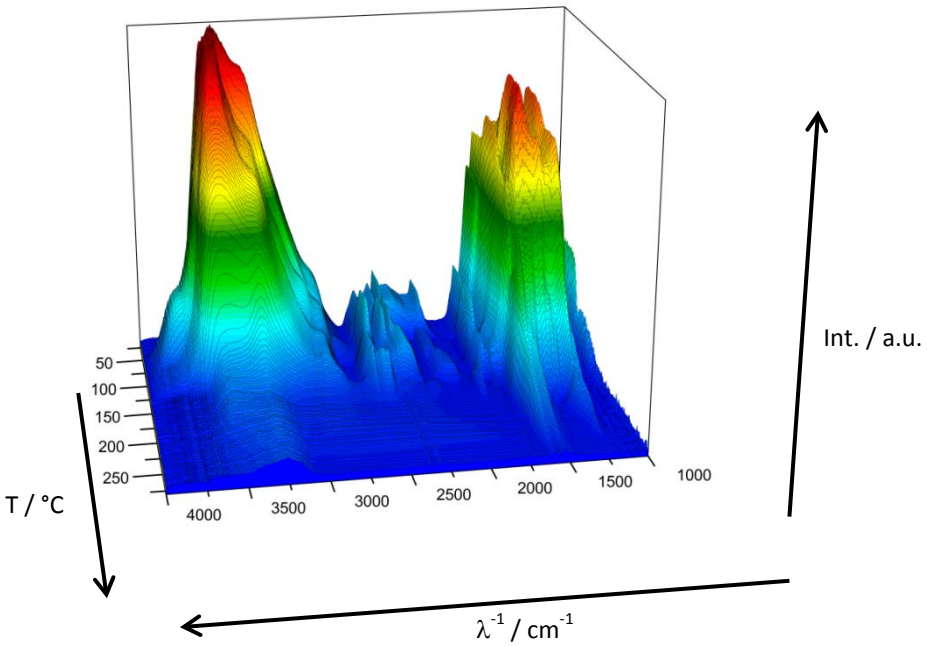

Figure S1: *In-situ* DRIFTS spectra recorded for IWI-08 catalyst under a flow of N_2.

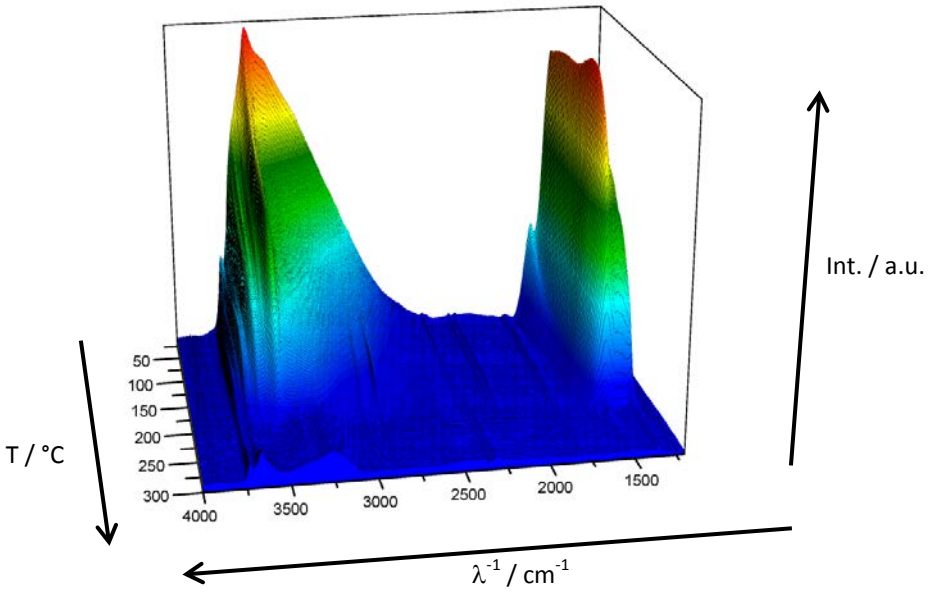

Figure S2: *In-situ* DRIFTS spectra recorded for DPU-08 catalyst under a flow of N_2.

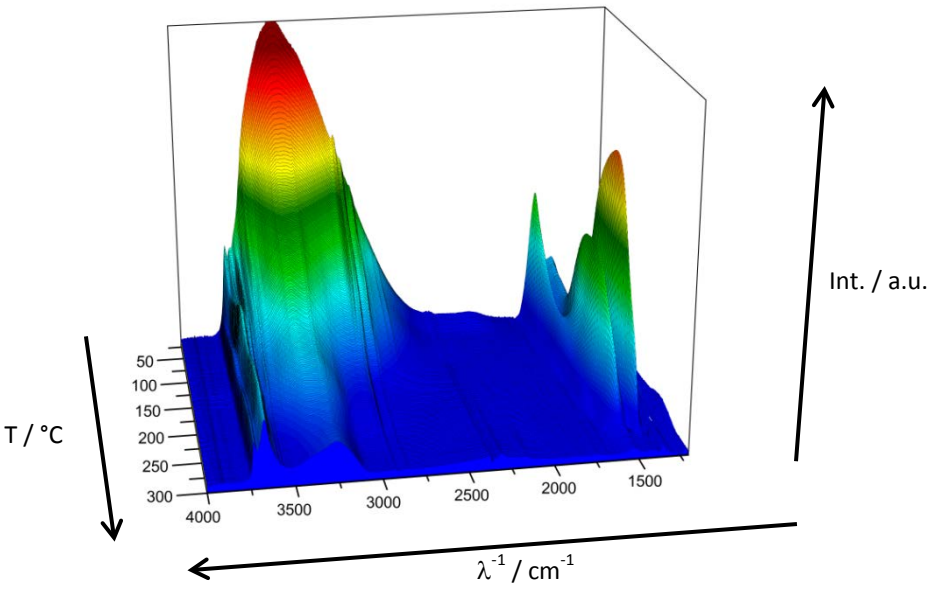

Figure S3: *In-situ* DRIFTS spectra recorded for DPA-08 catalyst under a flow of N_2.

Electron microscopy of microtomed catalysts

Studies of low magnification electron microscopy images show homogeneous contrast for catalyst prepared by both DP methods.(Figure S4) Images for impregnated catalysts (Figure S5) showed both high and low contrast areas. Using STEM-EDX, the darker areas shown in the figure were identified to be areas with high loading, while the lighter were found to be titania only.

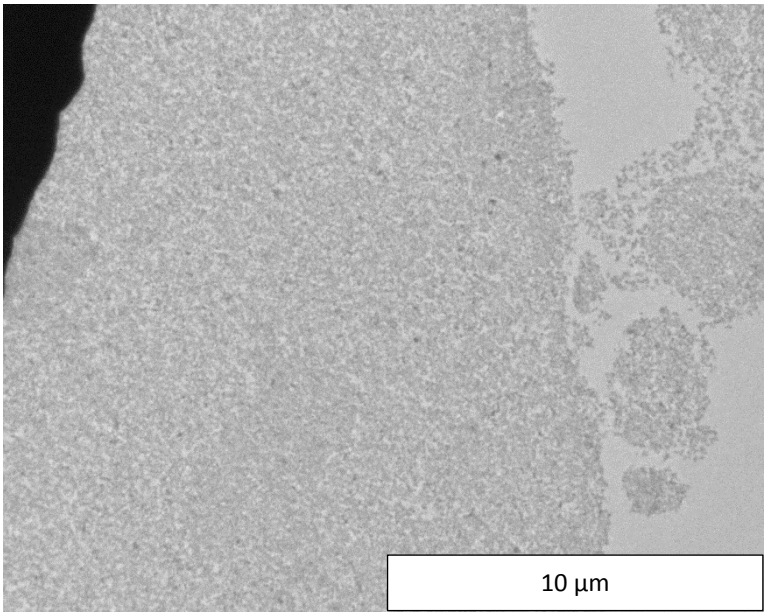

Figure S4: Representative TEM image of a microtomed section of DPA-08 catalyst.

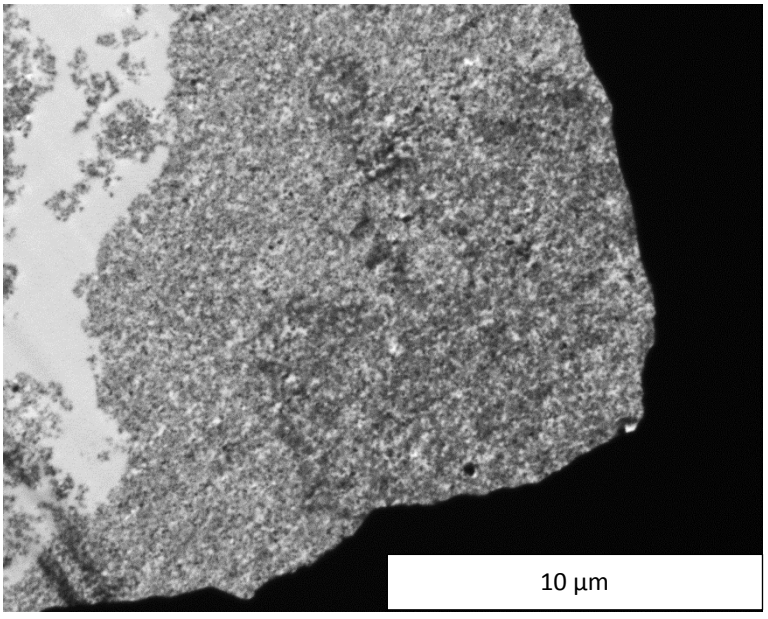

Figure S5: Representative TEM image of a microtomed section of IWI-08 catalyst.

Chapter 3

Deactivation behavior of Co/TiO_2 catalysts during Fischer-Tropsch synthesis

Abstract: Here we report on the preparation of Co/TiO_2 catalysts (8 and 16 wt.-% Co) using deposition precipitation by ammonia evaporation and incipient wetness impregnation with subsequent static drying (IWI-S) and fluidized bed drying (IWI-F). While the initial cobalt oxide dispersions were similar for catalysts with the same metal loading, the distribution of the nanoparticles over the support surface was found to increase in the order IWI-S < IWI-F < DPA. Initial activities during Fischer-Tropsch synthesis at 493 K, 20 bar were found to increase in the same order, while the C_{5+} selectivities were significantly higher for catalysts prepared by DPA. After 200 h of Fischer-Tropsch synthesis at 35 % X_{CO}, all systems studied had lost about 20 % of their initial activity, which could be completely attributed to loss in active metal surface area as shown by TEM histogram analysis. Deactivation constants determined using second order deactivation kinetics were in the same order of magnitude as for Co/SiO_2 catalysts studied previously, but were not affected by the distribution of cobalt. Catalysts tested at higher X_{CO} were found to show significantly faster deactivation, which could also be attributed to average cobalt particle growth.

Introduction

The Fischer-Tropsch reaction involves the catalytic conversion of synthesis gas into higher hydrocarbons and is a promising route to ultraclean fuels, lubricants and chemicals. Different feedstocks can be used for the generation of the synthesis gas, such as coal, biomass or natural gas, the latter being most interesting from an economic perspective in the context of stranded natural gas and shale gas.[1–6] Beside the choice of feedstock for synthesis gas generation, investment and operating costs, reactor technology and oil and gas price development, the performance of the catalyst system is a key factor for the economic viability of Fischer-Tropsch plants.[7,8] Catalyst performance can be divided into three aspects: activity, selectivity and stability. High activities per unit volume are favored, although mass transfer limitations may occur in industrially used catalyst pellets. More importantly, a high selectivity to heavier hydrocarbons (C_{5+}) is desired. Furthermore, the catalyst should feature a high stability under operating conditions. This criterion is especially important for fixed bed processes, in which exchanging catalysts is a more complex and time consuming operation compared to slurry bubble column processes. [7–9]

The problem of cobalt Fischer-Tropsch catalyst deactivation has been reviewed extensively.[10,11] The deactivation mechanisms discussed in literature include poisoning, carbon effects (e.g. coking, carbidization and fouling), re-oxidation, formation of cobalt-support compounds, cobalt surface rearrangement, mechanical disaggregation and loss of cobalt surface area by particle growth. Bulk oxidation has been found to be unlikely under typical Fischer-Tropsch process conditions, although surface oxidation at high water partial pressures may be possible.[11,12] Poisoning effects are highly dependent on the utilized feedstock for synthesis gas generation and the applied gas purification technology, making it an extremely complex phenomenon to be studied at laboratory scale.[13] Cobalt particle growth, however, has been a topic that has received attention both from industrial and academic side and has been identified to be a key factor in catalyst deactivation.[10,11,14–17]

Since the Hüttig temperature of cobalt (526 K) is close to the operating conditions of the low temperature Fischer-Tropsch synthesis (typically 473-553 K),[18] particle growth can occur either via particle migration and coalescence or via Ostwald ripening.[19] Both the

partial pressure of water and the formation of cobalt carbonyl species can play a role in the extent of the competing particle growth mechanisms.[16,19,20] Beside the operating conditions, the structure of the catalyst might play an important role for its stability against deactivation by particle growth. It has previously been shown for different catalytic systems that an enhanced spacing of supported nanoparticles can have a distinct positive effect on the catalyst stability against particle growth.[21–23] For the synthesis of catalysts with well-distributed supported nanoparticles, different techniques can be applied, such as improved drying and heat treatment protocols[21,22,24,25] including freeze-drying[23] for impregnated catalysts or using deposition precipitation as an alternative catalyst preparation method.[26–28]

We have previously demonstrated that in the synthesis of Co/TiO_2 catalysts the use of deposition precipitation via ammonia evaporation (DPA)[29] leads to an improved distribution of cobalt over the support material at similar cobalt particle sizes compared to a standard incipient wetness impregnation protocol with subsequent static drying (IWI-S). The more uniform distribution of cobalt was shown to lead to less particle growth during reduction of the catalyst and higher activities in the Fischer-Tropsch reaction under industrial conditions. It was also shown that the catalysts prepared by deposition precipitation feature distinctly higher selectivities to heavy hydrocarbons for a broad metal loading range (4-24 wt.-% Co), which is important for industrial applications.[26]

Here we report on the deactivation behavior for the first 200 hours on stream under industrially relevant conditions of the catalytic systems mentioned above. Furthermore, we apply incipient wetness impregnation with subsequent fluidized bed drying (IWI-F) in order to obtain an improved cobalt distribution without observing the selectivity effects present in catalysts prepared via deposition precipitation. We study the influence of the preparation methods on the cobalt distribution using transmission electron microscopy. The relative loss of activity of the catalysts at comparable CO conversion levels is discussed and the average cobalt particle sizes before and after the catalytic testing experiments are measured using transmission electron microscopy in order to determine the turnover frequencies (TOF) of the catalysts at the start and at the end of the catalytic tests. These values can be used in order to draw conclusions on the main reasons for catalyst deactivation on the timescale of the experiments carried out.

Materials and methods

Catalyst synthesis

Two methods were applied for the preparation of Co/TiO_2 catalysts by incipient wetness impregnation (IWI). TiO_2 (Aeroxide P25, Evonik Degussa, pore volume 0.3 ml/g, BET surface area 50 m^2/g, 70 % anatase, 30 % rutile) was pre-sieved to particles of 75-150 µm and dried under vacuum (50 mbar), before the support material was impregnated with an aqueous solution of $Co(NO_3)_2 \cdot 6H_2O$ (Acros, p.a.). The material was then dried in an oven under static air at 333 K overnight. After that, the catalyst was heat treated at 623 K (2 h, ramp 2 K/min) in a fluidized bed under a flow of N_2. These catalysts are labeled IWI-XXS, XX being the weight percentage of Co, assuming Co to be in the form of Co_3O_4. Alternatively, the material was dried in a fluidized bed under a flow of N_2 at 353 K, before the heat treatment was carried out at 623 K (2 h, ramp 2 K/min) in a fluidized bed under a flow of N_2. These catalysts are labeled IWI-XXF. It should be noted that metal loadings of 8 wt.-% Co (assuming Co to be in the form of Co_3O_4) were achieved with a single impregnation, while for catalysts with 16 wt.-% Co a second impregnation cycle was carried out after the heat treatment of the sample after the first impregnation.

The preparation method[30] of Co/TiO_2 catalysts by ammonia evaporation deposition precipitation was described before.[26] 24.75 g of $CoCO_3$ (Acros, p.a.) were dissolved in 255.6 g of 25 wt.-% ammonia solution (Merck, p.a.). 24.75 g of $(NH_4)_2CO_3$ (Acros, p.a.) were added and the mixture was diluted to give a total of 500 mL. 8 mL of this stock solution were mixed with 70 mL of 9 wt.-% ammonia solution and used to suspend an appropriate amount of TiO_2 powder (0.5-4.0 g) in a PTFE round-bottom flask. The flask was equipped with a reflux cooler and the suspension was stirred and heated to 373 K for 3 h while air was not excluded. After cooling to ambient temperature, the material was filtered off, washed thoroughly with water and dried at 333 K overnight. The obtained filter cake was crushed and sieved to 75-150 µm and then heat-treated in a flow of N_2 at 673 K (4 h, ramp 5 K/min). The catalysts are labeled DPA-XX.

Catalyst characterization

X-ray powder diffraction (XRD) was performed on a Bruker D2 Phaser with a Co K_α (λ = 1.789 Å) source. Co_3O_4 crystallite size estimation was performed using the Co_3O_4 peak at 37° 2Θ with an automatic calculation routine in DiffracEvaluation V2.0 software by Bruker, which is based on the Debye-Scherrer-equation.

For Transmission Electron Microscopy (TEM), the heat-treated catalysts were ground with a mortar, suspended in ethanol using an ultrasonic bath and dropped onto a copper grid with holey carbon film. Spent catalysts were prepared in the same way. The samples were analyzed using a Tecnai T10 or Tecnai T12 microscope, with electron beam voltage of 100 kV or 120 kV, respectively. Equivalent cobalt particle sizes are calculated from average Co_3O_4 particle sizes based on analysis of typically 200 particles by using the relation $d(Co)=d(Co_3O_4) * 0.75$. Spent catalysts showed metallic cobalt particles covered with a thin wax layer, therefore no correction factor was used.

Catalytic testing

Fischer-Tropsch synthesis was carried out in a 16 reactor catalytic setup (Flowrence, Avantium). The catalysts were diluted with SiC (200 µm) to arrive at the same amount of Co in every reactor, giving a catalyst bed volume of 200 µL. The catalysts were dried in a flow of He for 2 h and then reduced *in situ* in a flow of H_2/He (1:3 v/v) at 623 K (8 h, ramp 1 K/min). Subsequently, the reactors were cooled to 453 K and pressurized to 20 bar under a flow of H_2. After switching to H_2/CO (2:1 v/v) the temperature was increased to 493 K (ramp 1 K/min). At the end of the experiment, most of the products remaining in the catalyst bed were removed under a flow of H_2 at 473 K, before the setup was cooled down to room temperature under a flow of He. The products were analyzed using online gas chromatography (Agilent 7890A). The permanent gases were separated on a Shincarbon column and quantified against He as an internal standard using a TCD detector. CO conversions were calculated as

$$X_{CO} = (mol_{CO\ in}-mol_{CO\ out})/mol_{CO\ in} \quad (1)$$

Hydrocarbons (C1-C9) were separated on a PPQ column, detected using an FID detector and quantified against the TCD signal of the internal standard He. Selectivities to the lower hydrocarbon fractions S_{CX} were calculated from converted CO and the corresponding yields as

$$S_{CX} = Y_{CX}/(mol_{CO\ in}-mol_{CO\ out}) \quad (2)$$

The selectivities to products with 5 and more carbon atoms are calculated from the yields to lower hydrocarbons as

$$S_{C5+} = 1 - S_{C1-C4} \quad (3)$$

CO conversion levels during the experiments were between 25 and 35 %. Activities are reported as cobalt time yields (CTY, $mol_{CO}/(g_{Co}\cdot s)$) and weight time yields (WTY, $mol_{CO}/(g_{Cat}\cdot s)$). In order to analyze the deactivation of the catalysts, the activities a were determined by assuming first-order kinetics in hydrogen according to

$$a = GHSV * \log (1 - X_{H2}) \quad (4)$$

These activities were then normalized ($a_{norm}=a/a_{initial}$) and fitted according to a linearized form of second order deactivation kinetics as demonstrated previously.[21,22]

$$1/(a_{norm}(t)) = k_d*t + 1 \quad (4)$$

Results and discussion

The results for the Co_3O_4 particle size of the catalysts obtained after heat treatment determined from XRD and TEM (Table 1) showed that for comparable metal loadings similar particle sizes were obtained for all applied preparation techniques. As expected and in accordance with results reported previously,[26] the average particle sizes were found to be larger for the catalysts with higher metal loadings. TEM revealed that the supported Co_3O_4 particles were strongly clustered for the catalysts dried in static air. Distinctly less clustering was obtained for catalysts dried under a flow of nitrogen and uniform distributions were found for the catalysts prepared by deposition precipitation.(Figure 1) These results are in accordance with results reported previously indicating improved distributions of supported metal nanoparticles for fluidized bed drying[22,25] and deposition precipitation.[26]

Table 1: Co_3O_4 crystallite sizes determined from Scherrer-analysis of the XRD peak at 37° 2Θ and surface-average Co_3O_4 particle sizes determined by TEM.

Catalyst	IWI08S	IWI16S	IWI08F	IWI16F	DPA08	DPA16
XRD Co_3O_4 crystallite size / nm	8.4	12	6.9	12	8.5	13
TEM Co_3O_4 particle size / nm	8.2	11	7.8	10	7.0	11

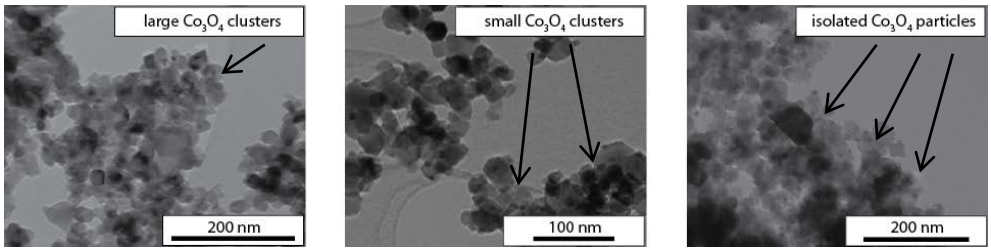

Figure 1: TEM images of IWI08S (left) showing strongly clustered supported Co_3O_4 particles, less clustered Co_3O_4 particles for IWI08F (center) and homogeneously distributed Co_3O_4 particles for DPA08 (right).

The performance of the catalysts was studied at 20 bar and 493 K and at similar CO conversion levels. (Table 2) For low and high metal loadings, the lowest cobalt time yields (CTY) were obtained for catalysts prepared by incipient wetness impregnation with subsequent static drying. Higher activities were found for catalysts prepared by incipient wetness impregnation with subsequent fluidized bed drying and even higher activities were determined for the catalysts prepared by deposition precipitation. These values correlate with the degree of cobalt oxide clustering prior to reduction and can be rationalized by a stronger tendency for particle growth during reduction in the case of the clustered catalysts as reported previously.[26] While for the static drying method, a higher cobalt time yield was found for higher metal loading, the opposite was the case for the catalysts prepared by fluidized bed drying. The C_{5+}-selectivities of all impregnated catalysts were similar between 83 and 85 wt.-%, while the results showed distinctly lower methane selectivities and higher C_{5+}-selectivities of 90 wt.-% for the DPA catalysts at very similar conversion levels, which has been reported before.[26]

Table 2: Results for Fischer-Tropsch synthesis at 493 K, 20 bar, H_2:CO v/v 2.0. Initial data for X_{CO}, S_{CH4} and, S_{C5+} and CTY after reaching synthesis conditions, final data after 200 h.

Catalyst	X_{CO} initial / %	X_{CO} final / %	CTY initial / 10^{-5} $mol_{CO}/(g_{Co}*s)$	CTY final / 10^{-5} $mol_{CO}/(g_{Co}*s)$	S_{CH4} / wt.-%	S_{C5+} / wt.-%
IWI08S	35.3	30.6	7.0	6.2	8	85
IWI16S	36.2	28.7	8.3	6.8	10	83
IWI08F	36.5	29.2	10.4	8.2	8	85
IWI16F	36.4	30.2	9.1	7.4	9	83
DPA08	36.1	30.7	11.2	9.0	6	90
DPA16	29.0	26.1	10.1	9.0	6	90

In order to obtain information on the cause of the activity loss of the catalysts, particle size analysis of the fresh and spent catalysts was carried out using electron microscopy. (Figure 2, Table 3) The results show that all catalysts with low cobalt loading show a significant extent of particle growth. For IWI08S, this can be rationalized by the short interparticle distances, while for IWI08F and DPA08 the low initial average particle sizes may be a driving factor for particle growth. Smaller increases of particle sizes were found

for the catalysts with higher metal loadings, presumably due to the higher initial particle sizes.

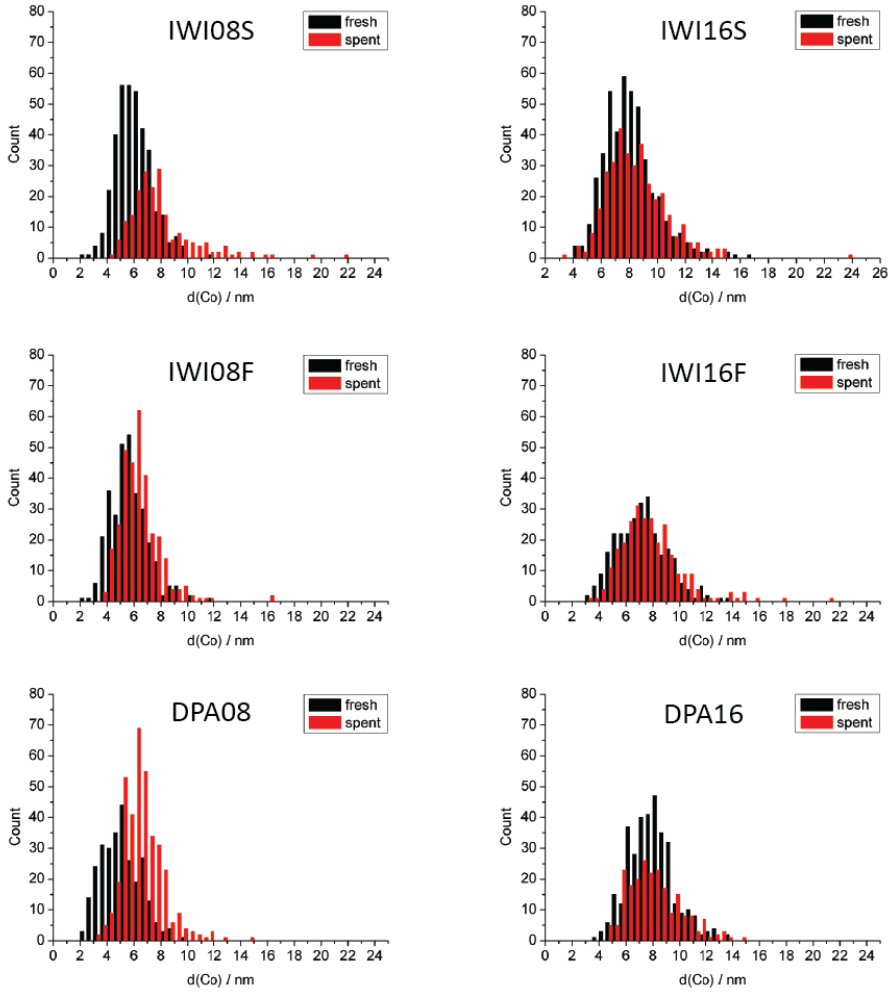

Figure 2: Histograms for TEM cobalt particle size analysis of fresh and spent catalysts.

Calculations of turnover frequencies for the beginning and for the end of the catalytic experiment were carried out based on the surface average TEM particle sizes. (Table 3) The results showed that for the catalysts with low cobalt loadings, no significant change in turnover frequencies were observed, indicating that particle growth explains the loss of activity quantitatively. This is in accordance with the literature listing a loss of active metal

surface area the most important factor in the deactivation of cobalt Fischer-Tropsch catalysts during the first hundreds of hours for cobalt Fischer-Tropsch catalysts in general[10,11] and Co/TiO_2 in particular. For catalysts with high metal loadings, somewhat lower turnover frequencies were obtained at the end-of-run. The higher values observed at the start for the highly loaded samples can either be attributed to average particle growth during reduction which was not taken into account in the calculations. Alternatively, the particle size of the fresh catalysts may be underestimated because TEM analysis might not be fully representative although large numbers of particles were measured. The reason for the TOF values reported here being lower than results previously reported[26] relates to the fact that the TOF in this work were calculated from TEM particle sizes rather than from hydrogen chemisorption uptake.

Table 3: Turnover frequencies (TOF) during Fischer-Tropsch synthesis at 493 K, 20 bar, H_2:CO 2.0 v/v, initial X_{CO} 35 % for the catalysts in the beginning of the catalytic testing experiment and after 200 h based on TEM surface average particle sizes of the fresh and spent catalysts.

Catalyst	d_{Co} fresh / nm	d_{Co} spent / nm	TOF initial / 10^{-3} s^{-1}	TOF final / 10^{-3} s^{-1}
IWI08S	6.1	7.9	24	24
IWI16S	8.3	8.5	39	34
IWI08F	5.7	6.4	33	30
IWI16F	7.3	7.8	37	33
DPA08	5.2	6.6	33	34
DPA16	8.0	8.1	43	37

To quantify the deactivation behavior over the timescale of the catalytic experiment, the activity curves based on H_2 conversion (Figure 3) were analyzed and fitted assuming 2^{nd} order deactivation kinetics (Figure 5).

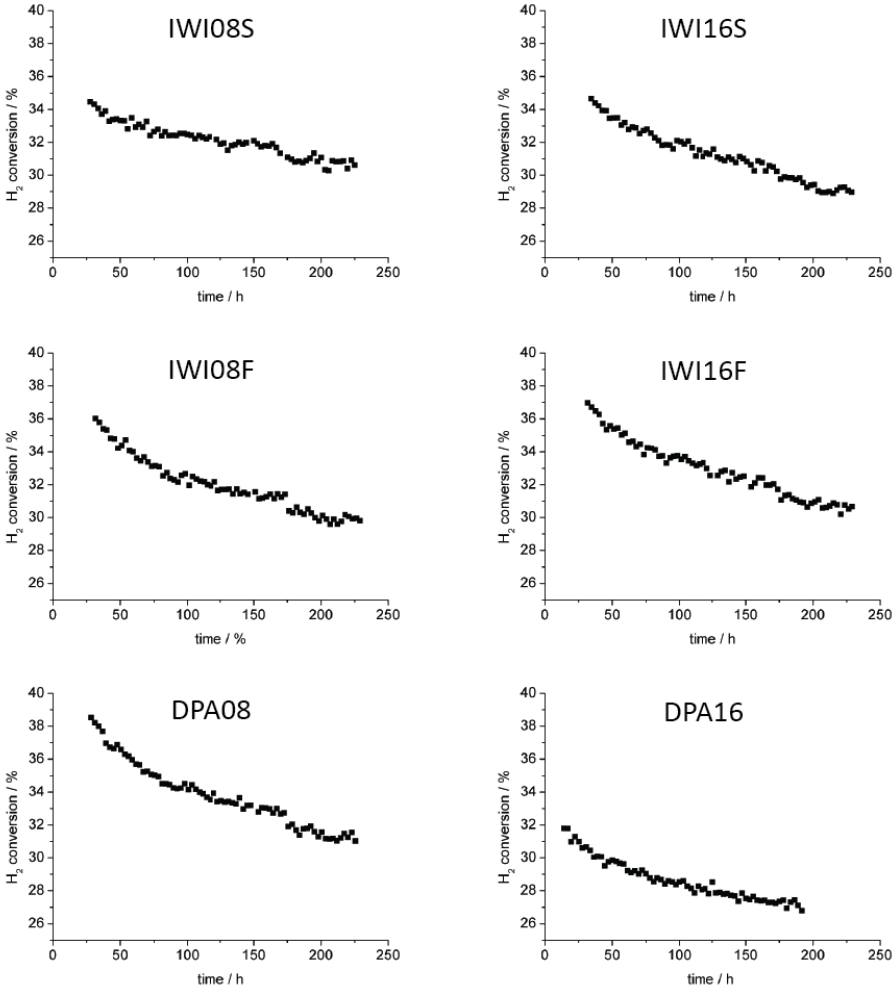

Figure 3: H_2 conversion curves during Fischer-Tropsch synthesis at 493 K, 20 bar, H_2:CO 2.0 v/v for catalysts tested at initial X_{CO} of 35 %.

Similar deactivation rates k_d were obtained for all catalysts, with only the values obtained for one impregnated catalyst with subsequent static drying being significantly lower. The

relative remaining activity for IWI08S and DPA16 are the highest obtained. The relative remaining activities for all other impregnated catalysts were similar. It should be noted that the ratio of final to initial CTY or WTY for all catalysts is similar and appears to be independent of the catalyst preparation method or the cobalt interparticle spacings of the systems studied in this research. (Table 4) The graphs of final CTY/WTY against initial CTY/WTY shows this point even more clearly.(Figure 4). The slope of the linear fit for WTY is about 0.8 in line with the loss of about 20% activity for most of the catalysts investigated for 200 h at 35% CO conversion.

Table 4: Fitting of deactivation curves during Fischer-Tropsch synthesis at 493 K, 20 bar, H_2:CO 2.0 v/v. Fitting is according to $1/(a_{norm}(t)) = k_d * t + 1$.

Catalyst	k_d / 10^{-4} h^{-1}	R^2	CTY_{final}/ $CTY_{initial}$
IWI08S	5.9	0.99	0.89
IWI16S	11.1	0.99	0.82
IWI08F	12.8	0.99	0.79
IWI16F	11.5	0.99	0.81
DPA08	13.4	0.99	0.80
DPA16	10.8	0.99	0.89

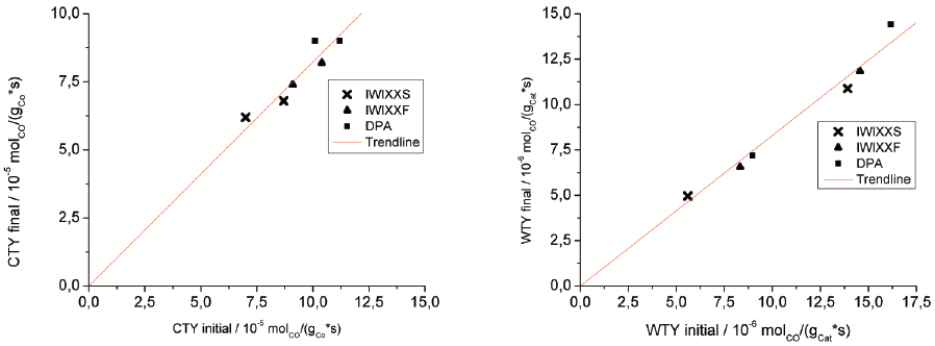

Figure 4: Final (after 200 h) against initial CTY and WTY during Fischer-Tropsch synthesis at 493 K, 20 bar, H_2/CO 2.0 v/v for all catalysts studied at initial X_{CO} 35 %. Linear fit with zero intercept; the slopes of the lines are 0.82 and 0.83 respectively.

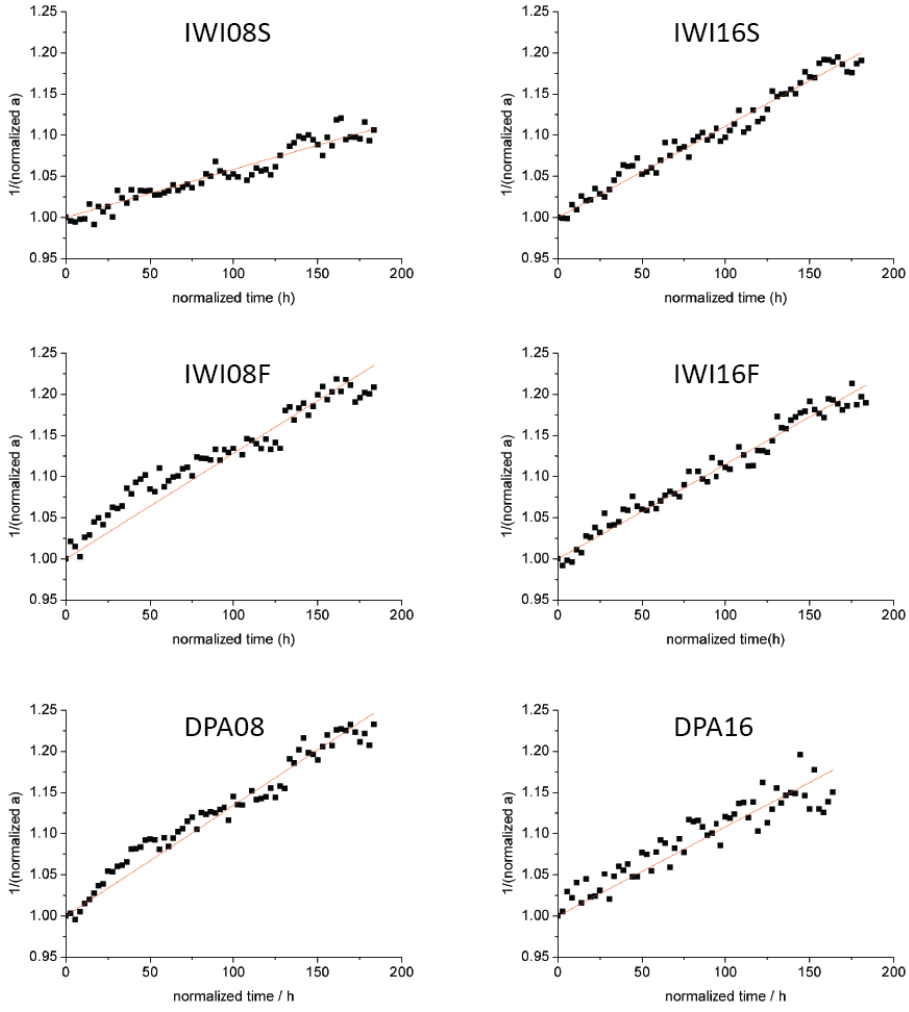

Figure 6: Fitted data sets for normalized activities as a function of time, Fischer-Tropsch synthesis at 493 K, 20 bar, H_2/CO 2.0 v/v, initial X_{CO} ~35 %. Fitting is according to $1/(a_{norm}(t)) = k_d * t + 1$.

Two catalysts were tested at lower GHSV in order to study the effect of higher conversions (Figure 6) on the activities and deactivation behavior. TEM histogram analysis of the spent catalysts revealed that average particle growth took place to a higher extent at higher conversions (Figure 7), which can be explained with higher water partial pressures in the reactors.[16] A look at the initial and final TOF frequencies (Table 5) shows that the loss in activity can mostly be attributed to average particle growth. Interestingly, the final turnover frequencies at high CO conversion levels of IWI16S are slightly higher and distinctly higher for DPA16 compared to the values obtained at lower CO conversion levels. This can be explained by the autocatalytic effect of water that has previously been demonstrated to have a positive effect on reaction rates of Co/TiO_2 catalysts.[31]

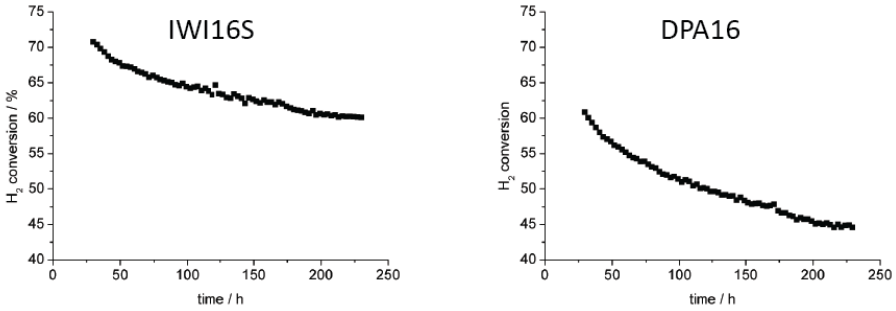

Figure 6: H_2 conversion curves during Fischer-Tropsch synthesis at 493 K, 20 bar, H_2:CO 2.0 v/v for catalysts tested at higher conversions.

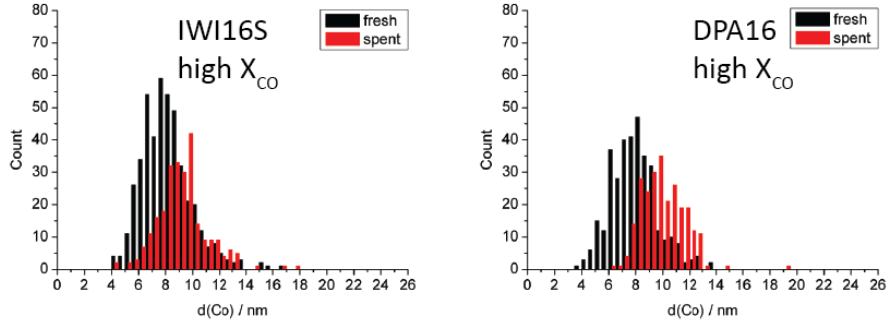

Figure 7: Histograms for TEM cobalt particle size analysis of fresh and spent catalysts tested at high X_{CO}.

Table 5: Turnover frequencies (TOF) during Fischer-Tropsch synthesis at 493 K, 20 bar, H_2:CO 2.0 v/v, different initial X_{CO} for the catalysts in the beginning of the catalytic testing experiment and after 200 h based on TEM surface average particle sizes of the fresh and spent catalysts.

Catalyst	X_{CO} initial / %	d_{Co} fresh / nm	d_{Co} spent / nm	TOF initial / 10^{-3} s^{-1}	TOF final / 10^{-3} s^{-1}
IWI16S	36.2	8.3	8.5	39	34
IWI16S	70.4	8.3	9.4	39	42
DPA16	29.0	8.0	8.1	43	37
DPA16	61.4	8.0	10.1	52	52

A look at the deactivation curves of catalysts tested at lower GHSV (Figure 9) showed higher deactivation rate constants for IWI16S and lower remaining activities in the end of the catalytic testing experiment for DPA16 (Table 6). These results indicate that higher water partial pressures enhance deactivation by particle growth as suggested previously.[16]

Table 6: Fitting of deactivation curves during Fischer-Tropsch synthesis at 493 K, 20 bar, H_2:CO 2.0 v/v. Fitting is according to $1/(a_{norm}(t)) = k_d * t + 1$.

Catalyst	X_{CO} initial / %	k_d / 10^{-4} h^{-1}	R^2	CTY_{final}/ $CTY_{initial}$
IWI16S	36.2	11.1	0.99	0.82
IWI16S	70.4	15.1	0.99	0.78
DPA16	29.0	10.8	0.99	0.89
DPA16	61.4	24.7	0.99	0.72

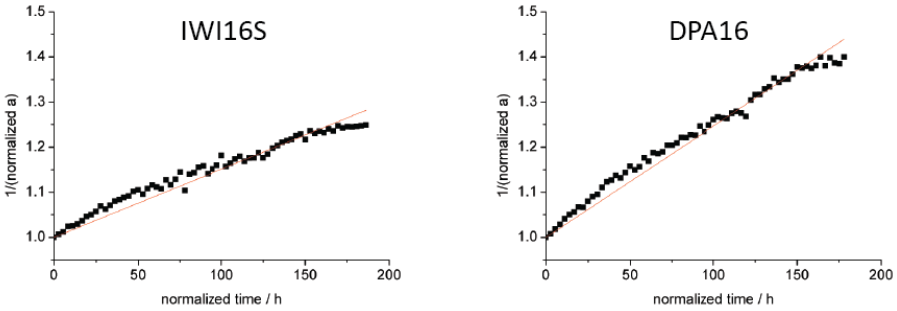

Figure 9: Fitted data sets for normalized activities as a function of time, Fischer-Tropsch synthesis at 493 K, 20 bar, H_2:CO 2.0 v/v. Fitting is according to $1/(a_{norm}(t)) = k_d * t + 1$.

Conclusions and outlook

The results show that the catalyst preparation method has a strong impact on the cobalt distribution on the titania support material. It was demonstrated that fluidized bed drying leads to more uniform cobalt distributions compared to conventional static drying, while the use of deposition precipitation led to even largely homogeneous cobalt distributions. Results from Fischer-Tropsch synthesis at 493 K and 20 bar revealed higher activities for systems with more uniform distribution of cobalt, which can be rationalized with the higher accessible cobalt surface area during Fischer-Tropsch synthesis. The C_{5+}-selectivity was not found to be affected by differences in cobalt distribution for the impregnated catalysts, but superior selectivities were found for the systems prepared by deposition precipitation as has been shown earlier.[26] Catalytic testing experiments for 200 h showed that all catalysts lose about 20% of their activity likely due to average particle growth, as was shown by TEM analysis of the fresh and spent catalysts and turnover frequency calculations. Constant turnover frequencies calculated for the catalysts with low metal loadings suggest that the loss in activity can be completely attributed to a loss of cobalt surface area, which is in accordance with results reported elsewhere.[17] The deactivation curves for catalysts at similar CO conversion levels showed that the relative loss in activity is comparable for all catalysts studied in this research and that the cobalt distribution over the support surface does not seem to play a crucial role in the particle growth mechanism, unlike previously shown for Co/SiO_2 Fischer-Tropsch catalysts[22] or other catalytic systems.[21] Catalytic testing of two catalysts at elevated CO conversion levels showed that the deactivation proceeded faster, e.g. higher deactivation rate constants and a higher relative activity loss were observed for IWI16S and DPA16. Also in this case, the loss in activity was found to correlate well with the loss of cobalt surface area during Fischer-Tropsch synthesis. In-situ X-ray spectroscopy[32] might be able to give more insight into the reasons of deactivation for these catalysts in the future. In order to study the mechanism of particle growth, e.g. Ostwald ripening or migration and coalescence and (quasi)-*in-situ* electron microscopy techniques[33] can be applied in order to obtain further insights.

Acknowledgements

We gratefully acknowledge Shell Global Solutions for financial support. We also thank Johan den Breejen, Heiko Oosterbeek and Sander van Bavel for fruitful discussions and Rien van Zwienen for technical assistance on high pressure catalytic testing. KPdJ acknowledges support from NWO-TOP, NRSCC and an ERC Advanced Grant.

References

[1] M.E. Dry, J. Chem. Technol. Biotechnol. 77 (2002) 43–50.

[2] M.E. Dry, Catal. Today. 71 (2002) 227–241.

[3] O.P.R. van Vliet, A.P.C. Faaij, W.C. Turkenburg, Energy Convers. Manag. 50 (2009) 855–876.

[4] G. Haarlemmer, G. Boissonnet, E. Peduzzi, P.-A. Setier, Energy. 66 (2014) 667–676.

[5] R. Zennaro, Fischer – Tropsch Process Economics, in: P.M. Maitlis, A. de Klerk (Eds.), Greener Fischer-Tropsch Pro, Wiley-VCH, 2013: pp. 149–169.

[6] E.B. Fox, Z.-T.Z.-W. Liu, Z.-T.Z.-W. Liu, Energy & Fuels. 27 (2013) 6335–6338.

[7] A. de Klerk, Y.-W. Li, R. Zennaro, Fischer – Tropsch Technology, in: P.M. Maitlis, A. de Klerk (Eds.), Greener Fischer-Tropsch Process. Fuels Feestocks, Wiley-VCH, 2013: pp. 53–79.

[8] A.Y. Khodakov, W. Chu, P. Fongarland, Chem. Rev. 107 (2007) 1692–1744.

[9] S.T. Sie, R. Krishna, Appl. Catal. A Gen. 186 (1999) 55–70.

[10] N.E. Tsakoumis, M. Rønning, Ø. Borg, E. Rytter, A. Holmen, Catal. Today. 154 (2010) 162–182.

[11] A.M. Saib, D.J. Moodley, I.M. Ciobîcă, M.M. Hauman, B.H. Sigwebela, C.J. Weststrate, J.W. Niemantsverdriet, J. van de Loosdrecht, Catal. Today. 154 (2010) 271–282.

[12] J. van de Loosdrecht, B. Balzhinimaev, J.-A. Dalmon, J.W. Niemantsverdriet, S.V. Tsybulya, A.M. Saib, P.J. van Berge, J.L. Visagie, Catal. Today. 123 (2007) 293–302.

[13] K. Aasberg-Petersen, I. Dybkjær, C.V. Ovesen, N.C. Schjødt, J. Sehested, S.G. Thomsen, J. Nat. Gas Sci. Eng. 3 (2011) 423–459.

[14] N.E. Tsakoumis, R. Dehghan-Niri, M. Rønning, J.C. Walmsley, Ø. Borg, E. Rytter, A. Holmen, Appl. Catal. A Gen. 479 (2014) 59–69.

[15] M.D. Argyle, T.S. Frost, C.H. Bartholomew, Top. Catal. 57 (2013) 415–429.

[16] G.L. Bezemer, T.J. Remans, A.P. van Bavel, A.I. Dugulan, J. Am. Chem. Soc. 132 (2010) 8540–1.

[17] S.L. Soled, G. Kiss, C. Kliewer, J. Baumgartner, E.-M. El-Malki, Learnings from Co Fischer-Tropsch catalyst studies, in: ACS Natl. Meet. Expo. New Orleans, 2013.

[18] J.A. Moulijn, A.E. van Diepen, F. Kapteijn, Appl. Catal. A Gen. 212 (2001) 3–16.

[19] B.H. Davis, Cobalt FT Catalysts, in: P.M. Maitlis, A. de Klerk (Eds.), Greener Fischer-Tropsch Process. Fuels Feestocks, First edit, 2013: pp. 193–207.

[20] M. Sadeqzadeh, S. Chambrey, S. Piché, P. Fongarland, F. Luck, D. Curulla-Ferré, D. Schweich, J. Bousquet, A.Y. Khodakov, Catal. Today. (2013).

[21] G. Prieto, J. Zečević, H. Friedrich, K.P. de Jong, P.E. de Jongh, Nat. Mater. 12 (2013) 34–9.

[22] P. Munnik, P.E. de Jongh, K.P. de Jong, J. Am. Chem. Soc. 136 (2014) 7333–40.

[23] T.M. Eggenhuisen, H. Friedrich, F. Nudelman, J. Zečevic, N.A.J.M. Sommerdijk, P.E. de Jongh, K.P. de Jong, Chem. Mater. 25 (2013) 890–896.

[24] T.O. Eschemann, W.S. Lamme, R.R. Manchester, T.E. Parmentier, A. Cognigni, M. Ronning, J Catal. 328 (2015) 130–138.

[25] P. Munnik, N.A. Krans, P.E. de Jongh, K.P. de Jong, ACS Catal. 4 (2014) 3219–3226.

[26] T.O. Eschemann, J.H. Bitter, K.P. de Jong, Catal. Today. 228 (2014) 89–95.

[27] K.P. de Jong, Deposition Precipitation, in: K.P. de Jong (Ed.), Synth. Solid Catal., Wiley-VCH, Weinheim, 2009: pp. 111–132.

[28] M.K. van der Lee, A.J. van Dillen, J.H. Bitter, K.P. de Jong, J. Am. Chem. Soc. 127 (2005) 13573–13582.

[29] C.M. Lok, EP 1 542 794, 2010.

[30] C.M. Lok, US 7,851,404, 2010.

[31] E. Iglesia, Appl. Catal. A Gen. 161 (1997) 59–78.

[32] K.H. Cats, I.D. Gonzalez-Jimenez, Y. Liu, J. Nelson, D. van Campen, F. Meirer, A.M.J. van der Eerden, F.M.F. de Groot, J.C. Andrews, B.M. Weckhuysen, Chem. Commun. (Camb). 49 (2013) 4622–4.

[33] T.W. Hansen, A.T. Delariva, S.R. Challa, A.K. Datye, Acc. Chem. Res. 46 (2013) 1720–30.

Chapter 4

Effects of noble metal promotion for Co/TiO_2 Fischer-Tropsch catalysts

Abstract: We report on the preparation of noble metal (Ag, Pt, Re, Ru) promoted Co/TiO_2 catalysts (~9 wt.- Co) with different atomic ratios of promoter to cobalt (0, 0.0035, 0.0070, 0.0140) by co-impregnation and subsequent fluidized bed drying. Initial cobalt oxide dispersions were found to be similar for all catalysts studied (TEM, XRD). Temperature-programmed reduction showed that all noble metal promoters shift the reduction of cobalt oxide to lower temperatures, an effect that was found to increase in the order Re < Ag < Ru < Pt and with increasing noble metal to cobalt ratios. All promoters were found to increase the activity of the catalysts during Fischer-Tropsch (FT) synthesis at 30 % CO conversion, which can be attributed to an increase in apparent turnover frequencies for all catalysts and additionally increased cobalt metal dispersions for Re-promoted catalysts. Interestingly and in contrast to previous studies on particle size effects, no decrease in turnover frequency was observed for highly dispersed Re-promoted Co/TiO_2 catalysts. *In-situ* XRD also indicated the formation of more active *hcp* cobalt species for a Ag-promoted catalyst. Turnover frequencies were found to be highest for low and medium promoter to cobalt ratios for Ag and Pt-promoted catalysts, while turnover frequencies were found to monotonically increase with increasing promoter to cobalt ratios for Ru and Re-promoted catalysts. For Re and Ag-promoted catalysts increased C_{5+} selectivities were found for all promoter loadings, for Ru-promoted catalysts the C_{5+} selectivity was found to increase with increasing promoter loadings. The addition of Pt led to decreased C_{5+} selectivities. Recent theoretical studies have indicated that the activity of Co for FT can be enhanced by increasing their hydrogenation activity in line with the present work.

Introduction

The Fischer-Tropsch reaction involves the conversion of synthesis gas to higher hydrocarbons, which can then further be converted to ultraclean fuels or chemicals. While the synthesis gas can be derived from biomass, coal, or natural gas, the latter is the most economical option given current market prices and the availability of stranded gas and shale gas reserves. A crucial aspect for the economic viability for Fischer-Tropsch plants lies in the performance of the catalyst.[1,2] Because of their low watergas-shift activity, their high selectivity to higher hydrocarbons, and their stability, supported cobalt catalysts are preferred for plants processing synthesis gas derived from natural gas.[3–7] Supported cobalt catalysts used in industrial applications typically do not only contain 15-30 wt.% of catalytically active cobalt, but also 1-10 wt.-% of metal oxides[8–11] and 0.1-1 wt.-% of noble metals[8,12] in order to improve the activity, selectivity and stability of the catalysts.[13]

While oxidic promoters are mainly used in order to ensure high selectivities to heavy products,[8,12] noble metals are used to either improve the degree of reduction or the dispersion of supported cobalt catalysts. The addition of noble metals can shift the temperature needed to reduce cobalt oxide to metallic cobalt to distinctly lower temperatures, but its effect on the degree of reduction has been reported to be rather minor. Instead, the improved activity of noble metal promoted cobalt catalysts has been mainly attributed to higher cobalt dispersions,[12,14–17] synergistic effects in the case of bimetallic particles,[12,18–20] or the suppression of cobalt-support compound formation.[12]

The activity of Fischer-Tropsch reaction has been found to linearly increase with the available metallic cobalt surface area, given constant turnover frequencies (TOF).[19] This holds for catalysts with cobalt particles above a critical size of ~6 nm, below which the TOF drops sharply.[21–23] Above this critical size, the TOF has also been found to be independent of the support material used and noble metals present.[12,16,19]

An exception on constant TOF has been reported earlier for the case of Ru-promoted Co/TiO_2 catalysts showing a threefold higher surface-specific activity than unpromoted catalysts.[18] Similar results have also been found for Pt-promoted Co/Nb_2O_5 catalysts.[24] While in most cases studies on the impact of noble metal promotion on TOF

were performed on Al_2O_3-supported catalysts, the support materials in the examples described above are reducible oxides that show strong metal support interactions towards group 8-10 metals, making them fundamentally different from other support materials typically used in Fischer-Tropsch catalyst preparation.[25–27]

Here we report on the structural and catalytic properties of noble metal promoted Co/TiO_2 catalysts prepared by co-impregnation with subsequent fluidized bed drying and heat treatment. Some of the most relevant noble metal promoters Ag, Pt, Ru, and Re were added in different atomic ratios. The heat-treated catalysts are characterized by TEM, XRD and TPR in order to obtain information on initial cobalt oxide dispersions and reducibility of the catalysts. Catalytic testing is carried out under industrial conditions in order to study the impact of noble metal addition on the catalytic properties. The spent catalysts are analyzed by TEM in order to calculate TOF during Fischer-Tropsch synthesis to answer the question whether the addition of noble metal promoters to cobalt supported on titania generally leads to higher intrinsic activity compared to unpromoted catalysts. In-situ XRD studies are carried out in order to investigate whether the addition of noble metal promoters also influences the metallic cobalt phase formed during reduction, eventually determining the activity and selectivity during Fischer-Tropsch synthesis.

Materials and methods

Catalyst synthesis

Noble metal promoted Co/TiO_2 catalysts were prepared by co-impregnation. Therefore, TiO_2 (Aeroxide P25, Evonik Degussa, pore volume 0.3 mL/g, BET surface area 50 m^2/g, 70 % anatase, 30 % rutile) was pre-sieved to 75-150 µm and dried under vacuum, before the support material was impregnated with an aqueous solution containing $Co(NO_3)_2{\cdot}6H_2O$ (4M, Sigma-Aldrich, 99.99%) and one of the noble metal precursors $HRe(OH)_4$ (Sigma-Aldrich, 99.99%), $Ru(NO)(NO_3)_3$ (Sigma-Aldrich, 98.2%), $[(NH_3)_4Pt](NO_3)_2$ (Sigma-Aldrich, 99.995%) or $AgNO_3$ (Sigma-Aldrich, 99%) in concentrations to achieve atomic noble metal to cobalt ratios of 0.0035, 0.0070 and 0.0140. After that, the material was dried in a fluidized bed under a flow of N_2 at 353 K, before the heat treatment was carried out at 523 K (2 h, 2 K/min) in a fluidized bed under a flow of N_2. These catalysts are labeled Co XX NM YY, NM being the noble metal used, XX the cobalt weight loading (typically 9 wt.-%

assuming Co to be in the form of Co_3O_4) and YY the noble metal weight loading (0.05 to 0.39 wt.-%). Unpromoted Co/TiO_2 catalysts were prepared analogously with a solution of $Co(NO_3)_2 \cdot 6H_2O$ (4M, Sigma-Aldrich, 99.99%) and are labeled Co XX.

Catalyst characterization

X-ray powder diffraction (XRD) was performed on a Bruker D2 Phaser with a Co K_α (λ = 1.789Å) source. Co_3O_4 crystallite size estimation was performed using the Co_3O_4 peak at 37° 2Θ with an automatic calculation routine in DiffracEvaluation V2.0 software by Bruker, which is based on the Debye-Scherrer-equation. Equivalent cobalt particle sizes are calculated from observed Co_3O_4 particle sizes by using the relation $d(Co)=d(Co_3O_4) * 0.75$. Spent catalysts were found to be metallic cobalt covered with a thin wax layer, therefore no correction factor was applied.

For Transmission Electron Microscopy (TEM), the heat-treated catalysts were ground with a mortar, suspended in ethanol using an ultrasonic bath and dropped onto a copper grid with holey carbon film. Spent catalysts were prepared in the same way. The samples were analyzed using a Tecnai T12/ Tecnai T20 microscope, with electron beam voltage of 120 kV, 200 kV, respectively. Equivalent cobalt particle sizes are calculated from observed Co_3O_4 particle sizes by using the relation $d(Co)=d(Co_3O_4) * 0.75$.

Temperature-programmed reduction (TPR) was carried out using a Micromeritics Autochem II ASAP 2920. Typically, 50 mg of the sample were dried in a flow of Ar at 373 K for 1 h and then reduced in a 50 NmL/min flow of H_2/Ar (1:19 v/v) at a temperature ramp of 5 K/min.

In-situ X-ray powder diffraction studies were carried out on a Bruker D8 Phaser with a Co K_α (λ = 1.789Å) source and equipped with an Anton Paar XRK reaction chamber. Typically 50 mg of the powdered catalysts were dried under a flow of He and then reduced under a flow of H_2/He 1:3 v/v at 623 K (2 h, ramp 1 K/min).

Catalytic testing

Fischer-Tropsch synthesis was carried out in a 16 reactor catalytic testing setup (Flowrence, Avantium). The catalysts (75-150 μm) were diluted with SiC (200 μm) to a total bed volume of 200 μL in order to obtain desired CO conversion levels of 30 %. The catalysts were dried in a flow of He for 2 h and then reduced in-situ in a flow of H_2/He (1:3 v/v) at 623 K (8 h, ramp 1 K/min). Subsequently, the reactors were cooled to 453 K and pressurized to 20 bar under a flow of H_2. After switching to H_2/CO (2:1 v/v) the temperature was increased to 493 K (1 K/min). In the end of the experiment, most of the products remaining in the catalyst bed were removed under a flow of H_2 at 473 K, before the setup was cooled down to room temperature under a flow of He. The products were analyzed using online gas chromatography (Agilent 7890A), the permanent gases were separated on a Shincarbon column and quantified against He as an internal standard using a TCD detector. CO conversions were calculated as

$$X_{CO} = (mol_{CO\ in}\text{-}mol_{CO\ out})/mol_{CO\ in} \quad (1)$$

Hydrocarbons (C1-C9) were separated on a PPQ column, detected using an FID detector and quantified against the TCD signal of the internal standard He. Selectivities to the lower hydrocarbon fractions S_{CX} were calculated from converted CO and the corresponding yields as

$$S_{CX} = Y_{CX}/(mol_{CO\ in}\text{-}mol_{CO\ out}) \quad (2)$$

The selectivities to products with 5 and more carbon atoms are calculated from the yields to lower hydrocarbons as

$$S_{C5+} = 1 - S_{C1\text{-}C4} \quad (3)$$

CO conversion levels during the experiments were between 25 and 35 %. Activities are reported as cobalt time yields (CTY, $mol_{CO}/(g_{Co}\cdot s)$) and weight time yields (WTY, $mol_{CO}/(g_{Cat}\cdot s)$). Turnover frequencies were calculated from TEM surface average particle sizes assuming spherical geometries and a surface area of one cobalt atom of 0.0628 nm^2.[21]

Results and discussion

The particle size analysis of the heat-treated catalyst precursors was carried out using TEM and XRD. (Figure 1) The results showed very similar initial particle sizes of 4 to 7 nm for all promoted catalysts. Deviations between the measurement techniques can be explained by the fact of XRD analyzing crystallite sizes rather than particle sizes and being a bulk technique instead of a local imaging technique as TEM. For the unpromoted catalyst similarly sized cobalt oxide particle sizes were determined.

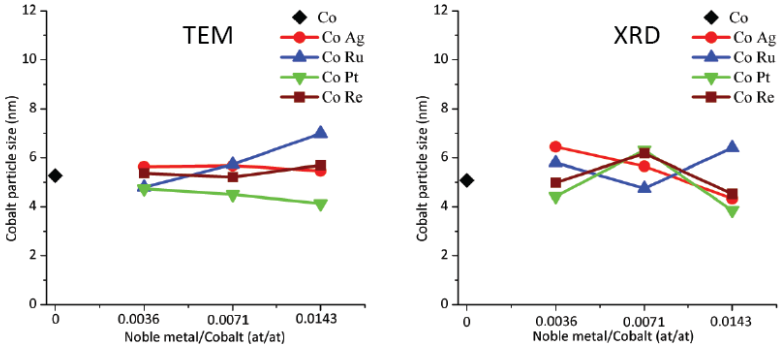

Figure 1: Surface average equivalent cobalt particle sizes derived from TEM (left) and equivalent cobalt crystallite sizes derived from XRD line broadening analysis of the Co_3O_4 peak at 37° 2θ (right) of the heat-treated catalysts.

TEM imaging of the catalysts (Figure 2) also revealed well-distributed supported cobalt oxide particles for unpromoted and promoted catalysts, which is in line with results previously reported.[28] From TEM imaging no clear statement can be made on whether the cobalt oxide particles are doped with the noble metal promoters or whether the metals are present separately on the support material.

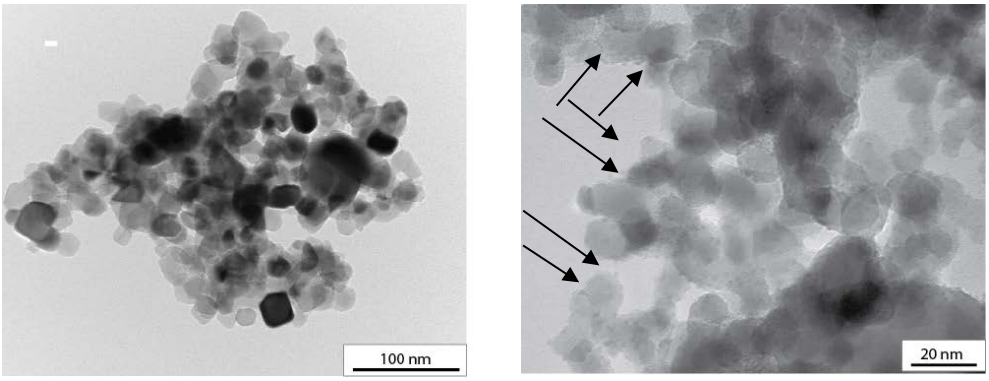

Figure 2: TEM images of the unloaded TiO_2 P25 support material (left), and the TiO_2-supported Co catalyst, sample Co8.8Ag0.23 (right). Note the sharp edged titania support particles in the left, and the more rounded off shape of the supported cobalt oxide particles in the right image. The arrows indicate the position of a few supported cobalt oxide particles.

The reduction behavior of the promoted and unpromoted catalysts was studied using TPR. (Figure 3) The TPR results of the unpromoted Co/TiO_2 catalysts showed the typical two-step reduction pattern of Co_3O_4 to CoO (centered at 530 K) and CoO to Co (670 K). The use of Ag as a promoter was found to lead to a shift of both reduction peaks to lower temperatures, which was more pronounced in case of higher Ag loadings (500 K and 600 K for the highest Ag loading), a trend previously reported for Ag-promoted Co/Al_2O_3 catalysts.[17] Promotion with different amounts of Pt led shifts of the reduction peaks to even lower temperatures (430 K and 530 K for the highest Pt loading). It could be noted that already the lowest amount of Pt added led to a strong shift of the reduction peaks to lower temperatures (450 K and 560 K), while the further shift with increasing Pt loadings was found to be less significant. These findings are in line with observations for Pt-promoted Co/Al_2O_3 catalysts previously reported.[16,17] Ru promotion also led to shifts in reduction temperature for both reduction steps. Largest shifts were found for the highest promoter loadings (450 K and 560 K). For Re-promoted catalysts the first reduction peak was not affected for low and medium promoter loadings, while a shift to higher temperatures was observed for high Re loadings, an effect that has previously been

attributed to the high reduction temperature of ReO_2 for the case of promoted Co/Al_2O_3 catalysts.[16] Only the second reduction peak was found to shift significantly to lower temperatures (620 K) As the initial cobalt oxide particle sizes were comparable for all catalysts, it can be assumed that all differences observed in the TPR patterns are due to the presence of the noble metal promoters and not dispersion effects.[29] A quantification of the TPR measurements in order to calculate the degree of reduction was not done because of the possibility of SMSI effects and its associated contribution to the TCD signal.[30]

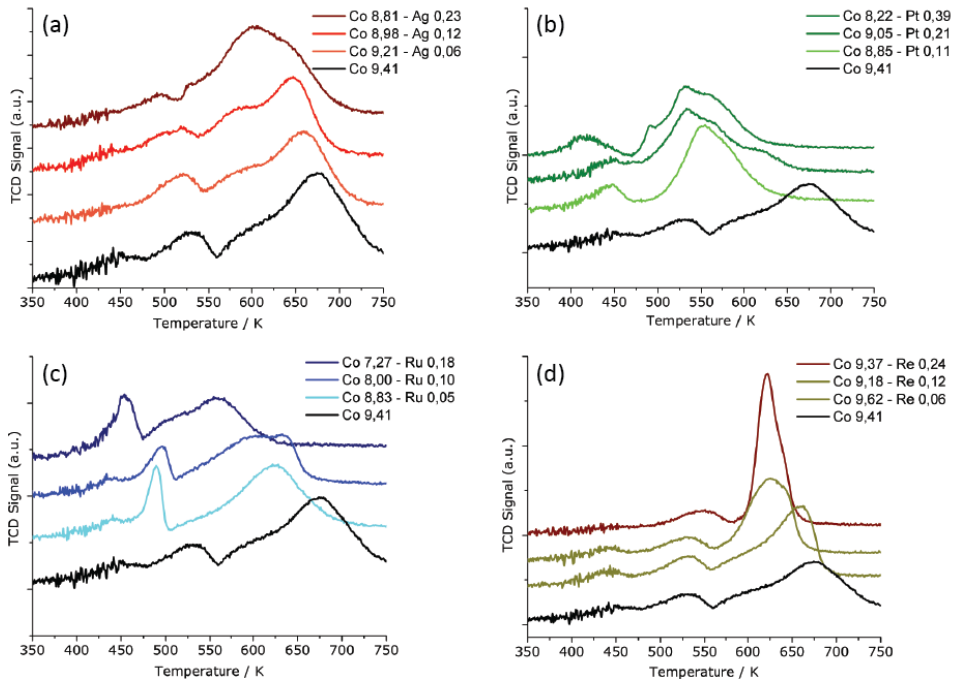

Figure 3: TPR profiles for Ag-promoted (a), Pt-promoted (b), Ru-promoted and Re-promoted (d) Co/TiO_2 catalysts. For comparison the TPR profile of an unpromoted catalyst is given in black. The legends in all graphs provide the cobalt and noble metal loadings in wt.-%.

Table 1: Catalytic performance of unpromoted and promoted Co/TiO_2 catalysts after 60 h of Fischer-Tropsch synthesis at 493 K, 20 bar, H_2/CO 2.0 v/v.

	Catalyst	X_{CO} / %	CTY / 10^{-5} $mol_{CO}/(g_{Co}*s)$	S_{CH4} / wt.-%	S_{C5+} / wt.-%
	Co 9.4	29.2	6.9	6.3	85
Ag-promoted	Co 9.2 Ag 0.06	30.3	10.0	6.5	89
	Co 9.0 Ag 0.12	33.9	11.9	6.4	89
	Co 8.8 Ag 0.26	33.1	10.5	7.0	87
Pt-promoted	Co 8.9 Pt 0.11	30.4	10.8	7.6	83
	Co 9.1 Pt 0.21	30.0	16.8	8.3	84
	Co 8.2 Pt 0.39	34.2	13.5	7.3	83
Ru-promoted	Co 8.8 Ru 0.05	26.4	7.2	6.9	82
	Co 8.0 Ru 0.10	30.3	14.5	9.3	84
	Co 7.3 Ru 0.18	31.8	13.5	7.0	88
Re-promoted	Co 9.6 Re 0.06	30.9	20.0	6.2	90
	Co 9.2 Re 0.13	26.7	18.6	6.7	88
	Co 9.4 Re 0.25	33.1	21.5	7.0	88

Fischer-Tropsch synthesis was carried out at 20 bar, 493 K and at very similar CO conversion levels. The results (Table 1) showed a cobalt time yield of 6.9 10^{-5} $mol_{CO}/(g_{Co}*s)$ and a C_{5+}-selectivity of 85 wt.-% for the unpromoted catalyst that are in good accordance with results published earlier.[31,32] The addition of Ag was also found to increase both activities (10-12 10^{-5} $mol_{CO}/(g_{Co}*s)$) and the C_{5+} selectivity significantly to 87-89 wt.-%. An increase of CTY was also found for the catalysts promoted with Pt, with an optimum found

for the addition of 0.21 wt.-% Pt. This activity gain was accompanied by decreased C_{5+} selectivities of only 82-84 wt.-% that can partly be attributed to the hydrogenolysis and methanation activity of Pt. The addition of Ru also resulted in an increased activity, most pronounced for the addition of 0.10 wt.-% Ru. Higher amounts of Ru were found to lead to higher C_{5+} selectivities. The addition of Re led to the most significant improvements in CTY and C_{5+} selectivity, comparable for all amounts of Re added.

Table 2: Equivalent cobalt particle sizes of the fresh and spent unpromoted and promoted Co/TiO_2 catalysts and TOF after 60 h of Fischer-Tropsch synthesis at 493 K, 20 bar, H_2/CO 2.0 v/v.

	Catalyst	d_{fresh} / nm	d_{spent} / nm	CTY / 10^{-5} $mol_{CO}/(g_{Co}*s)$	TOF_{spent} / s^{-1}
	Co 9.4	5.3	8.6	7.1	0.024
Ag-promoted	Co 9.2 Ag 0.06	5.6	11.8	10.0	0.066
	Co 9.0 Ag 0.12	5.7	10.3	11.9	0.068
	Co 8.8 Ag 0.26	5.8	10.1	10.5	0.059
Pt-promoted	Co 8.9 Pt 0.11	4.7	8.1	10.8	0.048
	Co 9.1 Pt 0.21	4.5	6.5	16.8	0.061
	Co 8.2 Pt 0.39	4.1	7.9	13.5	0.057
Ru-promoted	Co 8.8 Ru 0.05	5.5	8.1	7.2	0.032
	Co 8.0 Ru 0.10	5.7	10.5	14.5	0.084
	Co 7.3 Ru 0.18	7.0	7.8	13.5	0.057
Re-promoted	Co 9.6 Re 0.06	5.4	3.7	20.0	0.041
	Co 9.2 Re 0.13	5.2	3.7	18.6	0.039
	Co 9.4 Re 0.25	5.7	4.9	21.5	0.058

In order to study the reasons for the different activities, the cobalt particle sizes of the spent catalysts were determined by TEM in order to calculate turnover frequencies. (Table 2) For the unpromoted catalysts, increased cobalt particle sizes were found after the catalytic testing and the TOF was in the expected range. For all catalysts promoted with Ag, bigger cobalt particles were found in the spent catalysts. While the effect of increasing cobalt dispersions is discussed for various noble metals,[12,13] we only measure higher metal dispersions for Re-promoted catalysts. (Table 2, Figure 4) The TOF of the catalysts promoted by Pt, Ru or Re were determined to be a factor of 2 higher than the TOF of the unpromoted catalyst, however, no strong influence of Ag was found. Pt promoted catalysts showed less average particle growth and TOF slightly lower than those of the Ag promoted catalysts. Neither CTY nor TOF of the Ag promoted catalysts were found to depend strongly on the promoter loading. Pt promoted catalysts showed increasing activities and TOF with increasing promoter loading initially, with lower values obtained for higher amounts of Pt. The cobalt particle sizes of the Ru promoted catalysts were found to be comparable with the other catalysts, but as for the CTY, a strong dependency of the amount of Ru added on the TOF was found. A medium Ru loading of 0.10 wt.-% led to a threefold TOF increase compared to the unpromoted catalyst. For the catalysts promoted with Re, cobalt particle sizes were found to be lower than the initial equivalent cobalt particle sizes, which can be rationalized with the role of Re being a well-known dispersion enhancing noble metal promoter.[12] The TOF determined for these catalysts were around 0.04 s^{-1} for low and medium Re amounts and 0.06 s^{-1} for higher amounts of Re. These results suggest that for titania-supported cobalt catalysts a distinct increase in TOF can be observed upon the introduction of noble metal promoters, which is not observed for the addition of noble metal promoters on irreducible support materials.[18] It should be noted that possible differences in the degree of reduction were not considered in these calculations, although it has previously been reported that the effect of noble metal promotion on the degree of reduction is relatively small for Co/TiO_2 catalysts.[16,32–35]

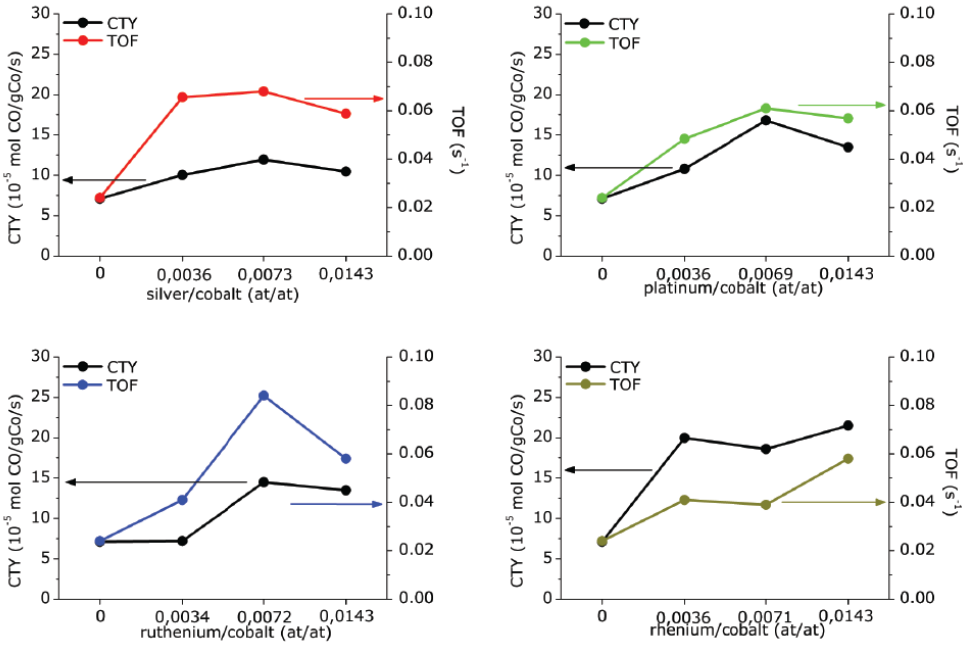

Figure 4: TOF based on surface average TEM particle sizes of spent catalysts and CTY during Fischer-Tropsch synthesis at 493 K, 20 bar, H_2/CO 2.0 v/v for unpromoted and promoted catalysts.

In order to obtain more information on the enhanced intrinsic activities of the promoted catalysts, *in-situ* XRD studies were carried out, mimicking the reduction of the catalysts. (Figure 5) The results revealed that for both unpromoted and promoted catalysts CoO was detected at 500 K. The CoO diffraction line disappeared at 623 K, while diffraction lines of metallic cobalt were found at this temperature. While for the unpromoted catalyst the peak was found to be at the expected diffraction angle for *fcc* Co, the peak was found to be broadened for the Ag-promoted catalyst, indicating the presence of at least small amounts of *hcp* Co. It has been found previously that the formation of *hcp* cobalt leads to higher activities[36–38] and C_{5+} selectivities[39] during Fischer-Tropsch synthesis. It has also been shown that *hcp* Co is less prone to average particle growth during Fischer-Tropsch synthesis than *fcc* Co.[37] Using in situ XRD, it has been demonstrated that this more active form can be formed by activation using synthesis gas[40] or by carbidization of cobalt oxide with subsequent hydrogenation of CoC_2.[41] The *hcp* structure is the

thermodynamically stable phase below 723 K,[1] although for particles below 20 nm the *fcc* structure is expected to prevail.[42] Nevertheless, the product typically formed upon reduction of Co_3O_4 particles under H_2 atmosphere at 623 K is *fcc* Co. Using TPR, we have demonstrated that the use of noble metal promoters leads to a shift of the reduction peaks to lower temperatures. It is thus suggested that an onset of the reduction at lower temperatures leads to the formation of *hcp* Co, the thermodynamically stable modification, (partly) explaining the higher activities of the noble metal promoted catalysts. While in earlier studies stacking faults or the porosity of *hcp* cobalt were considered to explain the superior catalytic performance,[36,38] recently DFT kinetic studies were carried out to shed light on the effect of the cobalt crystal structure on the elementary reaction steps of the Fischer-Tropsch reaction. It was demonstrated that CO activation proceeds with a higher rate on *hcp* Co, but also that it proceeds via direct dissociation, unlike H-assisted dissocation for *fcc* Co.[43]

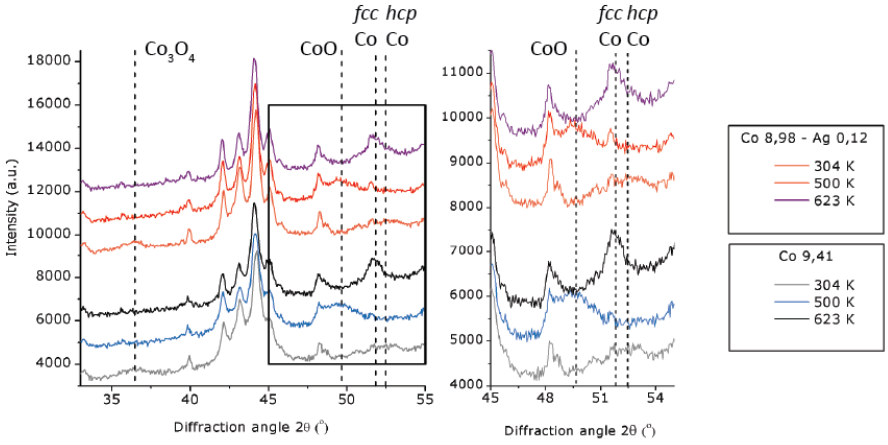

Figure 5: *In-situ* X-ray diffractograms for Ag-promoted and unpromoted Co/TiO_2 catalysts during and after reduction under a flow of H_2/He 1:3 v/v.

Conclusions and outlook

The XRD and TEM results showed that (co-)impregnation of TiO_2 with subsequent fluidized bed drying and heat treatment leads to a rather uniform distribution of similarly sized supported cobalt oxide particles for both unpromoted and promoted catalysts. TPR studies revealed that the addition of noble metals lead to decreased reduction temperatures of cobalt oxide, this effect being most pronounced for the addition of Pt and Ru and less pronounced for the addition of Re and Ag. The effect on the reduction temperature was found to increase with higher promoter loadings for all noble metals. The catalytic properties under industrial Fischer-Tropsch synthesis conditions were found to be strongly influenced by the addition of noble metals. While the addition of Ag, Re and higher amounts of Ru led to increased cobalt time yields and C_{5+}-selectivities, Pt-promoted catalysts showed only higher activities, but significantly lower C_{5+}-selectivities at very similar CO conversion. TEM studies of the reduced and spent catalysts showed that the cobalt particle sizes for the unpromoted and most promoted catalysts were similar, only Re-promoted catalysts showed distinctly lower particle sizes after the catalytic testing. TOF calculations based on the surface average TEM particle sizes of spent catalysts revealed that increased turnover frequencies were found for promoted catalysts as previously shown for Ru-promoted Co/TiO_2 and Pt-promoted Co/Nb_2O_5 catalysts,[18,19,24] while the effect of TOF increase was most pronounced for Ru and Pt. Again, the influence of different degrees of reduction cannot be excluded from the calculations. *In-situ* XRD studies revealed that for Ag-promoted catalysts, at least some *hcp* Co is formed, possibly contributing the higher intrinsic activities of these catalysts compared to the unpromoted system.

For Ru catalyzed Co/TiO_2, it was previously suggested that an interaction in bimetallic particles leads to reduced site blockage by carbonaceous species[18] or that the rate of surface oxygen and hydroxide removal was accelerated.[19] For Re-promoted catalysts, a close interaction of the promoter with the active metal was also discussed to rationalize the increased activities and selectivities.[32] Recent DFT studies[44] show that Co catalysts operate in a regime in which the overall reaction rate is controlled by CO dissociation and oxygen removal by water formation. It is widely accepted that the noble metals used as promoters are more active hydrogenation catalysts than cobalt,[12] which can lead to synergistic effects in CO hydrogenation.[45,46] We suggest that increased hydrogenation

activity in promoted catalysts accelerates water formation and/or gives rise to hydrogen-assisted CO dissociation.[47–49]

Acknowledgements

We gratefully acknowledge Shell Global Solutions for financial support. We also thank Johan den Breejen, Heiko Oosterbeek and Sander van Bavel for fruitful discussions and Rien van Zwienen for technical assistance on high pressure catalytic testing. KPdJ acknowledges support from an ERC Advanced Grant.

References

[1] A.Y. Khodakov, W. Chu, P. Fongarland, Chem. Rev. 107 (2007) 1692–1744.

[2] B.H. Davis, Cobalt FT Catalysts, in: P.M. Maitlis, A. de Klerk (Eds.), Greener Fischer-Tropsch Process. Fuels Feestocks, First edit, 2013: pp. 193–207.

[3] M.E. Dry, J. Chem. Technol. Biotechnol. 77 (2002) 43–50.

[4] M.E. Dry, Stud. Surf. Sci. Catal. 152 (2004) 533–600.

[5] M.E. Dry, Appl. Catal. A Gen. 189 (1999) 185–190.

[6] M.E. Dry, Appl. Catal. A Gen. 138 (1996) 319–344.

[7] J.L. Casci, C.M. Lok, M.D. Shannon, Catal. Today. 145 (2009) 38–44.

[8] F. Morales, B.M. Weckhuysen, Promotion Effects in Co-based Fischer – Tropsch Catalysis, in: J.J. Spivey, K.M. Dooley (Eds.), Catal. Vol. 19, The Royal Society of Chemistry, Cambridge, 2006: pp. 1–20.

[9] F. Morales, E. de Smit, F.M.F. de Groot, T. Visser, B.M. Weckhuysen, J. Catal. 246 (2007) 91–99.

[10] F. Morales, D. Grandjean, A. Mens, F.M.F. de Groot, B.M. Weckhuysen, J. Phys. Chem. B. 110 (2006) 8626–8639.

[11] J.P. den Breejen, A.M. Frey, J. Yang, A. Holmen, M.M. van Schooneveld, F.M.F. de Groot, O. Stephan, J.H. Bitter, K.P. de Jong, Top. Catal. 54 (2011) 768–777.

[12] F. Diehl, A.Y. Khodakov, Oil&Gas Sci. Technol. 64 (2009) 11–24.

[13] R. Oukaci, A.H. Singleton, J.G. Goodwin, Appl. Catal. A Gen. 186 (1999) 129–144.

[14] W. Chu, P. Chernavskii, L. Gengembre, G. Pankina, P. Fongarland, A.Y. Khodakov, J. Catal. 252 (2007) 215–230.

[15] G. Jacobs, W. Ma, P. Gao, B. Todic, T. Bhatelia, D.B. Bukur, B.H. Davis, Catal. Today. 214 (2013) 100–139.

[16] G. Jacobs, T.K. Das, Y. Zhang, J. Li, G. Racoillet, B.H. Davis, Appl. Catal. A Gen. 233 (2002) 263–281.

[17] T. Jermwongratanachai, G. Jacobs, W. Ma, W.D. Shafer, M.K. Gnanamani, P. Gao, B. Kitiyanan, B.H. Davis, J.L.S. Klettlinger, C.H. Yen, D.C. Cronauer, J.A. Kropf, C.L. Marshall, Appl. Catal. A Gen. 464-465 (2013) 165–180.

[18] E. Iglesia, S.L. Soled, R.A. Fiato, H. V Grayson, J. Catal. 143 (1993) 345–368.

[19] E. Iglesia, Appl. Catal. A Gen. 161 (1997) 59–78.

[20] E. Iglesia, S.L. Soled, R.A. Fiato, J. Catal. 137 (1992) 212–224.

[21] J.P. den Breejen, P.B. Radstake, G.L. Bezemer, J.H. Bitter, V. Frøseth, A. Holmen, K.P. de Jong, J. Am. Chem. Soc. 131 (2009) 7197–7203.

[22] J.P. den Breejen, J.R.A. Sietsma, H. Friedrich, J.H. Bitter, K.P. de Jong, J. Catal. 270 (2010) 146–152.

[23] G.L. Bezemer, J.H. Bitter, H.P.C.E. Kuipers, H. Oosterbeek, J.E. Holewijn, X. Xu, F. Kapteijn, A.J. van Dillen, K.P. de Jong, J. Am. Chem. Soc. 128 (2006) 3956–64.

[24] J.H. den Otter, K.P. de Jong, Top. Catal. 57 (2013) 445–450.

[25] S.J. Tauster, S.C. Fung, R.L. Garten, J. Am. Chem. Soc. 100 (1978) 170–175.

[26] S.J. Tauster, Acc. Chem. Res. 20 (1987) 389–394.

[27] F.M.T. Mendes, A. Uhl, D.E. Starr, S. Guimond, M. Schmal, H. Kuhlenbeck, S.K. Shaikhutdinov, H.-J. Freund, Catal. Letters. 111 (2006) 35–41.

[28] T.O. Eschemann, K.P. de Jong, ACS Catal. 5 (2015) 3181–3188.

[29] A.M. Saib, A. Borgna, J. van de Loosdrecht, P.J. van Berge, J.W. Geus, J.W. Niemantsverdriet, J. Catal. 239 (2006) 326–339.

[30] M. Voß, D. Borgmann, G. Wedler, J. Catal. 212 (2002) 10–21.

[31] T.O. Eschemann, J.H. Bitter, K.P. de Jong, Catal. Today. 228 (2014) 89–95.

[32] S. Storsæter, B. Tøtdal, J.C. Walmsley, B.S. Tanem, A. Holmen, J. Catal. 236 (2005) 139–152.

[33] J. Li, G. Jacobs, T. Das, B.H. Davis, Appl. Catal. A Gen. 233 (2002) 255–262.

[34] B. Jongsomjit, C. Sakdamnuson, J. Panpranot, P. Praserthdam, React. Kinet. Catal. Lett. 88 (2006) 65–71.

[35] A. Michalak, M. Nowosielska, W.K. Jóźwiak, Top. Catal. 52 (2009) 1044–1050.

[36] O. Ducreux, B. Rebours, J. Lynch, D. Bazin, Oil&Gas Sci. Technol. 64 (2009) 49–62.

[37] H. Karaca, O. V. Safonova, S. Chambrey, P. Fongarland, P. Roussel, A. Griboval-Constant, M. Lacroix, A.Y. Khodakov, J. Catal. 277 (2011) 14–26.

[38] M. Sadeqzadeh, H. Karaca, O. V. Safonova, P. Fongarland, S. Chambrey, P. Roussel, A. Griboval-Constant, M. Lacroix, D. Curulla-Ferré, F. Luck, A.Y. Khodakov, Catal. Today. 164 (2011) 62–67.

[39] M.K. Gnanamani, G. Jacobs, W.D. Shafer, B.H. Davis, Catal. Today. 215 (2013) 13–17.

[40] V. a. de la Peña O'Shea, N. Homs, J.L.G. Fierro, P. Ramírez de la Piscina, Catal. Today. 114 (2006) 422–427.

[41] L. Braconnier, E. Landrivon, I. Clémençon, C. Legens, F. Diehl, Y. Schuurman, Catal. Today. 215 (2013) 18–23.

[42] O. Kitakami, H. Sato, Y. Shimada, F. Sato, M. Tanaka, Phys. Rev. B. 56 (1997) 13849–13854.

[43] J.-X. Liu, H.-Y. Su, D.-P. Sun, B.-Y. Zhang, W.-X. Li, J. Am. Chem. Soc. 135 (2013) 16284–16287.

[44] I.A.W. Filot, R.A. Van Santen, E.J.M. Hensen, Angew. Chem. Int. Ed. Engl. 53 (2014) 12746–12750.

[45] L. Guczi, L. Borkó, Z. Schay, D. Bazin, F. Mizukami, 65 (2001) 51–57.

[46] Z.S. L. Guczi G. Stefler, F. Mizukami, J. Mol. Catal. A Chem. 141 (1999) 177–185.

[47] J. Yang, Y. Qi, J. Zhu, Y.A. Zhu, D. Chen, A. Holmen, J. Catal. 308 (2013) 37–49.

[48] M.R. Elahifard, M.P. Jigato, J.W. Niemantsverdriet, ChemPhysChem. 13 (2012) 89–91.

[49] S. Shetty, A.P.J. Jansen, R.A. van Santen, J. Am. Chem. Soc. 131 (2009) 12874–12875.

Chapter 5

Effect of support surface treatment on the synthesis, structure, and performance of Co/CNT Fischer-Tropsch catalysts

Abstract: We report the preparation of supported cobalt catalysts (9 wt.-% Co) on untreated (CNT) and surface-oxidized (CNT-ox) carbon nanotube materials by incipient wetness impregnation with solutions of cobalt nitrate in water, ethanol or 1-propanol. The results show that by a judicious selection of solvent and drying method, similar cobalt particle sizes in the range of 4-5 nm on CNT and CNT-ox support materials were obtained for the freshly reduced catalysts. Cobalt particles supported on unfunctionalized CNT showed higher initial activities and C_{5+} selectivities than catalysts on functionalized CNT, however, the former catalysts were more prone to cobalt particle growth due to the lack of anchoring sites. The activities and cobalt particle sizes of catalysts after 60 h on stream revealed for particles larger than 6 nm a turn over frequencies (TOF) of 0.07 s^{-1} for Co/CNT and 0.03 s^{-1} for Co/CNT-ox. *In-situ* XAS/XRD studies showed a similar degree of reduction for the catalysts on untreated and oxidized CNT and the formation of *hcp* cobalt metal on untreated CNT which rationalizes the higher activity and TOF of the Co/CNT catalysts.

Introduction

The Fischer-Tropsch synthesis (FTS) comprises the catalytic conversion of synthesis gas into hydrocarbons and is considered a promising process to produce a mixture of long chain hydrocarbons, which can further be upgraded to ultraclean transportation fuels, chemicals and lubricants.[1–3] Since synthesis gas can be generated from different sources such as natural gas, shale gas, coal or biomass, the FTS has awaked interest against the background of souring crude oil prices and geopolitical uncertainties. For the economic prospects of FT plants, good catalyst performance at affordable costs is crucial, making supported cobalt catalysts the material of choice for modern low temperature Fischer-Tropsch plants based on synthesis gas derived from natural gas.[4–8]

Industrially used cobalt catalysts contain both structural and electronic promoters[9–11] and are typically supported on refractory oxides such as alumina, silica or titania.[6,12–15] Highly active and selective catalysts have been developed,[16–21] however, these support materials often have the disadvantages of limited hydrothermal stability, low reducibility of cobalt oxide to metallic cobalt or strong metal support interactions (SMSI).[22–25] Various carbonaceous support materials have been introduced as promising alternatives to overcome these drawbacks, such as activated carbon (AC), carbon spheres (CS), carbon nanofibers (CNF) or carbon nanotubes (CNT).[26–31] These materials are chemically robust and do not form cobalt-support compounds.[32,33] Commercially available multiwalled carbon nanotubes (MWCNT) as used in this study consist of rolled up graphene sheets that are arranged in a Russian doll fashion, featuring a well-defined structure, a high pore volume, a high specific surface area and a largely unfunctionalized and thereby hydrophobic surface.[33]

In previous work carbonaceous materials were mostly functionalized prior to being used as support material for metal catalysts, in order to improve the wetting properties for aqueous solutions relevant for metal precursor deposition and to create anchoring sites for the metal nanoparticles.[26,34] Several approaches have been used previously to functionalize the surface of carbonaceous support materials, most importantly liquid phase oxidation using nitric acid, sulfuric acid or mixtures thereof.[33,35] Since these methods often severely damage the catalyst structure, milder methods have been developed, both for liquid-phase and gas-phase functionalization.[32,36,37] Few

publications focus on the impact of support functionalization on catalyst structure and performance, and often the conclusions are based on systems with very different metal dispersions or distributions. [38–44]

It is the goal of this work to study the influence of support functionalization on the properties of Co/CNT catalysts at comparable cobalt dispersions. While the physicochemical properties of untreated commercially available support material used in this work have been studied in detail before,[33] it is the goal of this work to focus on the most important structural changes introduced by the functionalization procedures and their impact on the catalyst synthesis process. Therefore, we used both liquid-phase and gas-phase oxidation[32] to modify the CNT surface properties and to introduce acidic groups. The materials were characterized by means of nitrogen physisorption, transmission electron microscopy, Raman spectroscopy and acid-base titrations. Supported cobalt catalysts were prepared on these CNT materials using incipient wetness impregnation with different solvents and a drying and heat treatment protocol that has been proven to lead to good distributions of the supported metal particles over the support surface.[45,46] The impact of the chosen materials and methods on dispersion and distribution of cobalt was studied by electron microscopy and x-ray diffraction. The catalysts were then tested under industrially relevant FTS conditions to study trends in activity, selectivity and stability, while special attention was paid to the extent of reduction under the process conditions using *in-situ* XANES.

Materials and methods

Catalyst synthesis

Commercially available multiwalled carbon nanotubes (CNT, Baytubes C 150 HP, Bayer Material Science) were functionalized using gas-phase oxidation in a setup as described elsewhere.[32] Typically, 0.4 g of CNT (grain size 75-150 µm) were dried in a sample holder for 2 hours at 398 K. Then, a condenser and a round bottom flask containing about 150 mL nitric acid (65 %, Merck) were fitted to the heated sample holder, its design preventing the contact of condensed nitric acid with the sample. Nitric acid was heated to reflux for 0.5-4 h, before the heating mantle was removed. Then, the acid was allowed to cool down while the sample holder was still heated to prevent condensation of any vapors in the sample. Afterwards, the oxidized carbon nanotubes (CNT-ox-Xh, X being the duration of oxidation) were dried in a static oven at 393 K overnight. Alternatively, the samples were functionalized using liquid-phase oxidation. Therefore, typically 2 g CNT were suspended in 40 mL nitric acid (65 %, Merck) and heated at 393 K for 2 hours. Afterwards the suspension was allowed to cool down and the material was filtered off and washed with water until the pH was close to neutral. The material was then dried in a static oven at 393 K overnight and designated as CNT-LPO-2h.

After drying the support material *in vacuo*, the carbon nanotubes were loaded by incipient wetness impregnation with 1.5 M solutions of cobalt nitrate hexahydrate (p.a., Acros) in water, ethanol or 1-propanol.The materials were then dried in a static oven at 333 K in air overnight or in in a down-flow tubular setup under nitrogen flow at a temperature about 20 K below the boiling point of the solvent used for impregnation. Therefore, the reactor was heated fast to the desired temperature, which was then held for 2 h. To decompose the cobalt precursor, the temperature was then increased to 523 K (2 K/min) and held for 4 h under a flow of nitrogen (GHSV~6000 h^{-1}). All cobalt loadings for the catalysts prepared were around 9 wt.-%, assuming Co to be in the form of Co_3O_4. The loadings were calculated by determining the mass of solution added during impregnation of the catalysts. The catalysts prepared on untreated and oxidized carbon nanotubes were named Co/CNT-solvent or Co/CNT-ox-solvent, respectively, with the solvents deionized H_2O, EtOH (Interchema, >99%) and 1-PrOH (Alfa Aesar, >99.5%) used during the impregnation step.

Catalyst characterization

Nitrogen physisorption was carried out using a Micromeritics Tristar 3000 setup. Prior to measurements, the samples were degassed at 498 K for 20 h with a ramp of 10 K/min. Physisorption was measured at 77 K from 0 to 0.995 p/p_0. Surface area was estimated using the BET approach, average pore size distributions were determined from the desorption branches of the isotherms using the BJH method. The micropore volume was approximated using the t-plot method, total pore volumes were determined from single point adsorption at p/p_0=0.995.

X-ray powder diffraction (XRD) was performed on a Bruker D2 Phaser with a Co K_α (λ = 1.789 Å) source. Co_3O_4 crystallite size estimation was carried out using the Co_3O_4 peak at 36.8° 2Θ with an automatic calculation routine in DiffracEvaluation V2.0 software by Bruker, which is based on the Debye-Scherrer-equation.

For transmission electron microscopy (TEM), the support materials or the heat-treated catalysts were carefully ground with a mortar, suspended in ethanol using an ultrasonic bath and dropped onto a copper TEM grid with holey carbon film. The samples were analyzed using a Tecnai T12 or a Tecnai T20 microscope with electron beam voltages of 120 kV and 200 kV, respectively. Image analysis was carried out with iTEM, the sizes of a at least 150 Co_3O_4 particles were measured and the average diameter was used to derive an equivalent value for the average metallic cobalt particle size by using the relation d(Co) = 0.75 d(Co_3O_4). The same relation was used for analyzing the spent catalysts.[47]

Temperature-programmed reduction (TPR) was carried out using a Micromeritics Autochem II ASAP 2920. Typically, 50 mg of the sample were dried in a flow of Ar at 393 K for 1 h and then reduced in a flow of H_2/Ar (1:19, v/v) using a ramp of 5 K/min.

Titrations were performed using a Radiometer Analytical TitraLab TIM880 titration manager. Typically, 25-50 mg of the sample was loaded and 60 mL 0.1 M KCl (aq) was added while stirring. In order to remove dissolved CO_2, the liquid was flushed with nitrogen for two minutes before adding the titrant. The sample was titrated using an aqueous solution containing 0.01 M NaOH and 0.1 M KCl until the pH reached 9 or until the added volume V was 5 mL. The inflection point was found by numerically calculating

the first derivative and then applying a second degree polynomial fit ($y = aV^2 + bV + c$) around the maximum, finding the inflection point by calculating $V_{inflection} = -b/2a$.

Raman spectroscopy was performed with a Kaiser Optical Systems Inc. Raman Spectrometer equipped with a 532 nm laser. Measurements were carried out at 50 mW with an exposure time of 7 s and 11 accumulations using Holograms 4.0 software.

Combined *in-situ* XANES/XRD studies were performed at the Swiss-Norwegian Beamline (SNBL) at the European Synchrotron Radiation Facility (ESRF), station BM01B. The dried catalysts were diluted with boron nitride (1:1 v/v) and loaded in a quartz capillary with an outer diameter of 1 mm and a wall thickness of 0.02 mm. The bed length was 10 mm and the catalyst bed was fixed using glass wool. The setup for the *in-situ* measurements was described elsewhere.[48] The wavelength used for XRD was 0.4944 Å and the data was converted to 1.78897 Å (Co K_α) using the software Winplotr. Calibration of the energy of the edge of the XAS spectra and linear combination fitting was done with the IFEFFIT program Athena. The Co K-edge energy of the reference compound was calibrated by setting the zero-crossing of the second derivative to 7709 eV and the edge energy of the spectra were chosen as a set fraction of the edge step. For the fitting, Co foil and CoO or Co_3O_4 diluted with BN (1:1 v/v) were used as standards. The first reduction was carried out at 623 K (5 K/min) using a flow of H_2/He (1:3 v/v). After 5 h at 523 K the system was cooled to 553 K and the feed mixture was changed to CO/H_2 (1:2.1 v/v). The pressure was increased to 15 bar and the temperature to 493 K. These conditions were kept constant for 10 h, afterwards the system was returned to ambient pressure and the setup was flushed with pure H_2. The second reduction step took place at 673 K (5 K/min) for 5 h. Afterwards, the temperature was decreased to 553 K and the gas flow was changed to CO/H_2 (1:2.1 v/v). Again, the pressure was increased to 15 bar and the temperature was set to 473 K, these conditions were held for another 3 h.

Fischer-Tropsch synthesis

Fischer-Tropsch synthesis was carried out in a 16 reactor catalytic testing setup (Flowrence, Avantium). The catalysts (75-150 μm) were diluted with SiC (200 μm) to arrive at the same amount of Co in every reactor, giving a catalyst bed volume of 200 μL. The catalysts were dried in a flow of He at 373 K for 2 h and then reduced *in situ* in a flow of H_2/He (1:3 v/v) at 623 K (8 h, ramp 1 K/min). Subsequently, the reactors were cooled to 453 K and pressurized to 20 bar under a flow of H_2. After switching to H_2/CO (2:1 v/v) the temperature was increased to 493 K (1K/min), the products were analyzed using online gas chromatography (Agilent 7890A). The permanent gases were separated on a ShinCarbon ST (#19043) column and quantified against He as an internal standard using a TCD detector. CO conversions were calculated as $X_{CO}=(mol_{CO\ in}-mol_{CO\ out})/mol_{CO\ in}$. Hydrocarbons (C1-C9) were separated on an Agilent J&W PoraBOND Q column, detected using an FID detector and quantified against the TCD signal of the internal standard He. Selectivities to the lower hydrocarbon fractions S_{CX} were calculated from converted CO and the corresponding yields as $S_{CX}=Y_{CX}/(mol_{CO\ in}-mol_{CO\ out})$. The selectivities to products with 5 and more carbon atoms were calculated from the yields to lower hydrocarbons as $S_{C5+}=1-S_{C1-C4}$. Stable CO conversions and hydrocarbon selectivities were reached after about 50 h on stream and were between 25 and 35 %. Activities are reported as cobalt time yields (CTY, $mol_{CO}/(g_{Co}\cdot s)$). At the end of the catalytic testing experiment, the waxes in the pores of the catalysts were stripped off the catalysts for 12 h under a flow of H_2 at 473 K, subsequently the reactors were cooled down to room temperature under a flow of Ar. When removing the catalysts from the reactors, these were exposed to air prior to further characterization by TEM. Although the purity of the CNT material was greater than 99% C, the support material contains small amounts of residual growth catalyst from the industrial manufacturing process, which might have an effect on the catalytic properties. Therefore, the activity of the blank support material was also tested in the catalytic experiments, but it was found to be negligible.

Results and discussion

Characterization of the support materials

Transmission electron microscopy (TEM) imaging (Figure 1) was used to obtain information on the local structural changes in the carbon nanotubes upon functionalization. While the untreated CNT show smooth parallel rolled up graphene sheets with disordered deposits both inside and outside as described in the literature,[33] distinct differences can be found in the modified nanotubes. The materials oxidized by gas phase oxidation show a roughening of the nanotube surface, while the structure otherwise seems intact. For the CNT oxidized by liquid phase oxidation, a severe distortion of the original structure is noted as the surface was roughened and few parallel graphene sheets are observed.

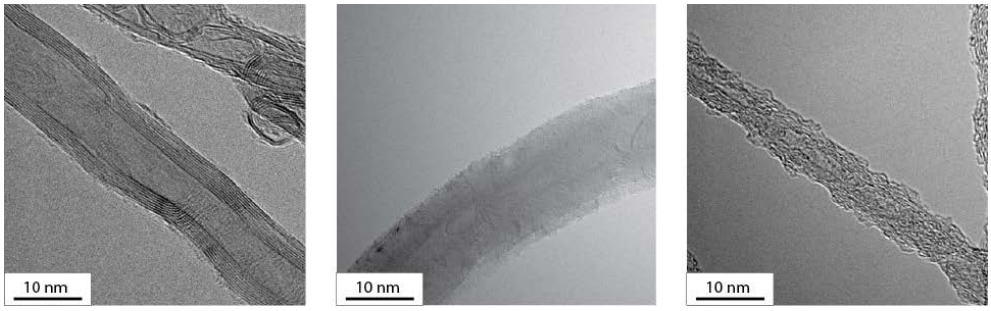

Figure 1: Representative TEM images of untreated (left), and 2 h gas phase oxidized (center) and 2 h liquid phase oxidized (right) carbon nanotubes.

The number of acidic groups on the functionalized materials was determined by acid-base titrations. Using this method, for the unfunctionalized materials no acidic groups were found. (Figure 2) The samples treated in the gas phase show that the number of acid sites increased with short oxidation times as expected, while longer times did not lead to significantly higher degrees of functionalization, a behavior that has been observed before. Note that the number of acid sites introduced for longer oxidation times was very similar to the result for liquid-phase oxidized nanotubes (0.40 mmol/g).[32,36] It should be noted that both for the untreated and functionalized CNT the amount of oxygen-containing groups may be higher than the amount of acid sites determined by titration.

For more accurate methods to quantitatively determine the amount of oxygen-containing groups, high-resolution XPS studies have been carried out successfully before.[49,50]

The degree of surface functionalization also played a key role in the wetting properties of the materials with different solvents. While oxidized CNT were wetted by water, ethanol or 1-propanol, the untreated materials floated on water indicating poor wetting properties. The untreated CNT materials, however, were wetted properly by ethanol or 1-propanol.

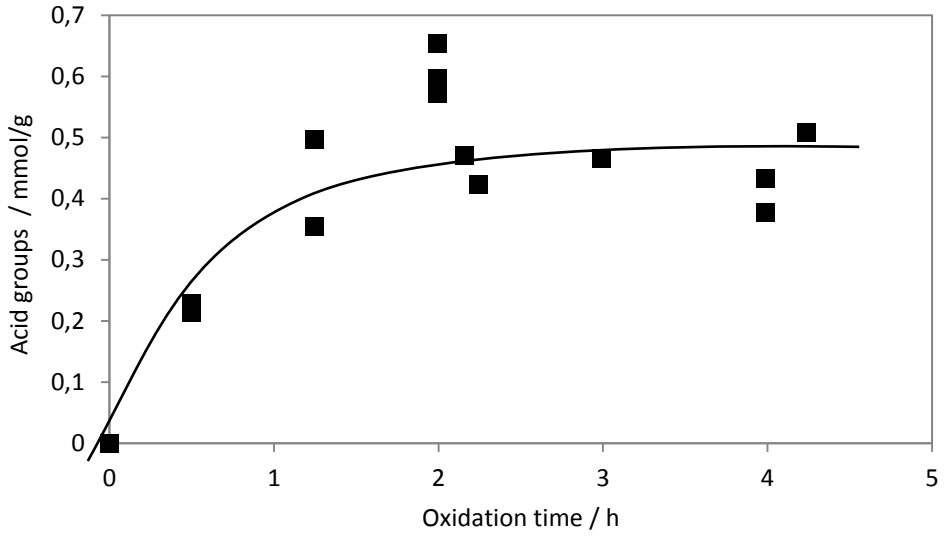

Figure 2: Number of acidic groups on the CNT surface for different gas phase oxidation times. The line through the points has been drawn to guide the eye.

Nitrogen physisorption on untreated and oxidized samples showed very similar adsorption-desorption curves (see appendix, Figure S3), that can be best described as IUPAC type IV isotherms with hysteresis at $p/p_0>0.9$. A slight increase of pore volume and BET surface area was noted for the gas phase oxidized CNT. (Table 1) The similarities in porosity suggest that the overall structure of the gas phase oxidized CNT has not been severely affected by the oxidation treatment, which is in line with the observations made with TEM. For liquid phase oxidized CNT a further increase in BET area is observed and the pore volume is found to be a bit lower than in the other materials.

Table 1: Influence of oxidation treatments on the porosity of the carbon support materials.

Support material	BET area / m^2/g	Total pore volume / mL/g
CNT	200	1.2
CNT-GPO-2h	250	1.4
CNT-LPO-2h	270	1.1

Raman spectroscopy was carried out to obtain further information how the different oxidation treatments had affected the CNT (Figure 3). The spectra of the untreated CNT show the typical pattern that has been discussed elsewhere in the literature,[33] featuring a distinct band at ~1580 cm^{-1} for the ideal graphitic lattice (G), at ~1340 cm^{-1} for disordered graphitic lattice (A_{1g} symmetry, D_1) and a shoulder on the G peak at ~1620 cm^{-1} that can also be assigned to disordered graphitic lattice (E_{2g} symmetry, D_2).[51] The relative intensity of the G band decreased for the gas phase oxidized sample and its D_2 shoulder becomes more apparent, indicating the increasing degree of disorder in the sample. For liquid phase oxidized CNT, the G band disappeared almost completely. The spectra were deconvoluted (for details see appendix) using Gaussian functions of the three contributions described above including a contribution of amorphous carbon (D_3) at ~1480 cm^{-1}. The increase of the I_{D1}/I_G ratio is in line with the observations from TEM images and suggests only slight structural distortions when using gas phase oxidation and severe structural damage for the samples using liquid phase oxidation. In contrast to what is reported elsewhere in the literature,[33] we found that both the D_1 and the G band became narrower going from the untreated sample to the gas phase oxidized CNT and to the liquid phase oxidized sample. Also, a distinct redshift of the D_1 band to ~ 1320 cm^{-1} is observed for the LPO sample. These effects have been interpreted as graphitic domains being smaller for related materials[52] and is in line with the other observations of the structural distortion.

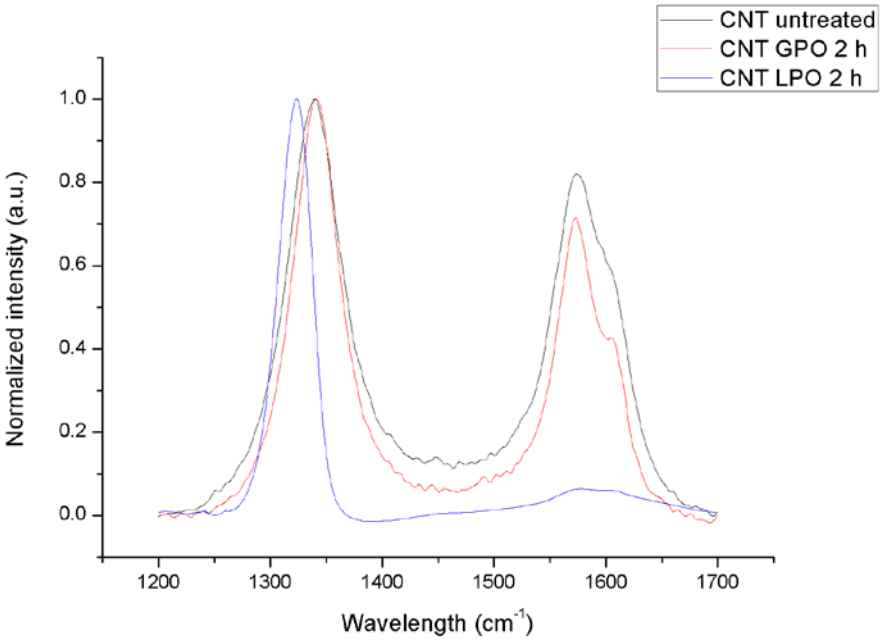

Figure 3: Raman spectra of untreated and functionalized carbon nanotubes.

Table 2: Raman data obtained for untreated and oxidized carbon nanotubes.

Support material	D_1 band FWHM / cm^{-1}	G band FWHM / cm^{-1}	I_{D1}/I_G
CNT untreated	59	57	1.2
CNT-GPO-2h	52	44	1.4
CNT-LPO-2h	36	85	39

Characterization of the heat-treated catalysts

XRD line broadening analysis was carried out on the heat treated CNT-supported catalysts to estimate the size of the Co_3O_4 crystallites. (Table 3) The results show relatively small cobalt oxide crystallites of 3-6 nm with little difference between the catalysts prepared on untreated and oxidized CNT. For both the catalysts on untreated and on oxidized CNT the largest crystallite sizes were found for the catalysts impregnated with aqueous solutions, while smaller crystallites were detected for impregnations with ethanol or propanol.

Table 3: Co_3O_4 crystallite sizes (nm) determined by XRD line broadening for 9wt% Co/CNT samples.

Support / Solvent	Water	Ethanol	1-Propanol
CNT	6	4	4
CNT-GPO-2h	5	5	3
CNT-LPO-2h	n/a	4	n/a

TEM particle size analysis results of the heat treated catalysts were in good accordance with the values deduced from XRD line broadening analysis. (See also table 5). Moreover, the images provided indications on the nanoscale distribution of the cobalt oxide particles over the CNT. The catalysts prepared by aqueous impregnations showed clusters of about 20 nm, while less clustering was observed for catalysts prepared by impregnations using cobalt nitrate solutions in ethanol and quite uniform distributions for the catalysts impregnated with solutions of 1-propanol. (Figure 4) When comparing the catalysts supported on untreated CNT with their counterparts on oxidized CNT, little difference in terms of cobalt oxide clustering was observed. (Figure 5) These results indicate that the solvent surface tension effects during drying have a larger impact than wetting of the support. In other words, if wetting suffices then surface tension effects dominate in agglomeration during drying. This finding is nicely in line with the elegant *in situ* TEM studies of Crozier et al.[53] comparing nickel nitrate distributions on silica showing that water as solvent led to more clustering than ethanol as solvent.

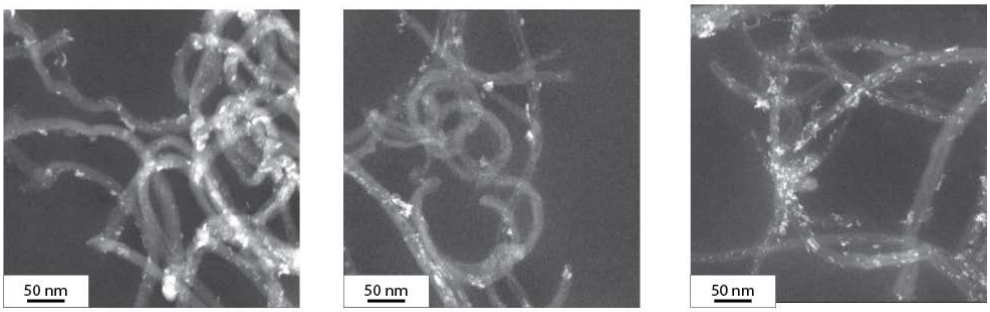

Figure 4: Representative STEM-HAADF images showing clustering of cobalt oxide particles for untreated CNT support impregnated with aqueous solutions (left, Co/CNT-H_2O) and a more homogeneous distribution for catalysts prepared by impregnation with solutions of cobalt nitrate in ethanol (middle, Co/CNT-EtOH) and uniform distribution when using isopropanol as solvent (right, Co/CNT-PrOH).

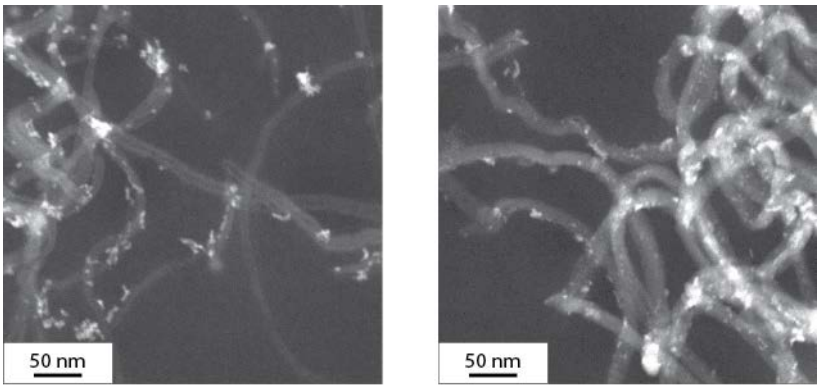

Figure 5: Representative STEM-HAADF images showing similar cobalt oxide particle distributions for propanol-impregnated catalysts on untreated support (left, Co/CNT-PrOH) and on oxidized support (right, Co/CNT-GPO-PrOH).

The reducibility of the catalysts was studied by temperature-programmed reduction (TPR). Similar patterns were found for all supported cobalt catalysts on untreated and oxidized CNT. (See Supporting Information, Figure S4) The patterns showed hydrogen uptake at ~ 473 K, indicating the presence of residual cobalt nitrate, and two broad peaks at ~ 573 K

and 673 K, resembling the typical two-step reduction pattern, that is of Co_3O_4 to CoO followed by reduction of CoO to metallic cobalt.[9] It can be seen that all reduction peaks in the sample supported on oxidized CNT had shifted to higher temperatures, indicating a reduction of cobalt oxide impaired by the presence of the functional groups, that has been reported before.[40,54] A quantification of the TPR data to determine the degree of reduction was difficult, since the hydrogen uptake from the reduction of cobalt oxide is likely to overlap with hydrogen consumption from gasification of the support.

Fischer-Tropsch synthesis and *in-situ* characterization

The results from catalytic testing at industrially relevant conditions revealed significant differences for the performance of the catalysts. All catalysts supported on untreated CNT showed distinctly higher CTY than their counterparts supported on gas phase oxidized or liquid phase oxidized CNT (Figure 6). For both series of cobalt catalysts supported on untreated and on gas phase oxidized CNT, the materials impregnated with aqueous solutions showed the lowest activity, while higher activities were found for the systems impregnated with solutions of cobalt nitrate in alcohols. In the case of catalysts supported on oxidized CNT, the catalysts impregnated with ethanol and 1-propanol displayed the same activity, whereas for catalysts on untreated CNT, the systems impregnated with ethanol showed superior activity. Regarding the selectivity to higher hydrocarbons, significantly higher C_{5+} selectivities were found for the catalysts on untreated CNT (88-91%) than for the catalysts on gas phase oxidized CNT (82-86%) and for the catalysts on liquid phase oxidized CNT (68%), although it should be mentioned that the CO conversions for the catalysts on untreated CNT were higher than for the ones supported on gas phase oxidized CNT and liquid phase oxidized CNT. (Table 4) A possible explanation is that for the untreated Co/CNT catalyst, the α-olefins primary products adsorb on the hydrophobic CNT surface thereby invoking re-adsorption on cobalt favoring additional chain growth. This re-adsorption step can be hampered by the presence of polar functional groups. For the surface-oxidized Co/CNT-GPO catalysts the support surface is expected to have a stronger interaction with polar molecules such as water. If water is preferably adsorbed on the surface, α-olefin re-adsorption can be inhibited leading to a reduced C_{5+}-selectivity. [55] Similar effects have also been discussed for Co/Al_2O_3 catalysts with different alumina phases where the C_{5+}-selectivity was found to be lower for catalysts supported on alumina phases with higher Lewis acidities.[56,57] We note that except for Co/CNT-LPO and

Co/CNT-H_2O, the measured C_{5+}-selectivities were found to correlate with CO conversion. (See appendix, Figure S6) However, the measured differences in C_{5+}-selectivities related to the differences in CO conversion ($\Delta S_{C5+}/\Delta X_{CO}$~0.4) are distinctly higher than was has been reported elsewhere in the literature (e.g $\Delta S_{C5+}/\Delta X_{CO}$~0.1 for Co/$Al_2O_3$[58]).

Table 4: Selectivity data for Co/CNT catalysts studied, 20 bar, 493 K, H_2/CO 2.0, GHSV ~2000 h^{-1}, 60 h on stream. [a] Data for Co/CNT-LPO-EtOH after 50 h on stream.

Catalyst	X_{CO} / %	S_{C1} / wt.-%	S_{C2-C4} /wt.-%	S_{C5+} / wt.-%
Co/CNT -H_2O	29	4	5	91
Co/CNT -EtOH	42	5	5	90
Co/CNT -PrOH	37	6	6	88
Co/CNT-GPO -H_2O	16	11	7	82
Co/CNT-GPO -EtOH	21	11	7	82
Co/CNT-GPO-PrOH	20	10	7	83
Co/CNT-LPO-EtOH[a]	18	19	12	69

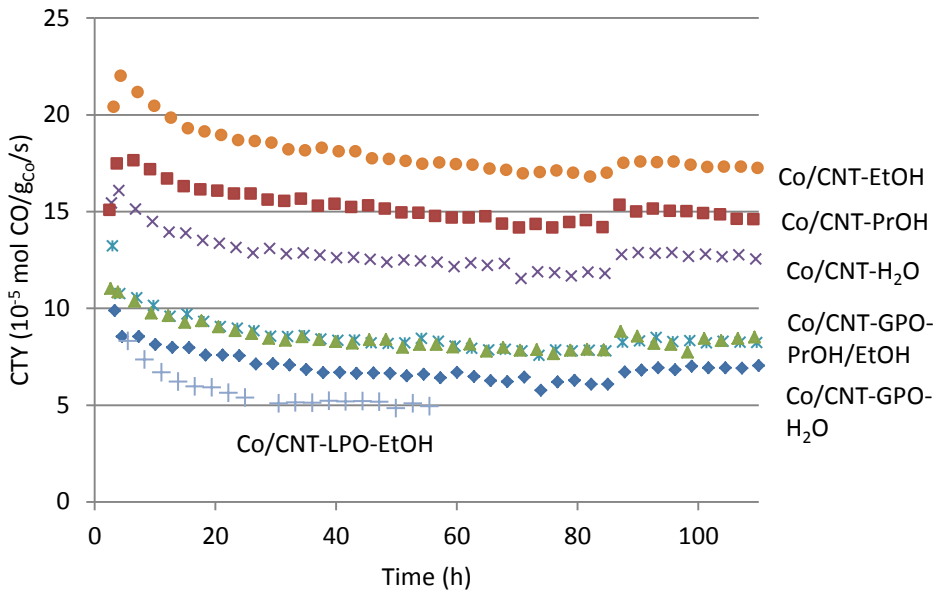

Figure 6: Cobalt-time-yields (CTY) for CNT-supported cobalt catalysts, Fischer-Tropsch synthesis at 20 bar, 493 K, H_2/CO 2.0 v/v, GHSV ~ 2000 h^{-1}.

In order to understand the reasons for the different activities and selectivities, the Co particle sizes before and after the catalytic experiments were determined by TEM. The results (Table 5) showed that the extent of average particle growth correlated with the degree of nanoparticle clustering found for the fresh catalysts (Figure 5). While initially the cobalt particle sizes in the catalysts were found to be very similar for all systems studied, the clustering in catalysts prepared by impregnations with aqueous solutions led to more severe particle growth and loss of metallic surface area during reduction and Fischer-Tropsch synthesis, explaining the superior activity of catalysts prepared with impregnation using organic solvents.

The turnover frequencies (TOF-final) based on the FT activity after 60 hours (Figure 7) and the cobalt particle sizes of the used catalysts for the catalysts supported on untreated CNT were significantly higher than the TOF-final found for the catalysts supported on gas phase oxidized CNT. The same trend is observed for the initial turnover frequencies based on the

particle sizes of the fresh catalysts. This indicates that the activity differences cannot be exclusively explained with differences of the active metal surface area. The fact that the activity for Co/CNT-PrOH was lower than that of Co/CNT-EtOH is rationalized by the fact that the average particle size of the material impregnated with 1-propanol was lower than the critical particle size of ~ 6 nm, below which the turnover frequency in FT decreases sharply.[17] This also holds for samples prepared on oxidized CNT using 1-propanol as a solvent. Also, all fresh catalysts feature cobalt particle sizes below 6 nm and show lower initial turnover frequency values, underlining the importance of particle size effects. (Table 5, Figure 7).

Table 5: Equivalent cobalt particle sizes (calculated from average TEM Co_3O_4 particle sizes using the relation $d_{Co} = d_{Co3O4} * 0.75$) of fresh and spent Co/CNT catalysts and cobalt time yields at 60 hours on stream. Initial TOF values are based on the equivalent cobalt particle sizes of the fresh catalysts and the initial data points in the catalytic testing. CTY and TOF final are based on the catalytic performance after ~60 hours and based on the cobalt particle sizes of the spent catalysts.

Catalyst	d_{Co} fresh / nm	d_{Co} spent / nm	CTY / 10^{-5} $mol_{CO}/(g_{Co}*s)$	TOF initial / 10^{-3} s^{-1}	TOF final / 10^{-3} s^{-1}
Co/CNT -H_2O	4.8	10.1	13	45	70
Co/CNT -EtOH	3.8	7.0	16	46	73
Co/CNT -PrOH	4.0	5.5	18	38	45
Co/CNT-GPO -H_2O	4.3	7.7	7.8	22	26
Co/CNT-GPO -EtOH	3.9	7.3	8.9	25	31
Co/CNT-GPO -PrOH	4.2	5.0	8.9	23	23
Co/CNT-LPO -EtOH	3.6	n/a	5.0	n/a	n/a

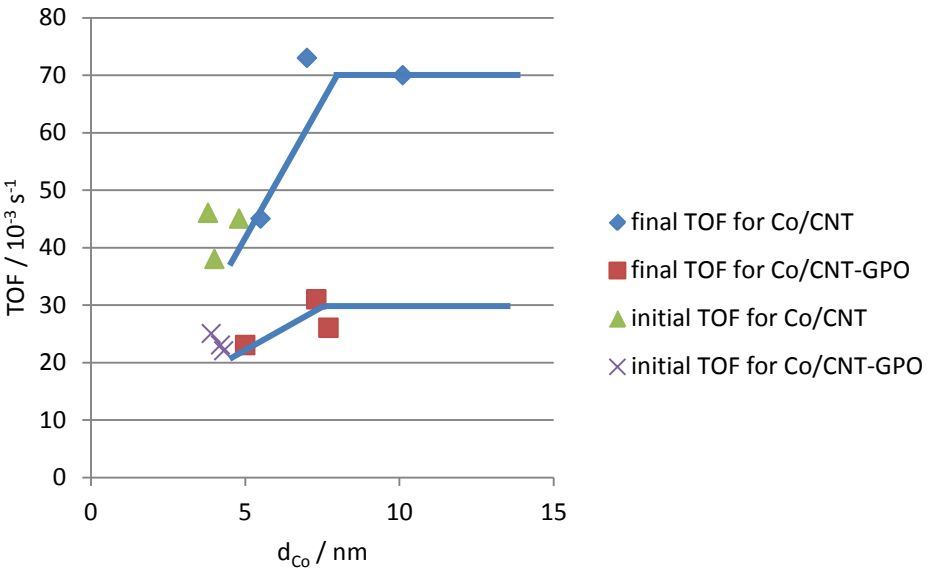

Figure 7: Initial and final TOF as a function of equivalent cobalt particle sizes. The lines are drawn as a guide to the eye.

Considering the results of the TEM particle size analysis and the turnover frequency calculations, the performance differences between the catalysts supported on untreated CNT and their counterparts supported on oxidized CNT is unlikely to arise from differences in dispersion of cobalt. Since the extent of reduction could not be determined from the TPR experiments, *in-situ*-XANES and XRD were used to probe the chemical nature of cobalt during process conditions. The results showed different reduction rates (Figure 8) for a catalyst on untreated CNT compared to a catalyst on oxidized CNT. While for the catalyst supported on untreated CNT, the reduction of Co_3O_4 to CoO came to completion after 40 min, there was still Co_3O_4 present for the catalyst supported on oxidized CNT after 80 min. This is in line with the TPR results indicating a hampered reduction for the catalysts supported on oxidized CNT, however, after two hours Co_3O_4 was fully reduced and the amounts of CoO and Co formed were very similar.

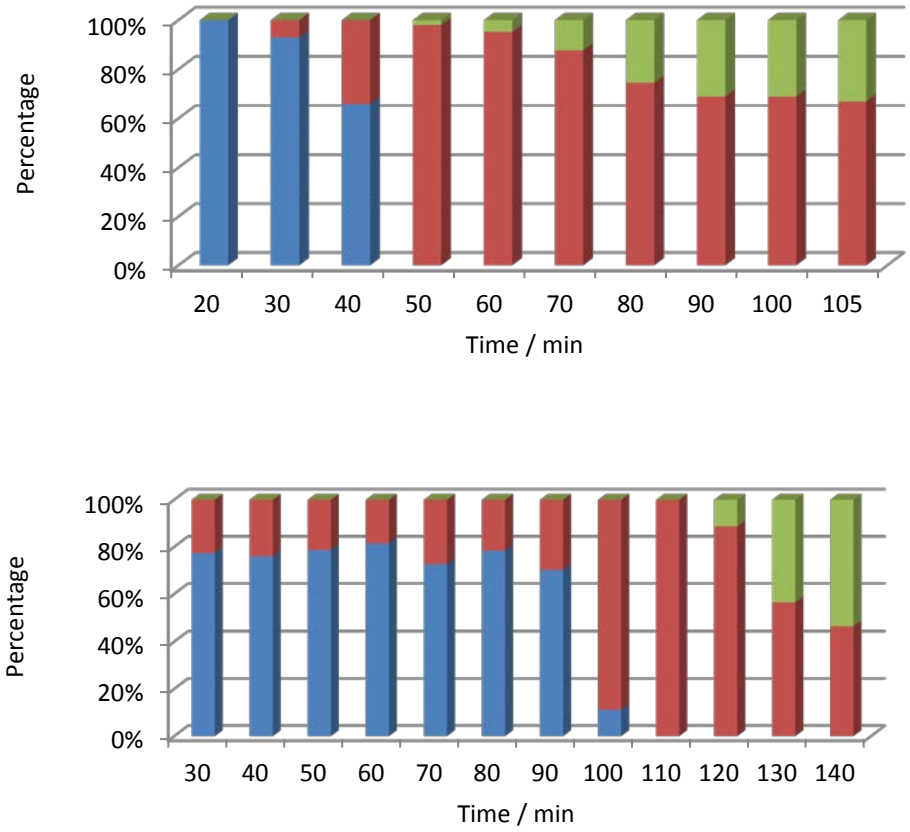

Figure 8: Phase composition of Co/CNT-PrOH (left) and Co/CNT-ox-PrOH (right) during reduction in a flow of He/H_2 (3.0 v/v) at 623 K (5 K/min), 1 bar, Co_3O_4 (blue), CoO (red), Co (green).

The extent of reduction was further determined during Fischer-Tropsch synthesis at conditions similar to the catalytic results reported above (Figure 9). After about 8 hours a steady state was reached and the degree of reduction was found to be 73% for the material on untreated CNT and 81% for the catalysts supported on oxidized CNT.

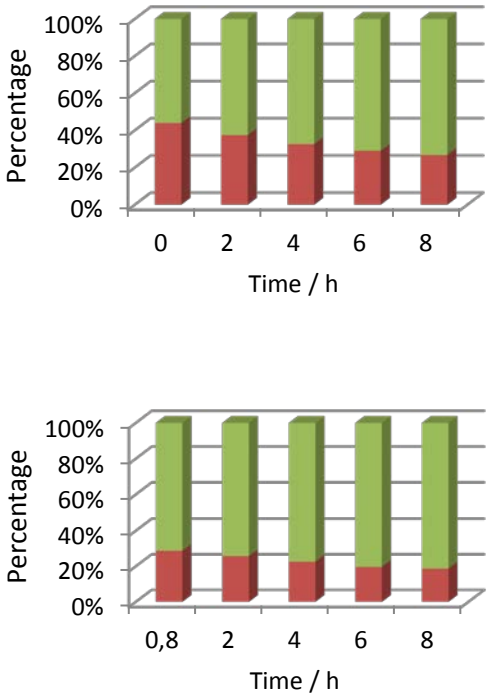

Figure 9: Phase composition of Co/CNT-PrOH (left) and Co/CNT-ox-PrOH (right) during Fischer-Tropsch synthesis at 493 K, 15 bar, H_2/CO 2.1 v/v, CoO (red), Co (green).

A second reduction at a higher temperature (673 K) and pressure (5 bar) was carried out, which led to a higher extent of reduction for both catalysts. Under these conditions the degree of reduction was found to be 84% for the catalyst on untreated CNT and 86% for the system on oxidized CNT. In the second Fischer-Tropsch synthesis cycle (see appendix, figure S5) the degree of reduction was found to be very similar for the two catalysts studied, 89% metallic Co was found for Co/CNT-PrOH, while 87% metallic Co was found for Co/CNT-ox-PrOH. (see appendix, figure S5 and S6)

The *in-situ* XRD-studies (Figure 10) performed during the first reduction step showed the disappearance of the Co_3O_4 peaks at 39, 67 and 74 ° 2θ in the course of time and the arising of CoO peak at 70° 2θ. For the catalyst supported on untreated CNT the appearance of a peak at 55° 2θ was observed, indicating the formation of *hcp* Co, while

this peak was not found for the catalyst on oxidized CNT. Since *hcp* Co is known to be more active in FTS than *fcc* Co,[59,60] these findings might (partly) explain the differences observed for the activities of the catalysts studied in this work.

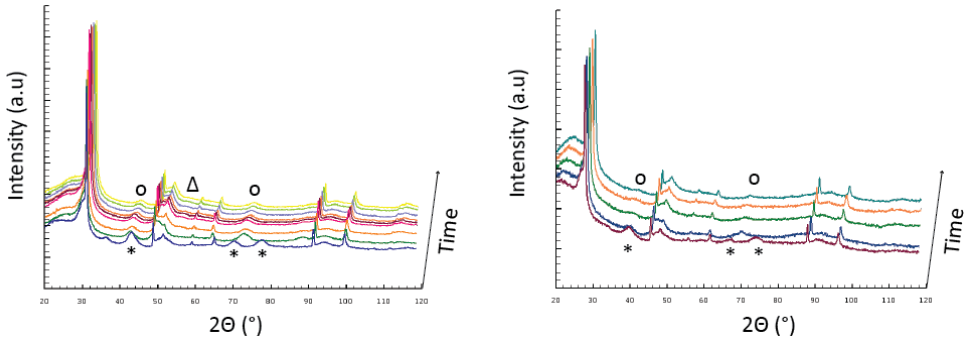

Figure 10: Diffractograms obtained from *in-situ* XRD studies during the first reduction step of a Co/CNT-PrOH (left) and Co/CNT-GPO-PrOH (right) catalyst. Note the disappearance of Co_3O_4 (*) and the appearance of CoO (o) for both catalysts, while a small peak for hcp Co (Δ) at 54° 2Θ is only observed for Co/CNT-PrOH. Conditions 1 bar, 623 K, H_2/He 1:3 v/v, diffractograms were recorded every hour during the reduction.

In order to compare the thermal stability between the catalysts supported on untreated and oxidized CNT, some catalysts were exposed to higher temperatures in several steps, before returning to the Fischer-Tropsch synthesis temperature of 493 K, where the catalyst performance was compared to that of the catalysts that had not been exposed to temperatures higher than 493 K. (Figure 11) The results showed that the activity increased stepwise with increasing the temperature as expected. Upon returning to the original synthesis temperature, however, only the catalyst supported on oxidized CNT returned to its original activity, while the catalyst supported on untreated CNT fell short. After the exposure to higher temperatures the catalyst on untreated CNT only showed a slightly higher activity than its counterpart on oxidized CNT.

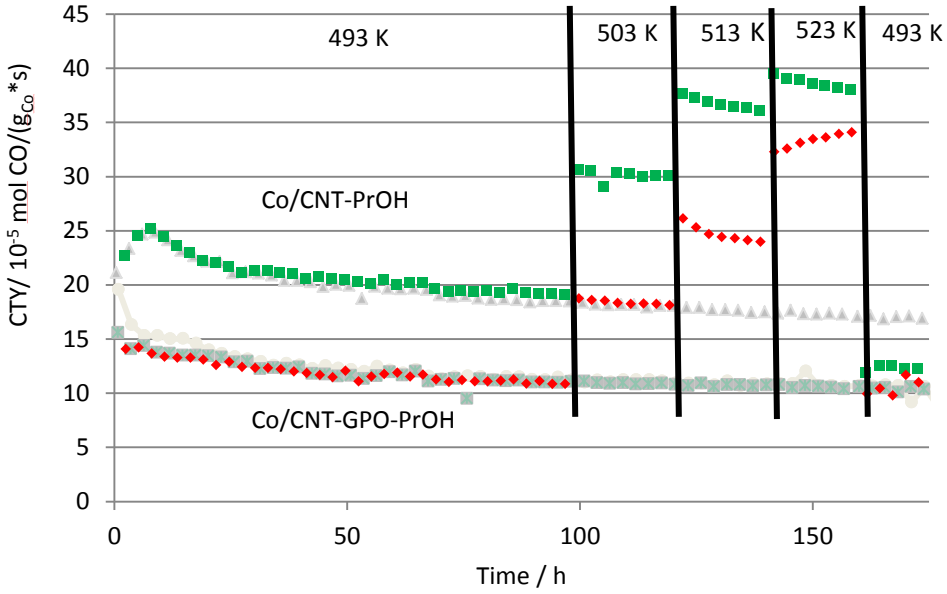

Figure 11: Cobalt-time-yields (CTY) for CNT-supported cobalt catalysts, Fischer-Tropsch synthesis carried out at 20 bar, 493/503/513/523/493 K, H_2/CO 2.0 v/v, GHSV ~ 2000 h^{-1}. The grey curves refer to the catalysts that have been exposed to 493 K for the whole duration of the experiment.

TEM studies of the spent catalysts showed similar particle size distributions for the catalysts on untreated and oxidized CNT that were used for FTS at 493 K only. For the catalysts exposed to higher temperatures, distinctly more particles greater than 10 nm were found for the catalysts on untreated CNT, while the histogram for the catalyst on oxidized CNT was similar to the one found for exposition to lower temperatures only. (Figure 12)

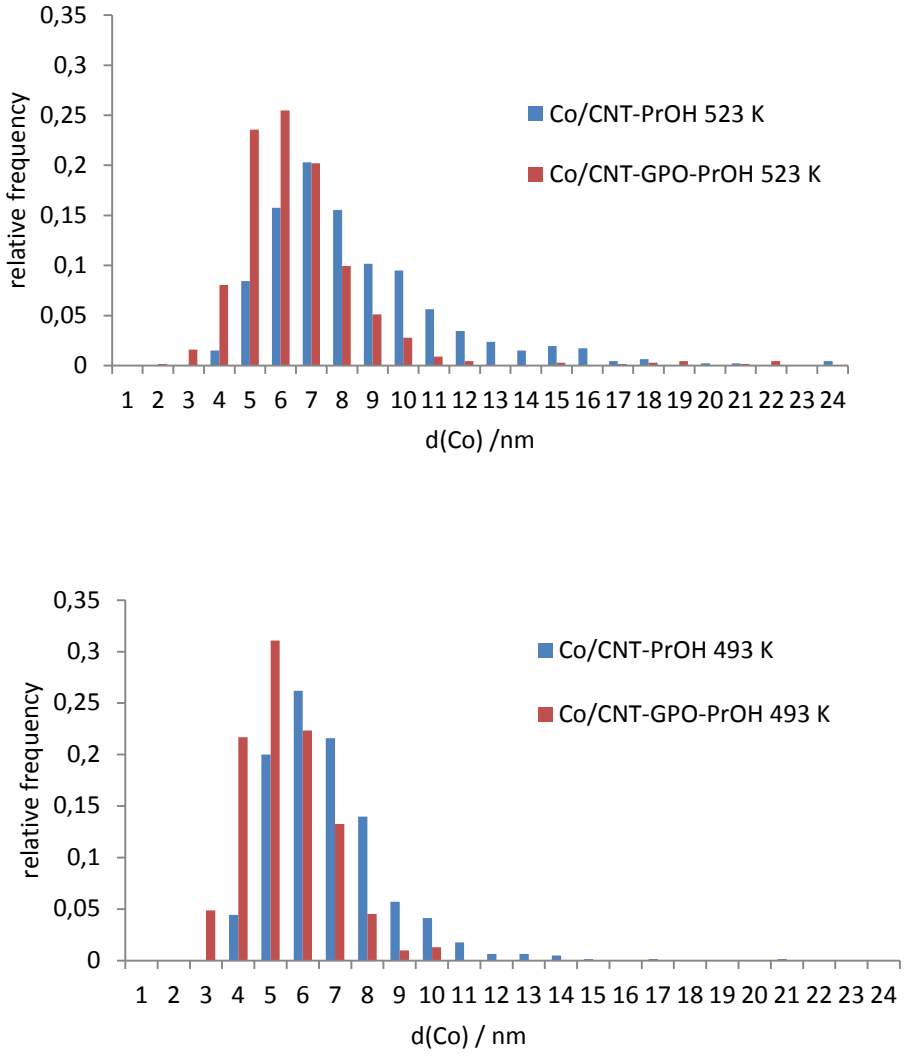

Figure 12: TEM Particle size distributions for catalysts exposed to 523 K (top) and 493 K (bottom).

Conclusions

Gas phase oxidation using nitric acid vapors was used as a versatile route to introduce functional groups on carbon nanotubes (CNT) surfaces without severely damaging the overall porous and crystalline structure of the material. The oxidized CNT materials exhibit improved wetting properties towards water, although proper wetting of the untreated CNT was also achieved using alternative solvents for impregnation, such as ethanol or 1-propanol. Both for unfunctionalized and oxidized CNT and for all solvents considered in this study, drying of the impregnated material under a flow of nitrogen about 20 K below the boiling point of the solvent led to similarly sized supported Co_3O_4 nanoparticles of 3-6 nm. Using TEM, it was shown that clustering of Co_3O_4 nanoparticles was reduced using ethanol as a solvent for impregnation and even further using 1-propanol for the impregnation. These findings indicate that the nature of the solvent (a.o. surface tension) and drying conditions are more important for the preparation of well-dispersed and well-distributed supported cobalt oxide nanoparticles than the surface functionalization on its own.

The catalytic experiments at 20 bar showed that both for the systems on untreated and on oxidized CNT, the catalysts prepared by impregnation with solutions of cobalt nitrate in alcohols showed a superior cobalt-weight based activity over those prepared from an aqueous solution, because the cobalt particles had grown less during reduction and Fischer-Tropsch synthesis, leading to higher specific metal surface areas. These results emphasize the importance of avoiding clustering of supported nanoparticles by choosing an appropriate solvent and drying procedure. The distinctly higher surface-specific activity (TOF) for the catalysts supported on untreated CNT (TOF = 0.07 s^{-1} for Co particles larger than 6 nm)) compared to functionalized CNT (TOF = 0.03 s^{-1} for particles larger than 6 nm)) could not be explained by differences in cobalt dispersion or the degree of reduction. Although TPR suggests a retarded reduction of cobalt oxides to cobalt for the catalysts on oxidized CNT and despite the different reduction kinetics observed by XANES, the extent of reduction under steady state Fischer-Tropsch synthesis in all cases was very similar and very high and neither explains the differences in activity nor in selectivity. However, *in-situ* XRD studies indicated that *hcp* Co was present for the catalysts on untreated CNT, while this was not the case for the catalysts on oxidized CNT, which rationalizes the superior activity of the catalysts on unmodified support materials.

While in terms of initial activity and selectivity of the catalysts, surface functionalization did not have a positive effect, gas phase oxidation brought about a higher stability of the materials. While catalysts supported on untreated CNT displayed a substantial loss of activity that could be attributed to average cobalt particle growth. The catalysts supported on oxidized CNT maintained their catalytic activity, presumably due to a stronger anchoring of the cobalt nanoparticles to the support surface. These observations showed that the design of ideal Fischer-Tropsch catalysts remains a challenging tasks and that trade-offs have to be made in order to balance initial catalytic performance and long term stability.

Acknowledgements

We gratefully acknowledge Shell Global Solutions for financial support. We also thank Jesper Sattler for carrying out Raman spectroscopy, Daniel Stellwagen for help with interpreting Raman spectra and Rien van Zwienen for technical assistance on high pressure catalytic testing. The Research Council of Norway is acknowledged for financial support through the SYNKNØYT programme, and the personnel of the Swiss-Norwegian Beamlines (SNBL) at ESRF are highly acknowledged for experimental assistance.

References

[1] M.E. Dry, Catal. Today. 71 (2002) 227–241.

[2] J.L. Casci, C.M. Lok, M.D. Shannon, Catal. Today. 145 (2009) 38–44.

[3] M.E. Dry, J. Chem. Technol. Biotechnol. 77 (2002) 43–50.

[4] M.E. Dry, Stud. Surf. Sci. Catal. 152 (2004) 533–600.

[5] E. Iglesia, Appl. Catal. A Gen. 161 (1997) 59–78.

[6] A.Y. Khodakov, W. Chu, P. Fongarland, Chem. Rev. 107 (2007) 1692–1744.

[7] Q. Zhang, J. Kang, Y. Wang, ChemCatChem. 2 (2010) 1030–1058.

[8] B.H. Davis, Cobalt FT Catalysts, in: P.M. Maitlis, A. de Klerk (Eds.), Greener Fischer-Tropsch Processes for Fuels and Feestocks, First edit, 2013: pp. 193–207.

[9] W. Chu, P. Chernavskii, L. Gengembre, G. Pankina, P. Fongarland, A.Y. Khodakov, J. Catal. 252 (2007) 215–230.

[10] F. Diehl, A.Y. Khodakov, Oil&Gas Sci. Technol. 64 (2009) 11–24.

[11] F. Morales, B.M. Weckhuysen, Promotion Effects in Co-based Fischer – Tropsch Catalysis, in: J.J. Spivey, K.M. Dooley (Eds.), Catal. Vol. 19, The Royal Society of Chemistry, Cambridge, 2006: pp. 1–20.

[12] R. Oukaci, A.H. Singleton, J.G. Goodwin, Appl. Catal. A Gen. 186 (1999) 129–144.

[13] C.H. Bartholomew, R.C. Reuel, J. Catal. 85 (1984) 78–88.

[14] G. Jacobs, T.K. Das, Y. Zhang, J. Li, G. Racoillet, B.H. Davis, Appl. Catal. A Gen. 233 (2002) 263–281.

[15] J. van de Loosdrecht, S. Barradas, E.A. Caricato, N.G. Ngwenya, P.S. Nkwanyana, M.A.S. Rawat, B.H. Sigwebela, P.J. van Berge, J.L. Visagie, Top. Catal. 26 (2003) 121–127.

[16] T.O. Eschemann, J.H. Bitter, K.P. de Jong, Catal. Today. 228 (2014) 89–95.

[17] J.P. den Breejen, P.B. Radstake, G.L. Bezemer, J.H. Bitter, V. Frøseth, A. Holmen, K.P. de Jong, J. Am. Chem. Soc. 131 (2009) 7197–7203.

[18] J.H. den Otter, K.P. de Jong, Top. Catal. 57 (2013) 445–450.

[19] C.M. Lok, EP 1 542 794 A1, 2010.

[20] S. Storsæter, Ø. Borg, E.A. Blekkan, B. Tøtdal, A. Holmen, Catal. Today. 100 (2005) 343–347.

[21] E. Iglesia, S.L. Soled, R.A. Fiato, H. V Grayson, J. Catal. 143 (1993) 345–368.

[22] A.R. de la Osa, A. De Lucas, A. Romero, J.L. Valverde, P. Sánchez, Catal. Today. 176 (2011) 298–302.

[23] V.A. de la Peña O'Shea, M.C.Á. Galván, A.E. Prats Platero, J.M. Campos-Martin, J.L.G. Fierro, Chem. Commun. 47 (2011) 7131–7133.

[24] B. Jongsomjit, C. Sakdamnuson, J.G. Goodwin Jr, P. Praserthdam, Catal. Letters. 94 (2004) 209–215.

[25] S.J. Tauster, S.C. Fung, R.L. Garten, J. Am. Chem. Soc. 100 (1978) 170–175.

[26] G.L. Bezemer, U. Falke, A.J. van Dillen, K.P. de Jong, Chem. Commun. (Camb). (2005) 731–733.

[27] P. Serp, M. Corrias, P. Kalck, Appl. Catal. A Gen. 253 (2003) 337–358.

[28] K.P. de Jong, J.W. Geus, Catal. Rev. 42 (2000) 481–510.

[29] H. Xiong, M.A.M. Motchelaho, M. Moyo, L.L. Jewell, N.J. Coville, J. Catal. 278 (2011) 26–40.

[30] H. Xiong, M.A.M. Motchelaho, M. Moyo, L.L. Jewell, N.J. Coville, Catal. Today. 214 (2013) 50–60.

[31] F. Rodriguez-Reinoso, Carbon. 36 (1998) 159–175.

[32] W. Xia, C. Jin, S. Kundu, M. Muhler, Carbon. 47 (2009) 919–922.

[33] J.-P. Tessonnier, D. Rosenthal, T.W. Hansen, C. Hess, M.E. Schuster, R. Blume, F. Girgsdies, N. Pfänder, O. Timpe, D.S. Su, R. Schlögl, Carbon. 47 (2009) 1779–1798.

[34] G.L. Bezemer, P.B. Radstake, V. Koot, A.J. van Dillen, J.W. Geus, K.P. de Jong, J. Catal. 237 (2006) 291–302.

[35] T.G. Ros, A.J. van Dillen, J.W. Geus, D.C. Koningsberger, Chemistry (Easton). 8 (2002) 1151–62.

[36] R.W. Gosselink, R. van den Berg, W. Xia, M. Muhler, K.P. de Jong, J.H. Bitter, Carbon. 50 (2012) 4424–4431.

[37] V. Likodimos, T.A. Steriotis, S.K. Papageorgiou, G.E. Romanos, R.R.N. Marques, R.P. Rocha, J.L. Faria, M.F.R. Pereira, J.L. Figueiredo, A.M.T. Silva, P. Falaras, Carbon. 69 (2014) 311–326.

[38] U.M. Graham, G. Jacobs, M.K. Gnanamani, S.M. Lipka, W. Shafer, C.R. Swartz, T. Jermwongratanachai, R. Chen, F. Rogers, B.H. Davis, ACS Catal. 4 (2014) 1662–1672.

[39] T. Fu, Z. Li, Catal. Commun. 47 (2014) 54–57.

[40] T. Fu, R. Liu, J. Lv, Z. Li, Fuel Process. Technol. 122 (2014) 49–57.

[41] Y. Yang, L. Jia, B. Hou, D. Li, J. Wang, Y. Sun, J. Phys. Chem. C. 118 (2014) 268–277.

[42] T. Fu, Y. Jiang, J. Lv, Z. Li, Fuel Process. Technol. 110 (2013) 141–149.

[43] A. Karimi, B. Nasernejad, A.M. Rashidi, A. Tavasoli, M. Pourkhalil, Fuel. 117 (2014) 1045–1051.

[44] Z. Yu, Ø. Borg, D. Chen, E. Rytter, A. Holmen, Top. Catal. 45 (2007) 69–74.

[45] G. Prieto, J. Zečević, H. Friedrich, K.P. de Jong, P.E. de Jongh, Nat. Mater. 12 (2013) 34–9.

[46] P. Munnik, P.E. de Jongh, K.P. de Jong, J. Am. Chem. Soc. 136 (2014) 7333–40.

[47] D. Schanke, S. Vada, E.A. Blekkan, A.M. Hilmen, A. Hoff, A. Holmen, J. Catal. 156 (1995) 85–95.

[48] N.E. Tsakoumis, R. Dehghan, R.E. Johnsen, A. Voronov, W. van Beek, J.C. Walmsley, Ø. Borg, E. Rytter, D. Chen, M. Rønning, A. Holmen, Catal. Today. 205 (2013) 86–93.

[49] T.I.T. Okpalugo, P. Papakonstantinou, H. Murphy, J. McLaughlin, N.M.D. Brown, Carbon. 43 (2005) 153–161.

[50] S. Kundu, Y. Wang, W. Xia, M. Muhler, J. Phys. Chem. C. 112 (2008) 16869–16878.

[51] A. Sadezky, H. Muckenhuber, H. Grothe, R. Niessner, U. Pöschl, Carbon. 43 (2005) 1731–1742.

[52] Y. Wang, D.C. Alsmeyer, R.L. McCreery, Chem. Mater. 2 (1990) 557–563.

[53] P. Li, J. Liu, N. Nag, P.A. Crozier, J. Phys. Chem. B. 109 (2005) 13883–13890.

[54] T. Fu, C. Huang, J. Lv, Z. Li, Fuel. 121 (2014) 225–231.

[55] E.W. Kuipers, I.H. Vinkenburg, H. Oosterbeek, J. Catal. 152 (1995) 137–146.

[56] S. Rane, Ø. Borg, J. Yang, E. Rytter, A. Holmen, Appl. Catal. A Gen. 388 (2010) 160–167.

[57] S. Rane, Ø. Borg, E. Rytter, A. Holmen, Appl. Catal. A Gen. 437-438 (2012) 10–17.

[58] D.B. Bukur, Z. Pan, W. Ma, G. Jacobs, B.H. Davis, Catal. Letters. 142 (2012) 1382–1387.

[59] L. Braconnier, E. Landrivon, I. Clémençon, C. Legens, F. Diehl, Y. Schuurman, Catal. Today. 215 (2013) 18–23.

[60] J.-X. Liu, H.-Y. Su, D.-P. Sun, B.-Y. Zhang, W.-X. Li, J. Am. Chem. Soc. 135 (2013) 16284–16287.

Appendix

Raman spectral deconvolution

The spectra were deconvoluted based on four Gaussian functions at ~1340 cm^{-1}, ~1480 cm^{-1}, ~1580 cm^{-1} and ~1620 cm^{-1}. The fittings of the individual peak curves and the cumulative fit are shown in figure S1.

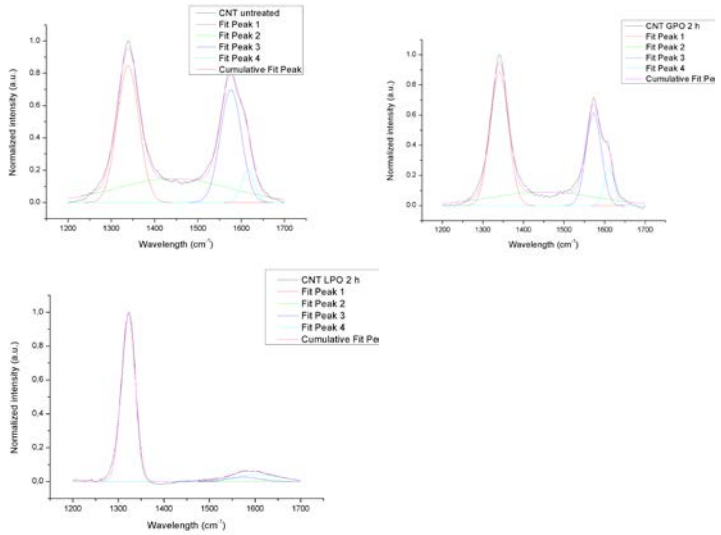

Figure S1: Fitted curves for the Raman spectra of untreated CNT (left), gas phase oxidized CNT (center) and liquid phase oxidized CNT (right).

Experimental setup for gas phase oxidation of CNT

Figure S2 shows a sketch and a photo of the actual setup used for the functionalization of the support material using gas phase oxidation. As the heating mantle was raised in temperature above the boiling point of nitric acid, the contact with liquid condensate was avoided. Also, the geometry of the setup diverted refluxing acid to bypass the sample.

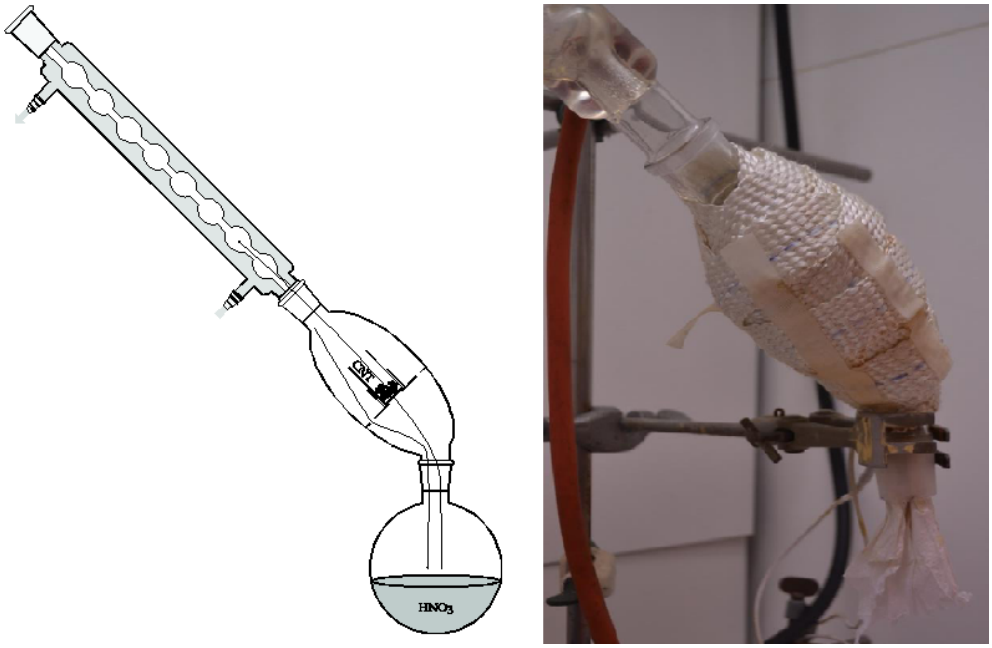

Figure S2: Sketch and photo of the GPO setup used in this work.

Nitrogen physisorption curves

Figure S3 shows the nitrogen physisorption curves for the support materials studied in this work.

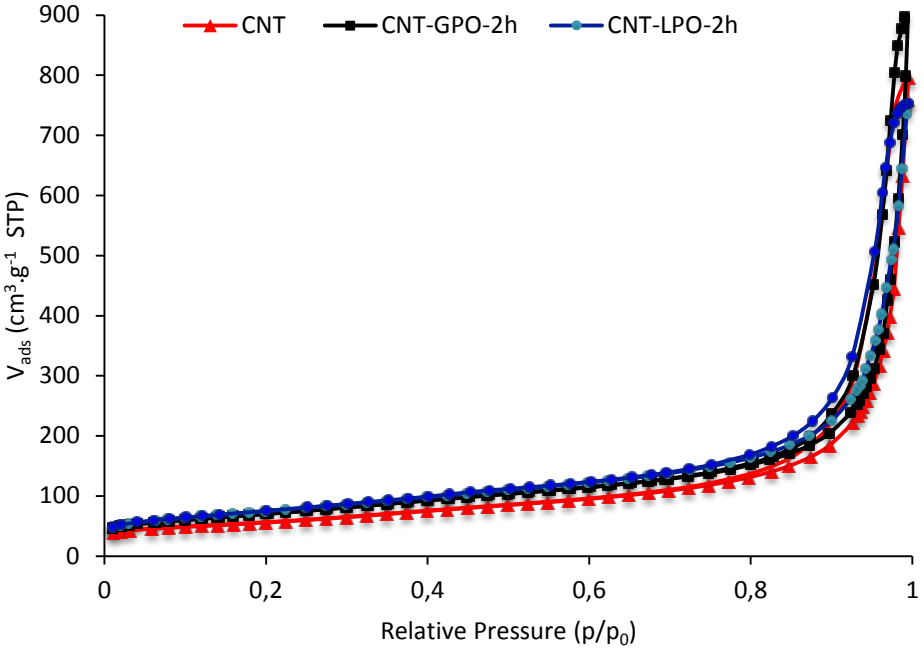

Figure S3: Nitrogen physisorption curves of the support materials used in this work.

Temperature programmed reduction

Figure S4 shows representative TPR patterns for the catalysts studied in this work.

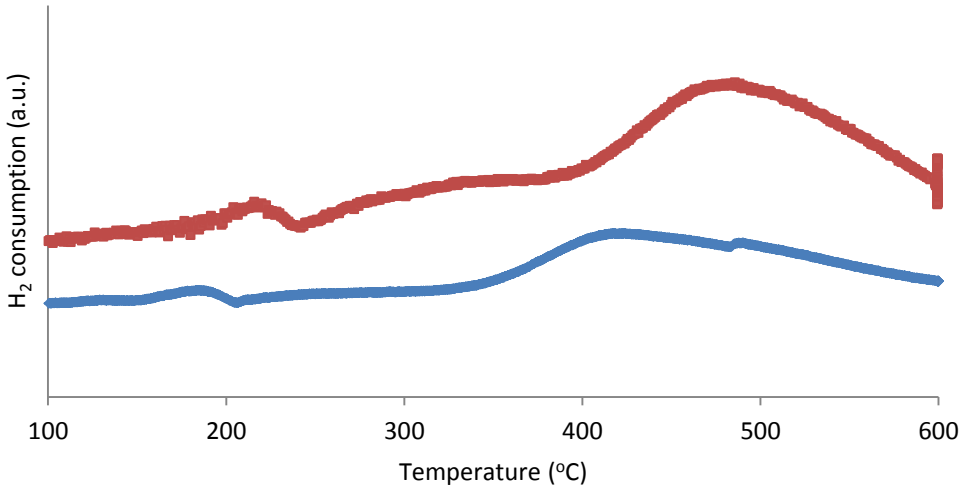

Figure S4: Representative TPR profiles for supported cobalt catalysts on untreated CNT (blue) and on oxidized CNT (red).

In-situ XANES

The figures S5 and S6 show the phase composition of the samples during the second reduction and the second FTS phase as discussed in the manuscript.

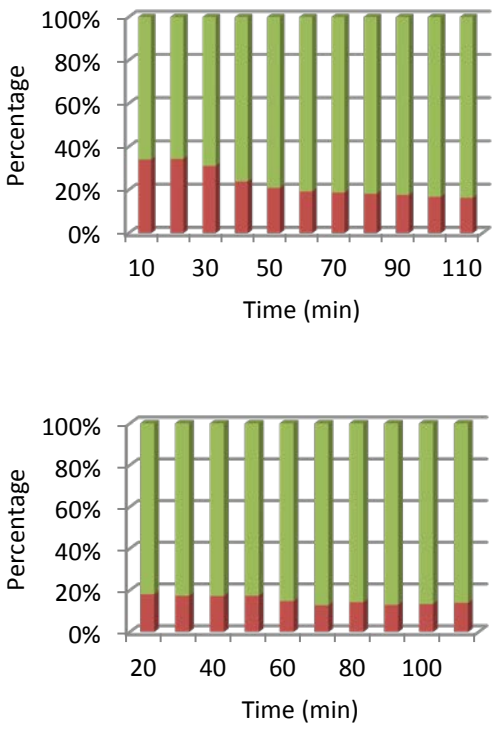

Figure S5: Phase composition of Co/CNT-PrOH (left) and Co/CNT-ox-PrOH (right) during reduction in a flow of He/H_2 (3.0 v/v) at 673 K (5 K/min), 5 bar, Co_3O_4 (blue), CoO (red), Co (green).

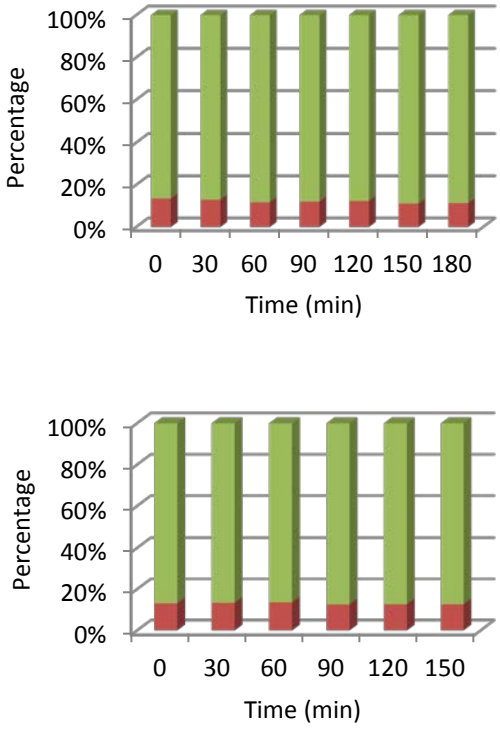

Figure S6: Phase composition of Co/CNT-PrOH (left) and Co/CNT-ox-PrOH (right) during the second Fischer-Tropsch synthesis cycle at 493 K, 15 bar, H_2/CO 2.1 v/v, Co_3O_4 (blue), CoO (red), Co (green).

Correlation of selectivity and CO conversion

Figure S7 shows that the observed C_{5+}-selectivities correlate well with the CO conversion for most catalysts studied.

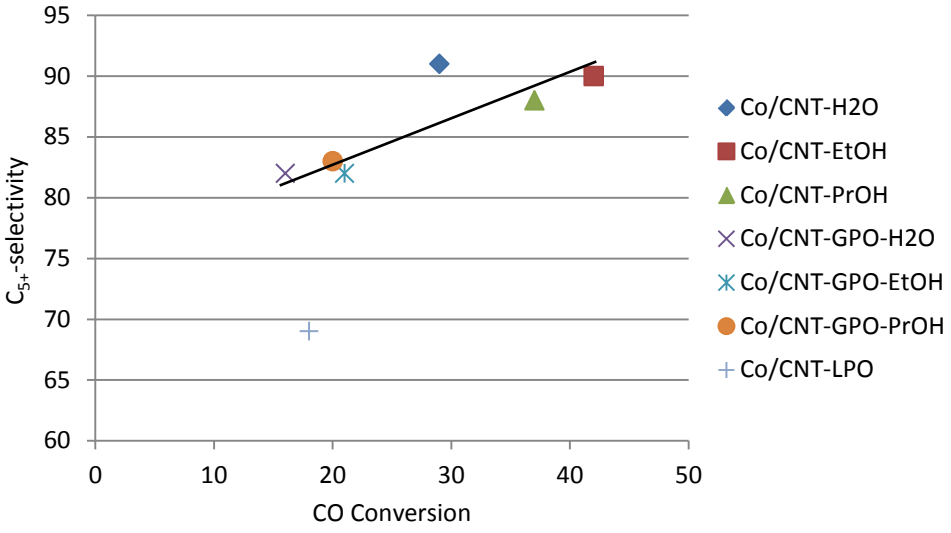

Figure S7: C_{5+}-selectivities plotted against the corresponding CO conversion. The line is a guide to the eye. 20 bar, 493 K, GHSV ~ 2000 h^{-1}, H_2/CO 2.0 v/v.

Chapter 6a

Summary and concluding remarks

The Fischer-Tropsch synthesis (FTS) involves the heterogeneously catalyzed conversion of synthesis gas into water and hydrocarbons and offers a promising route for the synthesis of ultraclean fuels, chemicals and lubricants. The synthesis gas can be generated from different feedstocks, such as coal (CTL), biomass (BTL) or natural gas (GTL), with the latter being the economically most interesting option. Therefore the Fischer-Tropsch synthesis might decrease dependencies on crude oil while allowing the indirect liquefaction of resources that are projected to be available longer than crude oil. The properties of the catalysts applied for the conversion of synthesis gas are crucial for the performance of XTL plants, demanding high activities, high selectivities to heavy hydrocarbons and high stabilities under process conditions. Titania-supported cobalt catalysts have previously been identified to be particularly well-suited catalysts for Fischer-Tropsch synthesis in the GTL process, especially because of their high hydrothermal stability and their high selectivity to heavy hydrocarbons. It is the goal of this research to provide new insights on how the preparation procedure affects the structural and catalytic properties of Co/TiO_2 catalysts during Fischer-Tropsch synthesis under industrial conditions.

In **chapter 2**, Co/TiO_2 catalysts (4-24 wt.-%) were prepared by conventional incipient wetness impregnation (IWI) with subsequent drying and compared with catalysts prepared by deposition precipitation starting from high (DPA) and low (DPU) pH. While average cobalt oxide particles (8 - 15 nm, XRD) were similar for catalysts with the same metal loadings, catalysts prepared by IWI showed the presence of agglomerated cobalt oxide particles. The supported cobalt particles were homogeneously distributed over the support surface for catalysts prepared by DPA, while the preparation of Co/TiO_2 catalysts by DPU led to the formation of very small (2-4 nm) supported cobalt oxide particles beside the formation of very large unsupported (200 nm) particles. This effect can be rationalized with the more extensive electrostatic interaction between the cobalt cations when starting at high pH compared to the method starting at low pH. Catalytic tests at 493 K and 20 bar showed that activities were found to increase in the order DPU < IWI < DPA over the whole cobalt metal loading range studied. The superior activity of DPA catalysts over IWI catalysts with comparable initial cobalt oxide dispersion is explained by their stability against average particle growth during reduction, which is supported by observations from hydrogen chemisorption and turnover frequency calculations. The low activity of catalysts prepared by DPU can be rationalized by the low specific cobalt surface area of the very large unsupported particles and the hampered reducibility of the very

small supported particles, which is apparent from TPR experiments. While C_{5+} selectivities were found to be comparable for IWI (79 %) and DPU (81 %) catalysts, significantly higher selectivities were found for catalysts prepared by DPA (86 %) for all metal loadings, an observation that cannot be explained by effects of available metal surface area. We suggest that partial dissolution of the support material during deposition precipitation at high pH leads to a TiO_2 decoration of the cobalt particles when the dissolved material is again precipitated. Such a decoration could lead to cobalt particles featuring relatively strong CO adsorption compared to impregnated catalysts. Techniques suitable for the detection of adsorbed species (CO-DRIFTS and SSITKA) can be used to gain further insights on the origin of the increased C_{5+} selectivities in the future.

In **chapter 3**, Co/TiO_2 catalysts (8 and 16 wt.-% Co) are discussed that were prepared by deposition precipitation using ammonia evaporation (DPA) and incipient wetness impregnation with subsequent static drying (IWI-S) and fluidized bed drying (IWI-F). While the presence of clustered particles for IWI-S and the homogeneous distribution of DPA catalysts has been discussed before, the IWI-F method leads to cobalt distributions more uniform than for IWI-S catalysts but not as uniform as for DPA catalysts. During Fischer-Tropsch synthesis at 493 K and 20 bar, the initial activities of the catalysts at 35 % CO conversion were found to increase with the homogeneity of the cobalt distribution. In order to study how the distribution of the active metal over the support surface influences catalyst stability, prolonged catalytic testing experiments (200 h) were carried out. Regardless the distribution of the active metal over the support, all catalysts were found to lose about 20 % of their initial activity over 200 h, which correlates well with the average particle growth during the experiment, as was demonstrated by TEM studies of the fresh and spent catalysts. Deactivation constants determined on the base of second order deactivation kinetics were found to be very similar for all catalysts studies and in the same order of magnitude as for Co/SiO_2 catalysts studied previously. In contrast to Co/SiO_2 Fischer-Tropsch catalysts and $CuZn/SiO_2$ catalysts for methanol synthesis, a more uniform distribution of the active metal over the titania support surface was not found to have a measurable positive effect on catalyst stability. For catalysts tested at higher CO conversions, higher activity losses and more severe particle growth was observed. From turnover frequency calculations based on TEM particle sizes, it can be concluded that average particle growth is the main factor in catalyst deactivation observed over the investigated time period, although no information was obtained on the degree of

reduction or surface rearrangements during Fischer-Tropsch synthesis. In the future, synchroton-based operando x-ray spectroscopy (XANES) and advanced microscopy techniques such as environmental TEM and/or STXM may address whether these factors also play a role during the experimental timespans.

While the first chapters of this thesis are dedicated to unpromoted catalysts, **chapter 4** addresses the effect of noble metal promotion on structural and catalytic properties of Co/TiO_2 catalysts in order to study how the promoters affect the intrinsic activities when using a reducible oxide support material. Catalysts with different amounts of noble metals (Ag, Pt, Ru, Re) were prepared by co-impregnation, leading to systems with similar initial cobalt oxide dispersions according to TEM and XRD. TPR showed that the addition of noble metal promoters shifts the cobalt reduction peaks to lower temperatures in the order Re < Ag < Ru < Pt and to an increasing extent with higher promoter loadings. Studies using in-situ XRD indicated that the reduction of Ag-promoted catalysts leads to the formation of hcp cobalt, which has previously been reported to lead to higher activities and C_{5+} selectivities. For Fischer-Tropsch synthesis at 493 K, 20 bar and 30 % X_{CO}, the use of all promoters led to increased cobalt time yields (10-12 10^{-5} $mol_{CO}/g_{Co}/s$ for $AgCo/TiO_2$, 10-17 10^{-5} $mol_{CO}/g_{Co}/s$ for $PtCo/TiO_2$, 7-15 10^{-5} $mol_{CO}/g_{Co}/s$ for $RuCo/TiO_2$ and 19 to 22 10^{-5} $mol_{CO}/g_{Co}/s$ for $ReCo/TiO_2$ compared to 6 10^{-5} $mol_{CO}/g_{Co}/s$ for Co/TiO_2), which indicated higher turnover frequencies for all systems studied. The highest increases in turnover frequencies were found for high Re loadings and medium Ru and Pt loadings. For $ReCo/TiO_2$ distinctly higher dispersions (d(Co) ~ 4 nm) were found in the spent catalysts, while the cobalt particle sizes remained unaffected by the addition of Ag, Ru or Pt (d(Co) 8 – 15 nm). Interestingly, no sharp decrease in the turnover frequencies is observed for the $ReCo/TiO_2$ catalysts, unlike in previous studies on particle size effects on carbon, silica and alumina supports. Compared with the unpromoted catalyst (85 %), the C_{5+} selectivity of Ag and Re promoted catalysts was significantly increased for all promoter loadings. For $RuCo/TiO_2$ catalysts, the C_{5+} selectivity was found to increase with higher promoter loadings. Pt-promoted catalysts, on the other hand, showed reduced C_{5+} selectivity, presumably due to the methanation activity of Pt. While the results suggest that the intrinsic activities of cobalt Fischer-Tropsch catalysts supported on reducible titania support can be increased by noble metal promotion, it should be noted that no information could be obtained on the degree of cobalt reduction during Fischer-Tropsch synthesis. Also, the location of the promoters could not be clearly determined by

conventional electron microscopy. These issues can be addressed by synchrotron based x-ray spectroscopy (XANES and EXAFS) and/or element specific microscopy techniques (STEM-EELS and STXM) in the future.

In all previous chapters, the titania support material is kept constant in the preparation studies. In **chapter 5**, we report on the impact of surface functionalization on the structural and catalytic properties of carbon nanotube (CNT) supported cobalt catalysts. Commercially available CNT (Baytubes 150 HP) consist of graphene sheets rolled up in a Russian doll fashion and are functionalized by liquid- (LPO) and gas-phase oxidation (GPO). Both surface treatment protocols led to similar numbers of acid groups and did not significantly affect the nitrogen physisorption properties of the support material, but the surface appeared to be roughened for CNT functionalized by GPO, while the graphitic structure was found to be severely distorted for CNT functionalized by LPO. Incipient wetness impregnation of the functionalized and unfunctionalized support materials was carried out with solutions of cobalt nitrate in water, ethanol and 1-propanol, yielding supported cobalt oxide particles of 4-5 nm. The distribution of cobalt was found to become more uniform in the order H_2O < EtOH < 1-PrOH. The activity of the catalysts during Fischer-Tropsch synthesis at 493 K and 20 bar correlated with the homogeneity of cobalt distribution, which can be explained by supported particles with a more homogeneous distribution having a lower tendency for particle growth during reduction. Supported cobalt catalysts on unfunctionalized CNT showed distinctly higher activities (13 – 17 10^{-5} $mol_{CO}/g_{Co}/s$) than their counterparts on functionalized CNT (5 – 9 10^{-5} $mol_{CO}/g_{Co}/s$). C_{5+} selectivities of catalysts on untreated CNT (88 – 91 %) were also found to be higher than in the case of functionalized materials (69 % for LPO and 82-83 % for GPO), which could not be exclusively explained by differences in CO conversion. While it is often assumed that the presence of acid groups hampers the reduction to metallic cobalt, using in-situ XANES we could demonstrate that the degree of reduction after reaching steady state did not significantly differ for catalysts supported on functionalized and untreated CNT. In-situ XRD studies indicated the formation of *hcp* cobalt for catalysts supported on unfunctionalized catalysts exclusively, possibly explaining the higher observed activities and C_{5+} selectivities for these catalysts. Alternatively, the higher selectivities can be explained by the unfunctionalized support surface favoring re-adsorption of α-olefins inducing further chain growth, while this pathway will be less favoured for functionalized supports due to the presence of functional groups. Supported cobalt catalysts

impregnated with solutions of 1-PrOH on functionalized and unfunctionalized CNT were used in Fischer-Tropsch synthesis at 493 K for 180 h, while the same catalysts were exposed to Fischer-Tropsch synthesis at higher temperatures (503 – 523 K). It was found that after returning to 493 K, the catalyst on untreated CNT showed decreased activities, while the activity of the catalyst on functionalized CNT remained unaffected. The higher stability of the catalyst on functionalized CNT against average particle growth at elevated temperature can be rationalized by oxygen containing support sites acting as anchoring points and thus inhibiting the mobility of cobalt nanoparticles over the support surface.

Chapter 6b

Samenvatting

De Fischer-Tropsch synthese (FTS) is de heterogeen gekatalyseerde omzetting van synthesegas tot koolwaterstoffen (en water) en biedt een veelbelovend alternatief voor de synthese van zeer schone transportbrandstoffen, chemicaliën en smeermiddelen. Het synthesegas kan gegenereerd worden uit verschillende grondstoffen, zoals steenkool (CTL), biomassa (BTL) of aardgas (GTL), met het laatstgenoemde als economisch meest interessante optie. Daarom zou de Fischer-Tropsch synthese de afhankelijkheid van aardolie kunnen verminderen, omdat het de mogelijkheid biedt om vloeibare transportbrandstoffen te maken uit bronnen die vermoedelijk langer beschikbaar zijn dan aardolie. De eigenschappen van de katalysatoren voor de omzetting van synthesegas zijn cruciaal voor de economie van de XTL fabrieken, want er is een hoge activiteit, hoge selectiviteit naar zware koolwaterstoffen en hoge stabiliteit onder procescondities nodig. Titania-gedragen kobalt katalysatoren zijn eerder geïdentificeerd als erg geschikte katalysatoren voor de Fischer-Tropsch synthese, vooral vanwege hun hoge hydrothermale stabiliteit en hun hoge selectiviteit tot zware koolwaterstoffen. Het doel van dit onderzoek is om nieuwe inzichten te krijgen hoe de bereidingsmethode de structurele en katalytische eigenschappen onder industriële condities van Co/TiO_2 katalysatoren in de Fischer-Tropsch synthese beïnvloed.

In **hoofdstuk 2** werden Co/TiO_2 katalysatoren (4-24 gew.-%), bereid door droge impregnatie (IWI) met een daaropvolgende statische droogstap, vergeleken met katalysatoren bereid door depositie precipitatie van hoge (DPA) en lage (DPU) pH. Terwijl de gemiddelde kobaltoxide deeltjesgroottes ongeveer even groot waren (8-15 nm volgens röntgendiffractie) voor katalysatoren met dezelfde metaal belading, werden er geclusterde kobaltoxide deeltjes voor de IWI katalysatoren gevonden. De gedragen kobaltoxidedeeltjes waren homogeen over het oppervlak van de drager verdeeld voor de DPA katalysatoren, terwijl de bereiding van Co/TiO_2 katalysatoren door de DPU methode leidt tot de vorming van heel kleine (2-4 nm) gedragen kobaltoxidedeeltjes en grote (200 nm) deeltjes los van de drager. Dit effect kan verklaard worden door de relatief sterkere electrostatische interactie tussen de kobalt-kationen en het oppervlak van de drager bij een hoge pH. Katalytische tests bij 493 K en 20 bar toonden dat de activiteit toenam in de orde DPU < IWI < DPA voor alle metaalbeladingen. De hogere activiteit van de DPA katalysatoren vergeleken met de IWI katalysatoren bij vergelijkbare kobaltoxide dispersies, kan verklaard worden door hun hogere stabiliteit tegen deeltjes groei tijdens de reductie, wat overeenkomt met waterstof chemisorptie experimenten en berekeningen voor de omzettingsfrequenties (TOF). De lage activiteit van de DPU-

katalysatoren kan aan de hand van TPR-experimenten beredeneerd worden, vanwege het lage specifieke oppervlak van de grote kobaltoxide deeltjes en een moeilijke reduceerbaarheid van de kleine gedragen deeltjes. Terwijl de selectiviteiten van de IWI (79 %) en DPU (81 %) katalysatoren vergelijkbaar waren, werden er significant hogere selectiviteiten gevonden voor de katalysatoren bereid door de DPA methode (86 %) voor alle metaal beladingen, een effect dat niet door de oppervlakte van het metaal verklaard kan worden. Wij stellen voor dat bij depositie precipitatie bij een hoge pH, een kleine deel van de drager opgelost wordt en vervolgens afgezet wordt op de kobaltdeeltjes als het materiaal weer neerslaat. Een dergelijke decoratie zou tot kobaltdeeltjes kunnen leiden, waarbij CO sterker gebonden kan worden dan in IWI-katalysatoren. Technieken voor de detectie van geadsorbeerde species kunnen in de toekomst gebruikt worden om de verhoogde selectiviteiten van deze katalysatoren beter te begrijpen.

In **hoofdstuk 3** worden Co/TiO_2 katalysatoren (8 en 16 gew.-%) besproken, die door middel van depositie precipitatie bij hoge pH (DPA) en droge impregnatie met een daaropvolgende statische droogstap (IWI-S) of een droogstap in een wervelbed (IWI-F) zijn gemaakt. Terwijl de aanwezigheid van geclusterde deeltjes voor IWI-S en de homogene verdeling voor DPA katalysatoren al besproken is, werden er voor de IWI-F katalysatoren homogenere verdelingen gevonden vergeleken met IWI-S, maar niet zo homogeen als voor DPA. Tijdens Fischer-Tropsch synthese bij 493 K en 20 bar werden hogere activiteiten voor katalysatoren met een homogenere verdeling van kobalt gevonden. Om de invloed van de verdeling van kobalt op de stabiliteit van de katalysatoren te kunnen bestuderen, werden er langere katalytische tests (200 uur) uitgevoerd. Ongeacht de verdeling van het kobalt over de drager, verloren alle katalysatoren ongeveer 20 % van hun initiële activiteit, wat goede overeenkomt met de deeltjesgroei tijdens het experiment, zoals werd geobserveerd met een electronenmicroscopische studie van de gebruikte katalysatoren. De deactiveringsconstanten, berekend op basis van tweede-orde kinetiek, waren vergelijkbaar voor alle katalysatoren en zaten in dezelfde orde van grootte als de Co/SiO_2 katalysatoren die eerder bestudeerd waren. In tegenstelling tot wat het geval is voor Co/SiO_2 Fischer-Tropsch katalysatoren en $CuZn/SiO_2$ katalysatoren voor de synthese van methanol, was er dus geen positief effect van een meer homogene metaalverdeling over de drager op de stabiliteit tijdens katalyse. Voor de katalysatoren die bij hogere CO-conversie zijn getest, werd een hoger activiteitsverlies en meer deeltjesgroei waargenomen. Van de omzettingsfrequenties en de TEM studies kunnen wij concluderen dat deeltjesgroei de belangrijkste factor in de deactivering over de bestudeerde tijdschaal

is, ondanks dat we niets over de reductiegraad of een herschikking van de kobalt oppervlakte kunnen zeggen. In de toekomst zouden er operando röntgenspectroscopie (XANES) en geavanceerde microscopietechnieken (TEM en/of STXM) gebruikt kunnen worden om te studeren of deze factoren ook een rol in de deactivering van de katalysatoren spelen.

Terwijl niet gepromoteerde katalysatoren werden besproken in de eerste hoofdstukken, rapporteren we in **hoofdstuk 4** de effecten van edelmetaal-promotoren op de structurele en katalytische eigenschappen van Co/TiO_2 katalysatoren, om te kijken of de promotoren de intrinsieke activiteit verhogen, wanneer er een reduceerbaar oxide als drager wordt gebruikt. Katalysatoren met verschillende hoeveelheiden edelmetaal (Ag, Pt, Ru, Re) werden bereid door middel van co-impregnatie, waardoor de initiële dispersie van kobaltoxide vergelijkbaar was volgens TEM en röntgendiffractie. TPR experimenten toonden dat edelmetalen de temperatuur voor de reductie van kobaltoxide verlaagden, in de volgorde Re < Ag < Ru < Pt, een effect dat sterker werd naar mate de belading van de promotor hoger werd. In-situ röntgendiffractie toonde aan dat de reductie van Ag-gepromoteerde katalysatoren tot de vorming van *hcp* kobalt leidt, waarvan bekend is dat de TOF hoger is dan voor *fcc* kobalt. Tijdens Fischer-Tropsch synthese bij 493 K en 20 bar vertoonden alle katalysatoren verhoogde activiteiten (10-12 10^{-5} $mol_{CO}/g_{Co}/s$ voor $AgCo/TiO_2$, 10-17 10^{-5} $mol_{CO}/g_{Co}/s$ voor $PtCo/TiO_2$, 7-15 10^{-5} $mol_{CO}/g_{Co}/s$ voor $RuCo/TiO_2$ en 19 to 22 10^{-5} $mol_{CO}/g_{Co}/s$ voor $ReCo/TiO_2$ vergeleken met 6 10^{-5} $mol_{CO}/g_{Co}/s$ for Co/TiO_2). De grootste verhoging van de omzettingsfrequentie werd gevonden voor hoge Re beladingen en lagere Ru en Pt beladingen. Voor $ReCO/TiO_2$ katalysatoren werden hogere kobaltdispersies in de gebruikte katalysatoren gevonden, terwijl de dispersie van de katalysatoren met Ag, Pt en Re ongeveer het zelfde was als voor de niet gepromoteerde katalysator (8-15 nm). Vergeleken met de niet gepromoteerde katalysator werden er significant verhoogde C_{5+} selectiviteiten voor alle katalysatoren met Ag en Re gevonden. Verder werden voor de $RuCo/TiO_2$ katalysatoren verhoogde selectiviteiten bij een hogere promotor belading gevonden, terwijl de katalysatoren met Pt een lagere selectiviteit toonden, waarschijnlijk vanwege de activiteit van Pt voor hydrogenolyse. Terwijl de resultaten suggereren dat edelmetaalpromotoren de TOF voor kobaltkatalysatoren op titania als reduceerbare oxide verhogen, moet er rekening gehouden worden met het feit dat dit onderzoek geen uitsluitsel geeft van de invloed van de edelmetalen op de reductiegraad van het kobalt. Verder kon de locatie van de edelmetaalatomen niet met behulp van gewone electronenmicroscopie bepaald worden. Deze punten kunnen in de

toekomst met behulp van röntgenspectroscopie (XANES en EXAFS) en/of element specifieke microscopie technieken (STEM-EELS en STXM) aangepakt worden.

Terwijl de drager in de vorige hoofdstukken overal titania was, rapporteren we in **hoofdstuk 5** over de invloed van oppervlaktefunctionalisering op de structurele en katalytische eigenschappen van kobaltkatalysatoren aangebracht op koolstofnanobuizen (CNT). Commercieel verkrijgbare CNT (Baytubes 150 HP) bestaand uit opgerolde grafietlagen en werden gefunctionaliseerd door oxidatie in vloeibare fase (LPO) en in de gasfase (GPO). Beide methodes voor de functionalisering leiden tot een vergelijkbare hoeveelheid zure groepen en hebben geen grote invloed op de stikstof fysisorptie resultaten voor de materialen, hoewel de drager onder de electronenmicroscoop er verruwd uit zag voor de GPO-CNT en de gehele grafitische structuur verstoord was voor de LPO-CNT. Droge impregnaties werden uitgevoerd met oplossingen van kobalt nitraat in water, ethanol en 1-propanol, wat tot gedragen kobaltoxide deeltjes leid van 4-5 nm. De verdeling van de nanodeeltjes over het oppervlak van de drager werd meer uniform in de volgorde H_2O < EtOH < 1-PrOH. De activiteit tijdens Fischer-Tropsch synthese correleerde met de verdeling van het kobaltoxide, waarmee beredeneerd kan worden dat homogeen verdeelde deeltjes minder samenklonteren tijdens de reductie en de eerste uren van de Fischer-Tropsch synthese. Gedragen kobalt katalysatoren op niet gefunctionaliseerde CNT toonden duidelijk hogere activiteiten (13 – 17 10^{-5} $mol_{CO}/g_{Co}/s$) dan de katalysatoren op gefunctionaliseerde CNT (5 – 9 10^{-5} $mol_{CO}/g_{Co}/s$). Ook de selectiviteiten voor katalysatoren op onbehandelde CNT (88 – 91 %) waren hoger dan voor katalysatoren op gefunctionaliseerde dragers (69 % for LPO and 82-83 % for GPO), wat niet alleen door verschillen in de verdeling van kobalt verklaard kan worden. Terwijl vaak aangenomen wordt dat de aanwezigheid van zure groepen de reduceerbaarheid van kobalt verlaagd, konden wij met behulp van in-situ XANES demonstreren dat de reductiegraad tijdens Fischer-Tropsch synthese vergelijkbaar was. In-situ röntgendiffractie studies toonden de vorming van *hcp* kobalt in het geval van de katalysatoren op niet gefunctionaliseerde dragers aan, wat een deel van de activiteitsverhoging zou kunnen verklaren. Een andere mogelijkheid is dat de verhoogde selectiviteiten veroorzaakt worden door de voorkeur voor re-adsorptie in het geval van niet gefunctionaliseerde dragers, waardoor α-olefines verder kunnen groeien. Gedragen kobaltkatalysatoren op gefunctionaliseerde en op onbehandelde dragers werden in de Fischer-Tropsch synthese bij hogere temperaturen (503-523 K) getest. Nadat de temperatuur tot 493 K was verlaagd, bleek dat de activiteit van de katalysatoren op gefunctionaliseerde CNT hetzelfde was gebleven, terwijl de

katalysatoren op onbehandelde CNT duidelijk minder actief geworden waren. De verhoogde stabiliteit tegen deeltjesgroei van de katalysatoren op gefunctionaliseerde CNT kan door de aanwezigheid van zure groepen verklaard worden, die als ankers dienen en de mobiliteit van de nanodeeltjes verlagen.

Acknowledgements

Probably everyone who has made it this far has to think hard once more. By now it is quite a while ago when I started my studies in Utrecht and I enjoy recalling the past when I write these words.

Krijn, first of all I would like to thank you for giving me the opportunity to carry out this project in your group. With your enthusiasm and your attention for detail you create a unique work atmosphere that helped me a lot. You also managed to always see the positive side of things, to leave some room for freedom and to still follow the project closely. It has been a pleasure working with you! I would also thank you for giving me the opportunity to follow my M.Sc. studies in Aachen in parallel to this project.

Shell Global Solutions is acknowledged for their financial support and many helpful discussions. Here I would like to particularly thank Johan den Breejen, Sander van Bavel, Heiko Oosterbeek and Leendert Bezemer for their advice on this project.

I would also like to acknowledge Magnus Rønning from NTNU Trondheim and Jorge Gascon, Vera Santos and Iulian Dugulan from TU Delft for supporting our project by giving us the opportunity to jointly carry out experiments in your facilities.

One of the things that makes this place special is the great group of people permanently supporting our projects. Dymph, Monique and Iris, thanks a lot for all the support and advice, especially in the last phase of my work. Rien, thank you for all the support in the setup, startup and maintenance of our workhorse setup, which brought this project a great step forward. Ad and Ad, thanks a lot for helping me with so many things over the last years, for keeping the setups going in a safe way. I would also like to thank Hans and Cor for a lot of support on the imaging part of this work, not just with me, but also with my students. Fouad, thanks for the IT and ordering support, Marjan, thank you for XRD and TGA. Herrick, Oscar, Pascal, it has been great to work with you.

Not all the experiments described in this thesis were carried out by myself, but by my enthusiastic students, which I am very grateful for. Rene and Wouter, thanks for all the intense work you put into your M.Sc. projects and that led to the results of chapter 5! Jogchum, you did a great job on carrying out your M.Sc. research that led to chapter 4.

Tanja and Wouter, thanks for taking samples from this work to NTNU and STCA to support this work with your external internships. Carl and Tom, your literature projects were a great contribution to the understanding of the matter of this thesis, too. Also thanks a lot to our group of second year students, Petra, Ludo, Rob and Sven, who validated some of the work described in chapter 2. It was a great pleasure working with all of you and I wish you all the best for your further careers!

Throughout the last couple of years I learned a lot from all colleagues around me about various subjects, but especially from the people in the syngas and catprep team. Thanks for getting me started in the group, Peter, and all the work we carried out together with Arjan on our setup. Petra, Harry, Gonzalo, Ard, Hirsa, Jovana, Rafael, Cedric, Roy, Nazila, Jeroen, Marianna, thanks for all shared insights and your advice on my work.

The thing I am definitely going to miss the most is the good atmosphere and the great people around. Joe, Dimitrije, Elena, Fiona, Gareth, Ilona, Peter, Peter, Peter, Carlo, Arjan, Hendrik, Jesper, Wenhao, Zafer, Daniël, Roy, Marianna, Ines, Ara, Christoph, Javi, Monica, Sam, Jan, Zoran, Gang, Korneel, Qingyun, Dilek, Jovana, Gonzalo, Jelle, Wouter, Tom, Rene, JX, Nazila, Jamal, Ara, Rob, Ard, Hirsa, Arjen, Lucian, Fouad, Jeroen, Ramon, thanks for making this time so special and thank you for the countless memories of pub quizzes, borrels, football, defense parties, mountain biking, quality music in the lab, courses and conferences and the travelling around Europe, Qatar and the U.S. that came with it, nights out in Utrecht and Amsterdam or simply good conversations and fun coffee breaks. Special thanks go out to the greatest indoor football team ever and everyone who came to wear the team colors and to cheer for us. These Thursday nights were more than 21 seconds of fun for sure and always a true highlight of the week, no matter the result. I hope to stay in touch with you. Keep it up!

Last but certainly not least I would like to thank my family for encouraging and supporting me over so many years. Maren and Maximilian, thanks for everything.

List of publications and presentations

Written publications

Eschemann, T.O., Bitter, J.H., de Jong, K.P.:
Effects of loading and preparation method of titania-supported cobalt catalysts for Fischer-Tropsch synthesis
Catalysis Today 228, 2014, 89-95.

Eschemann, T.O., Lamme, W.S., Manchester, R.L., Parmentier, T.E., Rønning, M., de Jong, K.P.:
Effect of support surface treatment on the structure and catalytic properties of Co/CNT Fischer-Tropsch catalysts
Journal of Catalysis 328, 2015, 130-138.

Eschemann, T.O., de Jong, K.P.:
Deactivation behavior of Co/TiO_2 catalysts during Fischer-Tropsch synthesis
ACS Catalysis 5, 2015, 3181-3188.

Eschemann, T.O., Oenema, J., de Jong, K.P.:
Effects of noble metal promotion for Co/TiO_2 Fischer-Tropsch catalysts
Catalysis Today, accepted for publication.

Welby, C.E., Eschemann, T.O., Unsworth, C.A., Smith, E.J., Thatcher, R.J., Whitwood, A.C., Lynam, J.M.:
Ruthenium acetate complexes as versatile probes of metal-ligand interactions: Insight into the ligand effects of vinylidene carbine, carbonyl, nitrosyl and isocyanide
European Journal of Inorganic Chemistry 9, 2012, 1493-1506.

Oral presentations

Eschemann, T.O., Bitter, J.H., de Jong, K.P.:
Preparation, characterization, activity and stability of titania-supported cobalt Fischer-Tropsch catalysts
10th Natural Gas Conversion Symposium, 03/2013, Doha, Qatar.

Eschemann, T.O., Bitter, J.H., de Jong, K.P.:
Preparation, characterizationg and performance of titania-supported cobalt Fischer-Tropsch catalysts
14th Dutch Chemistry and Catalysis Conference, 03/2013, Noordwijkerhout, The Netherlands.

Eschemann, T.O., Bitter, J.H., de Jong, K.P.:
Studying the influence of the synthesis procedure on the stability of titania-supported cobalt Fischer-Tropsch catalysts
23rd North American Catalysis Society Meeting, 06/2013, Louisville, KY, United States.

Eschemann, T.O., Manchester, R.L., Lamme, W.S., de Jong, K.P.:
Studying the role of support surface modification in the case of CNT-supported cobalt Fischer-Tropsch catalysts
15th Dutch Chemistry and Catalysis Conference, 03/2014, Noordwijkerhout, The Netherlands.

Poster presentations

Eschemann, T.O., Bitter, J.H., de Jong, K.P.:
Impact of preparation methods on structure and performance of cobalt Fischer-Tropsch catalysts
13th Dutch Chemistry and Catalysis Conference, 03/2012, Noordwijkerhout, The Netherlands.

Eschemann, T.O., Bitter, J.H., de Jong, K.P.:
The impact of loading and synthesis method on the properties of Co/TiO_2 Fischer-Tropsch catalysts
11th European Congress on Catalysis, 09/2013, Lyon, France.

Lamme, W.S., Eschemann, T.O., de Jong, K.P.:
Co/CNT Fischer-Tropsch catalysts: Influence of surface functionalization and impregnation solvent on structure and performance
15th Dutch Chemistry and Catalysis Conference, 03/2014, Noordwijkerhout, The Netherlands.

Eschemann, T.O., Lamme, W.S., Manchester, R.L., de Jong, K.P.:
Studying the role of support surface modification in the case of Co/CNT Fischer-Tropsch catalysts
47. Jahrestreffen Deutscher Katalytiker, 03/2014, Weimar, Germany.

Eschemann, T.O., Lamme, W.S., Manchester, R.L., de Jong, K.P.:
Studying the role of support surface modification in the case of Co/CNT Fischer-Tropsch catalysts
11th Symposium on Scientific Bases for the Preparation of Heterogeneous Catalysts, 07/2014, Leuven, Belgium.

Curriculum Vitae

Thomas Oliver Eschemann was born October 5, 1984 in Leverkusen, Germany. After graduating from Gymnasium Odenthal, he chose to enroll for chemistry at RWTH Aachen University in 2005. During his studies, he quickly realized that he was most interested in catalytic conversion and carried out several research projects in this field. Thomas took the opportunity to carry out some of the curricular research projects externally, e.g. at the University of York and at the Jülich Research Center. He chose to focus on heterogenous catalysis and joined the Institute for Fuel Chemistry and physical-chemical Process Technology, where he carried out his graduation project on “New synthesis routes to diphenyl carbonate” in cooperation with Evonik Industries as industrial partner.

After completing his chemistry studies in Aachen with honors in 2010, Thomas joined the Inorganic Chemistry and Catalysis group at Utrecht University to carry out his Ph.D. project under supervision of Prof. dr. ir. Krijn P. de Jong. His research project was titled “New stable Co/TiO_2 catalysts for the Fischer-Tropsch reaction” and carried out in cooperation with TU Delft and Shell Global Solutions. The results of his studies are described in this thesis. During his time as a Ph.D. student, Thomas was responsible for the dimensioning, acquisition and use of a high throughput catalytic testing setup as well as for temperature-programmed reduction and combined calcination/reduction setups. He was involved in undergraduate teaching, the supervision of several M.Sc. students and represented the group in the Ph.D. student committee of the Debye Institute for Nanomaterial Science, where he was responsible for the organization of the Debye Meeting Days 2013 and the Debye Summer School 2012 supporting program.

Thomas is married and the father of one son. He is enthusiastic about football, mountain biking, travelling and cooking. In his free time, he chose to study Economics at RWTH Aachen University, from which he successfully graduated in 2014. As of March 2015, Thomas has joined BASF Catalysts Germany GmbH as an Application Engineer in the field of mobile emissions catalysts.